REGULATION AND FUNCTION OF APOER2 AND VLDLR IN THE CENTRAL NERVOUS AND REPRODUCTIVE SYSTEMS

APPROVED BY SUPERVISORY COMMITTEE

_____

Joachim Herz M.D.
Professor of Biophysics and Molecular Genetics

_____

Amelia Eisch Ph.D.
Assistant Professor of Psychiatry

_____

Ege Kavalali Ph.D.
Associate Professor of Neuroscience

_____

Malu Tansey Ph.D.
Assistant Professor of Physiology

DEDICATION

I would like to dedicate this thesis to my husband Chaz.

I am forever grateful for your love, support, patience, and encouragement.

REGULATION AND FUNCTION OF APOER2 AND VLDLR IN THE CENTRAL NERVOUS AND REPRODUCTIVE SYSTEMS

by

IRENE MASIULIS BOWEN

DISSERTATION

Presented to the Faculty of the Graduate School of Biomedical Sciences

The University of Texas Southwestern Medical Center at Dallas

In Partial Fulfillment of the Requirements

For the Degree of

DOCTOR OF PHILOSOPHY

The University of Texas Southwestern Medical Center at Dallas

Dallas, Texas

April, 2009

Copyright

by

Irene Masiulis Bowen, 2009

All Rights Reserved

ACKNOWLEDGMENTS

I would first like to acknowledge my mentor Dr. Joachim Herz for giving me the opportunity to work, learn, and grow in his laboratory. His plethora of fantastic project ideas is astounding and his excitement for scientific investigation infectious.

I need to thank the fabulous scientists that made up my thesis committee: Dr.'s Amelia Eisch, Malu Tansey, Ege Kavalali, and for a brief period, Masahide Kikkawa. Thank you for all of your support, encouragement, and expert advice.

A great lab cannot exist without great scientists. I am indebted to many members of the Herz Lab both past and present. Thank you to everybody who has worked inside the doors of L5.154 and L5.156. I would like to thank Dr. Uwe Beffert who served as a second mentor for my first three years. I received indispensible technical support from both Wen-Ling Niu and Hui-Chuan Reyna, thank you. I would like to thank Priscilla Rodriguez, Isaac Rocha, and Megan Davenport for their hard work in maintaining and genotyping the 30+ strains of my mouse colony. I also need to acknowledge Dr. Li Zhou for teaching me the ES cell cloning techniques amongst many other things, and Dr. Murat Durakoglugil for teaching me how to slice brains and measure LTP. Finally, thank you to all of the friends I have made in the lab especially those who have offered great scientific advice and support over the past six years: Dr. Martin Dietrich, Dr. Hong Choi, Dr. Ying Chen, and Dr. Eric Johnson.

I also need to thank Richard Gibson for his help in generating the polyclonal antibodies used in these studies; Lisa Beatty and the Molecular Genetics Tissue Culture Core for their cell culture support; Jeff Cormier for his help with the qRT-PCR; Liz Lummus and Dr. Robert Hammer for their invaluable help with the generation of the KI

and BAC transgenic animals; and finally Dr. Timothy Quill for teaching me how to measure sperm viability and motility.

I would like to thank all of my life long friends, especially, Aleksa Valiulis Westwater and my college roommate Erinn Howard. Your friendships are priceless to me. Thank you to all of my new found Texas friends, in particular, Priscilla Rodriguez and the soon to be Dr. Gina Rodriguez, for keeping me sane and motivated.

Most importantly I would like to thank my parents for their selfless love, support (even if I move 1,200 miles away), and for teaching me the value of a good education. Nida, my sister, I would not have made it through graduate school without your phone calls, you are my best friend and my rock. Also, thank you to my in-laws who have accepted me as their own daughter. You make me feel loved.

I would not have chosen to go into science had it not been for my aunt, Dr. Ana Jonas. She has been an inspiration and a role model throughout my life and for that I am forever grateful.

Last but not least I would like to thank my husband for his sacrifices that allowed me to start and complete my graduate school career. You were the strength that I needed to get through the rough times and you helped me celebrate the good. I am indebted to my Kiwi for keeping my papers warm as I typed my thesis. And finally, thank you to my puppies that were never mad when I worked 14 hour days and always greeted me at the door with wagging tails; you help me enjoy the simple things in life.

REGULATION AND FUNCTION OF APOER2 AND VLDLR IN THE CENTRAL NERVOUS AND REPRODUCTIVE SYSTEMS

Publication No. _____

IRENE MASIULIS BOWEN, Ph.D.

The University of Texas Southwestern Medical Center at Dallas, 2009

JOACHIM HERZ, M.D.

The LDL receptor gene family is an evolutionarily ancient family of membrane spanning proteins composed of a diverse collection of receptors that share common domains and mediate a variety of organismal functions. Members of this family, Apoer2 and Vldlr, are highly similar receptors and are both involved in the Reelin signaling pathway. This pathway controls neuronal migration and organization of the brain during development as well as synaptic function in adulthood. Although both receptors partially compensate for one another during Reelin signaling, the generation of knockin mutant animals has allowed us to begin to uncover the unique and independent functions of these receptors that have not yet been explored.

For example, a single amino acid mutation in Vldlr determines binding of the Pafah1b complex to the cytoplasmic tail of the receptor. Mice expressing this L838R mutation were created using ES cell homologous recombination techniques and will be useful in exploring the effects of the mutation in brain development and synaptic function *in vivo*.

Vldlr independent functions that are unique to Apoer2 have been explored in more depth. These include binding of scaffolding proteins PSD95 and JIPs to an alternatively spliced exon within the cytoplasmic tail of Apoer2, which is not found in any other LDLR family member. This exon has been shown to mediate increased LTP induction after Reelin stimulation. Apoer2 knockin animals, expressing splice variants lacking another alternatively spliced exon encoding the O-linked sugar domain, show receptor stabilization through the inhibition of Apoer2 proteolytic processing. This causes increased Apoer2 levels in both the brain and testis. While lack of exon 16 has no known consequences in the testis, it does cause disrupted synaptic transmission and defective LTP induction after reelin stimulation in the brain.

Apoer2 was recently found to be involved in selenium uptake into the testis and brain. Through the use of various Apoer2 intracellular domain mutant mice, a differentiation was made between the Apoer2 functional domains involved in cell signaling and the function of the receptor in selenium endocytosis.

Further use of the aforementioned knockin mouse lines will help uncover previously unexplored functions of Vldlr and Apoer2 and advance our understanding of their potential involvement in neurological diseases such as Alzheimer's disease.

TABLE OF CONTENTS

PRIOR PUBLICATIONS

Beffert, U., Weeber, E.J., Durudas, A., Qiu, S., **Masiulis, I.**, Sweatt, J.D., Li, W.P., Adelmann, G., Frotscher, M., Hammer, R.E. et al. (2005). Modulation of synaptic plasticity and memory by Reelin involves differential splicing of the lipoprotein receptor Apoer2. Neuron *47*, 567-579.

Beffert, U., Nematollah Farsian, F., **Masiulis, I.**, Hammer, R.E., Yoon, S.O., Giehl, K.M., Herz, J. (2006). ApoE receptor 2 controls neuronal survival in the adult brain. Current Biology *16*, 2446-2452.

Masiulis, I., Quill, T.A., Burk, R.F., Herz, J. (2009). Differential functions of the Apoer2 intracellular domain in selenium uptake and cell signaling. Biological Chemistry *390*, 67-73.

Herz, J., Chen, Y., **Masiulis, I.**, Zhou, L. (2009). Expanding functions of lipoprotein receptors. Journal of Lipid Research, In press.

LIST OF FIGURES

CHAPTER ONE: General introduction and literature review

CHAPTER TWO: The interaction between Vldlr and the Pafah1b complex and its role in neuronal migration and synaptic function

CHAPTER THREE: The alternatively spliced O-linked sugar domain regulates Apoer2 processing

CHAPTER FOUR: The role of the Apoer2 cytoplasmic tail functional domains in selenium uptake and sperm function

LIST OF TABLES

CHAPTER FOUR: The role of the Apoer2 cytoplasmic tail functional domains in selenium uptake and sperm function

LIST OF ABBREVIATIONS

ACSF – Artificial Cerebrospinal Fluid
AD – Alzheimer's Disease
APOE – Apolipoprotein E
APOER2 – Apolipoprotein E Receptor 2
APP – Amyloid Precursor Protein
Aβ – Amyloid Beta Peptide
BAC – Bacterial Artificial Chromosome
BAEC – Bovine Aortic Endothelial Cells
BLRP – Biotin Ligase Recognition Peptide
BMP-4 – Bone morphogenetic protein 4
BSA – Bovine Serum Albumin
BWW – Biggers-Whitten-Whittingham
CNS – Central Nervous System
CREB – cAMP-response element binding protein
CSF – Cerebrospinal Fluid
CSN – Corticospinal Neuron
DAB1 – Disabled
DAPT – γ-secretase inhibitor
DBP – Vitamin-D Binding Protein
EGFP – Enhanced Green Fluorescent Protein
EPSC – Excitatory Postsynaptic Current
ER – Endoplasmic Reticulum
ES cell – Embryonic Stem Cell
FACS – Fluorescent Activated Cell Sorting
FCS – Fetal Calf Serum
FH – Familial Hypercholesterolemia
FTD – Frontotemporal Dementia
GABA – γ-aminobutyric acid
GP330 – Megalin
GSK3β – Glycogen Synthase Kinase 3β
ICD – Intracellular Domain
I/O – Input/Output
IPTG - Isopropyl Thiogalactoside
JIP – JNK Interacting Protein
JNK – c-Jun N-terminal Kinase
KI - Knockin
KO – Knockout
LB – Luria Broth
LDLR – Low-density Lipoprotein Receptor
LIF – Leukemia Inhibitory Factor
LPS – Lipopolysaccharide
LRP1 – Low-density Lipoprotein Receptor-Related Protein 1
LRP1b – Low-density Lipoprotein Receptor-Related Protein 1b
LRP2 – Megalin
LRP4 – MEGF7
LTP – Long Term Potentiation
MAP-2 – Microtubule Associated Protein 2
MEGF7 – Multiple epidermal growth factor containing protein 7

MLS – Multiple Cloning Site
MMP – Matrix Metalloproteinase
mz – Marginal Zone
NLS – Nuclear Localization Signal
NMDAR – *N*-methyl-D-aspartate receptor
NMJ – Neuromuscular Junction
NUDEL – Nuclear Distribution Element-Like
p3 – non-amyloidogenic APP peptide
PAF – Platelet-Activating Factor
PAFAH1b – PAF Acetylhydrolase 1b
pBSKS – pBluescriptII KS(+) vector
PDGF – Platelet-Derived Growth Factor
PI3K – Phosphatidylinositol-3-kinase
PKB – Protein Kinase B
PKC – Protein Kinase C
PKMζ – Protein Kinase M zeta
PMA – Phorbol 12-myristate 13-acetate
pp – Preplate
PPF – Paired Pulse Facilitation
PPI – Prepulse Inhibition
RAP – Receptor Associated Protein
Sepp1 – Selenoprotein P
SFK – Src Family Kinase
SHH – Sonic hedgehog
sp – Subplate
τ – Tau, a microtubule-associated protein
TB – True Blue
UTR – Untranslated Region
VLDLR – Very-low-density Lipoprotein Receptor
WT – Wild-type

CHAPTER ONE

GENERAL INTRODUCTION AND LITERATURE REVIEW

The LDL Receptor Family

The low-density lipoprotein (LDL) receptor family is a highly conserved and evolutionarily ancient family of transmembrane spanning proteins (Figure 1.1). Homologues of the LDL receptor family, with similarly arranged domains, can be found even in primitive organisms such as *C. elegans* (LRP) (Yochem and Greenwald, 1993) and *D. melanogaster* (LpR2) (Culi et al., 2004). The early appearance of the archaic LDL family-like receptors gives some insight into the importance of these proteins throughout the evolution of more complex organisms.

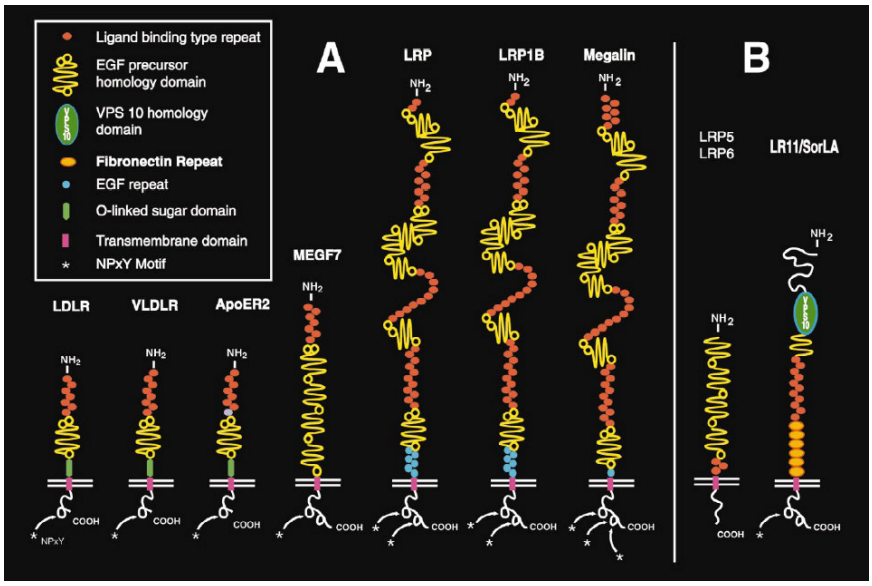

Figure 1.1: The LDL Receptor Family. (A) The seven core members of the LDL receptor family share common structural domains. (B) LRP5, LRP6 and LR11/SorLA, more distantly related proteins, share some similarity in domain structure with the main members of the family. (Herz, 2001)

The seven core members of the LDL receptor family are: the low-density lipoprotein receptor (Ldlr), very-low-density lipoprotein receptor (Vldlr), apolipoprotein E receptor 2 (Apoer2/Lrp8), multiple epidermal growth factor containing protein 7 (Megf7/Lrp4), LDL receptor-related protein (Lrp1), Lrp1b, and megalin (Lrp2/gp330) (Figure 1.1). Structurally, the members of the LDL receptor family are made up of similar "building blocks". Their extracellular domains contain multiple ligand binding repeats. The ligand binding domain is generally followed by an EGF precursor homology domain. Ldlr, Vldlr, and Apoer2 all contain O-linked sugar domains just prior to the transmembrane spanning region. This O-linked sugar domain contains numerous serine and threonine residues that serve as attachment sites for O-linked sugars.

The cytoplasmic tails of the family members show less similarity between receptors. There is, however, one small tetra-amino acid motif that the LDL receptor family members do share: the NPxY motif (x = any amino acid). The intracellular tails of the receptors contain anywhere from one to three of these motifs. This four amino acid sequence functions in protein interaction/signal transduction and endocytosis. In some of the family members, endocytosis is the primary function of the motif (Chen et al., 1990). This is true for the Ldlr, as the motif is responsible for endocytosis of the lipid bound receptor which is essential for mediating cholesterol homeostasis (Brown and Goldstein, 1986). In other family members the motif mainly functions in protein interaction and signal transduction (Howell et al., 1999b; Trommsdorff et al., 1998). Apoer2 is a prime example, as its endocytosis coefficient is very low (Beffert et al., 2006a) and the primary function of the motif is signal transduction across the membrane to the adaptor protein

Disabled (Dab1), which interacts with the receptor tail through the NPxY motif (Hiesberger et al., 1999; Howell et al., 1999a).

After the identification and characterization of the founding member of the LDL receptor the family, Ldlr, all subsequent family members were initially assumed to be involved in lipid metabolism based on the involvement of Ldlr in cholesterol homeostasis (Herz et al., 1988). However, it is now well established that, besides lipid metabolism, members of this family are also involved in extracellular matrix protein clearance, cellular signal transduction, endocytosis of various ligands, vitamins and other nutrients, synaptic function, and brain lamination (Reviewed in (Beffert et al., 2004; Herz, 2001; May et al., 2005; Willnow et al., 1999)). In order to appreciate the functional diversity represented by these receptors, it is essential to look at each member more closely on an individual basis.

Ldlr – The 95kDa Ldlr is ubiquitously expressed throughout the body, most notably in hepatocytes and the CNS. Ldlr plays the indispensible role of regulating cholesterol homeostasis throughout the body and in the brain. The receptor binds to LDL particles rich in cholesterol, clusters, and participates in clathrin coated pit mediated endocytosis of the receptor and attached lipoprotein particle (Brown and Goldstein, 1979). Mutations in the *LDLR* gene are responsible for familial hypercholesterolemia (FH), a disease in which Ldlr function is impaired, leading to increased plasma cholesterol concentrations causing premature cardiovascular disease (Fass et al., 1997; Hobbs et al., 1990).

Megf7/Lrp4 – Megf7 is the intermediately sized receptor, with a molecular weight of about 200 kDa. It has recently been found to play an important role in

development, more specifically in limb, kidney, lung, tooth, and neuromuscular junction formation (NMJ) (Johnson et al., 2005; Ohazama et al., 2008; Simon-Chazottes et al., 2006; Weatherbee et al., 2006). The most prominent phenotype of the Megf7 null mice visible externally is fully penetrant polysyndactaly. Similar phenotypes have been observed in humans (Hamosh et al., 2005) and a mutation in *Megf7* introducing a premature stop codon is the cause of the bovine mulefoot disease which exhibits the fusion of hooves in cows (Johnson et al., 2006). The limb and tooth phenotypes are thought to be a result of impaired involvement of Megf7 in the canonical Wnt signaling pathway (Johnson et al., 2005; Ohazama et al., 2008). In the past year, Megf7 was also found to be the missing link in the agrin/MuSK receptor complex involved in normal NMJ formation (Zhang et al., 2008).

Lrp1 – Lrp1 is one of the largest and most versatile receptors in the family. The 600 kDa receptor is cleaved by the furin protease to form an 85 kDa membrane spanning fragment non-covalently bound to an extracellular 515 kDa fragment (Herz et al., 1990). Lrp1 can specifically bind over 40 different ligands including ApoE, proteinase/inhibitor complexes, α2-macroglobulin, PDGF, and APP (Herz, 2001; May et al., 2005). Expressed in many tissues including the liver, brain, and vasculature, Lrp1 plays many important roles both as an endocytic receptor and a signaling protein (Herz and Strickland, 2001). Here are a few examples of its many essential functions: Lrp1 is involved in cholesterol homeostasis by acting as a receptor for chylomicron remnants as well as lipases (Beisiegel et al., 1991); Lrp1 regulates extracellular proteolytic activity by clearing matrix metalloproteinases (MPPs) (Barmina et al., 1999) and proteinase/inhibitor complexes (Herz et al., 1992); Lrp1 can also regulate APP expression and Aβ production,

suggesting possible involvement in the pathogenesis of Alzheimer's Disease (AD) (Kounnas et al., 1995; Ulery et al., 2000).

Lrp1b – Lrp1b is also around 600kDa in size and is approximately 59% identical to Lrp1. The structural and functional domains of Lrp1b and Lrp1 are organized in a highly similar manner. However, Lrp1b has an extra repeat in the fourth ligand binding domain, an additional 33 amino acid fragment in the cytoplasmic tail, and a slower endocytosis rate (Knisely et al., 2007; Liu et al., 2000b). Lrp1b has been classified as a tumor suppressor gene, as it is mutated or deleted in about 40-45% of all non-small cell lung carcinomas (Liu et al., 2000a) and other cancers (Langbein et al., 2002; Sonoda et al., 2004). Lrp1b is expressed in the CNS and has been shown to increase APP retention at the cell membrane and decrease Aβ production (Cam et al., 2004).

Megalin/Lrp2/gp330 – Like Lrp1/Lrp1b, megalin is also a large receptor (600 kDa) that can bind numerous extracellular ligands. These ligands include various vitamins, nutrients, apolipoproteins, sonic hedgehog (Shh), and bone morphogenetic protein 4 (BMP-4). Megalin is expressed in certain epithelial cells of the kidney, lung, and intestines (May et al., 2005). It is most prominently known for the endocytosis of low molecular weight proteins such as the vitamin-D binding protein (DBP) in the proximal tubules of the kidney (Nykjaer et al., 1999). Megalin null animals suffer from holoprosencephaly (Willnow et al., 1996a), a forebrain developmental defect which displays fusion of the two hemispheres of the forebrain, highlighting the importance of this receptor during development.

Vldlr and Apoer2/Lrp8 – The very-low-density lipoprotein receptor (Vldlr, 100 kDa) and apolipoprotein E receptor 2 (Apoer2, 160 kDa) share similar organization of

domains with the LDL receptor. However, differences include one more ligand binding repeat in Vldlr and a unique alternatively spliced exon expressing a part of the cytoplasmic tail of Apoer2. Both receptors are almost exclusively expressed in the brain. However, some Vldlr expression has also been found in muscle and vascular endothelial cells (Wyne et al., 1996) and Apoer2 has been found in the testis with minimal levels in the ovary (Kim et al., 1996). Through their extracellular ligand binding domains, the receptors bind two essential proteins found in the brain, Reelin and Apolipoprotein E (ApoE) (D'Arcangelo et al., 1999; Herz, 2001), making Apoer2 and Vldlr components of the Reelin signaling pathway. The receptors are required for the transmission of the Reelin signal across the plasma membrane (Hiesberger et al., 1999). In the Reelin signaling pathway, Apoer2 and Vldlr are involved in the proper lamination of the cortex and Purkinje cell localization in the cerebellum during development (Mariani et al., 1977; Trommsdorff et al., 1999). The Reelin signaling pathway is also involved in regulating synaptic function and plasticity during adulthood (Weeber et al., 2002). Although Apoer2 and Vldlr function in a concerted manner to transmit the Reelin signal, there are amino acid differences between the two, which suggest that they also have the capacity to perform specific functions independent of one another. For example, Apoer2 is also expressed in the testis and Apoer2 KO males suffer from infertility due to defects in sperm tail morphology and motility (Andersen et al., 2003). Less is known about the unique functions of Vldlr. However recent findings suggest a specific interaction between Vldlr and the Pafah1b complex (Zhang et al., 2007). The Pafah1b complex inactivates the platelet activating factor (PAF) by hydrolysis. PAF has been shown to inhibit neural growth and migration *in vitro* (Bix and Clark, 1998; Clark et al., 1995).

However, the significance of the interaction between Vldlr and the Pafah1b complex, *in vivo*, has not yet been explored but will be discussed in Chapter 2.

Reelin Signaling

Both Apoer2 and Vldlr are integral members of the Reelin signaling pathway which is extremely important for the proper development and function of the brain (Herz and Chen, 2006). Reelin is a very large (400 kDa) extracellular matrix glycoprotein which is expressed in the brains of many vertebrate species (Perez-Garcia et al., 2001). In mammals, Reelin is expressed by Cajal Retzius neurons in the outer layers of the developing neocortex (D'Arcangelo et al., 1995). It is during this time that Reelin helps guide newly born neurons to their correct positions in the cortex in an inside out fashion; the new neurons migrate past older ones to get closer to the surface of the cortex (Goffinet, 1992). In the cerebellum Reelin is expressed in the external granule layer where it mediates Purkinje cell localization and monolayer formation (Mariani et al., 1977; Schiffmann et al., 1997). After the cessation of developmental neuronal migration, Reelin expression changes so that it is expressed only by a specific subset of GABAergic interneurons within the cortex and glutamatergic granule cells in the cerebellum (Pesold et al., 1998). This drastic change in the expression pattern of Reelin between development and adulthood suggests very different functions of the protein during the two stages of life.

Reelin is a proteolytically processed protein which is cleaved into three different pieces (Ignatova et al., 2004; Lambert de Rouvroit et al., 1999). The Reelin protein begins with a signal peptide followed by a region with some similarity to the protein

F-spondin. Further downstream are 8 repeats of about 350 amino acids each, and it is between repeats two and three where the first cleavage occurs, the second between repeats six and seven (Lambert de Rouvroit et al., 1999). The central piece of Reelin, containing repeats three through six, is the functional piece required for binding to Apoer2 and Vldlr (Jossin et al., 2004) (Figure 1.2). Reelin forms a disulfide bound homodimer through interactions of the N-terminal sequence of the protein both *in vitro* and *in vivo* (Kubo et al., 2002). This homodimer binds to Apoer2 and Vldlr, clustering the receptors at the plasma membrane (Strasser et al., 2004). Receptor clustering induces Dab1 binding to the cytoplasmic tails of the receptors and subsequent phosphorylation of the adaptor protein by Src Family Kinases (SFKs) (Hiesberger et al., 1999; Howell et al., 1999a). Dimerization of Reelin is required for Dab1 phosphorylation and the transmission of the Reelin signal across the membrane (Kubo et al., 2002). Interestingly, phosphorylated Dab1 can in turn activate more SFKs by stimulating phosphorylation of the activating tyrosine-418, which is conserved in SFK family members (Arnaud et al., 2003; Ballif et al., 2003; Bock and Herz, 2003).

N-methyl-D-aspartate receptors (NMDARs) mediate neurotransmission, synaptic plasticity, and are functionally implicated in learning and memory (Collingridge and Bliss, 1995). Through the activation of SFKs, Reelin signaling has the ability to regulate NMDAR activity and thus affect synaptic function (Chen et al., 2005). The SFK, Fyn is responsible for the phosphorylation of the NR2B subunit of the NMDAR (Hisatsune et al., 1999; Nakazawa et al., 2001). Phosphorylation and activation of NMDARs is also regulated through the interaction of the adaptor protein PSD95 with both the NMDAR and the cytoplasmic tail of Apoer2 (Beffert et al., 2005; Sornarajah et al., 2008).

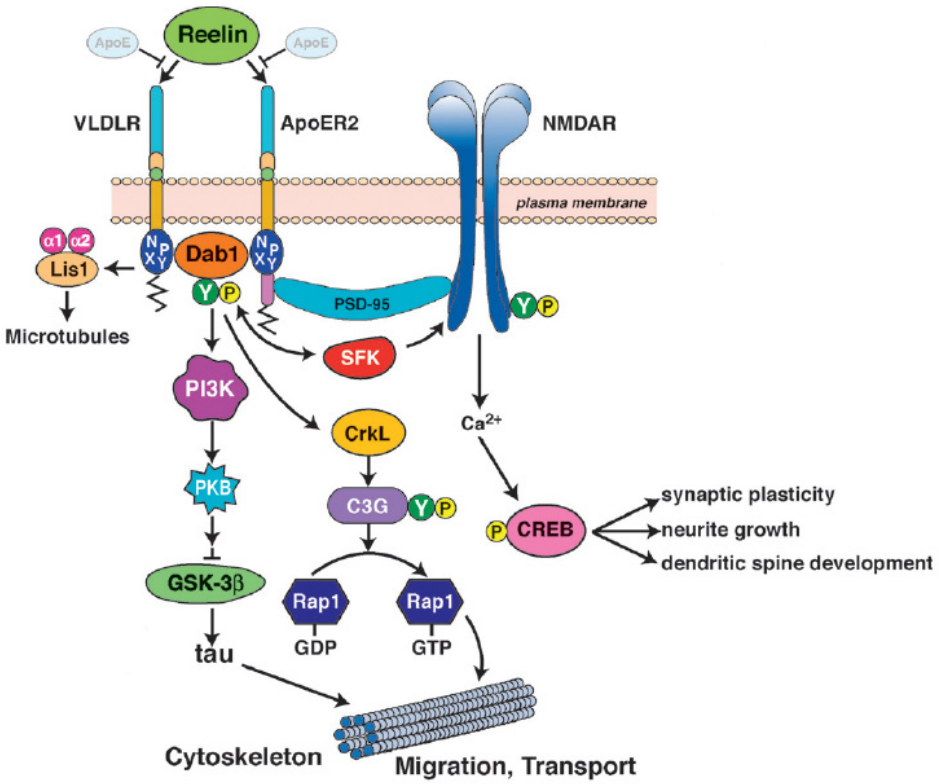

Figure 1.2: The Reelin Signaling Pathway. The Reelin signaling pathway beings with Reelin binding to the Apoer2 and Vldlr receptors causing receptor clustering. This clustering initiates the phosphorylation of the adaptor protein Dab1 bound to the cytoplasmic tails of the receptors. SFKs are responsible for Dab1 phosphorylation which can, in turn, promote increased activation of more Src family kinases. Reelin signaling plays a role in phosphorylation dependent NMDAR activation through the increase in SFK activity. Increased calcium influx from the activated NMDA receptors phosphorylates CREB which may transcriptionally regulate synaptic plasticity and neuronal development. Phosphorylated Dab1 interacts with CrkL whose downstream targets affect actin cytoskeleton stability. Phospho-Dab1 can also activate PI3K and PKB, which subsequently inhibit GSK-3β, helping to prevent tau hyperphosphorylation and aggregation. Lastly, in a phosphorylation dependent manner, Dab1 can also interact with Lis1, the regulatory subunit of the Pafah1b complex affecting microtubule dynamics. The alpha subunits of the Pafah1b complex also bind to the cytoplasmic tail of Vldlr, an interaction whose significance has not yet been determined. (Figure adapted from (Herz et al., 2008))

Phosphorylation of the NMDAR results in the opening of the ion channel and an influx of calcium into the neuron (Chen et al., 2005; Wang and Salter, 1994). NMDAR dependent influx of calcium promotes cAMP-response element binding (CREB) protein phosphorylation (Chen et al., 2005). Phospho-CREB may transcriptionally regulate genes important in synaptic plasticity along with neurite and dendritic spine development.

Phosphorylated Dab1 also interacts independently with various proteins that modulate microtubule organization and neuronal migration. Phospho-Dab1 activates phosphatidylinositol-3-kinase (PI3K), which activates protein kinase B (PKB/Akt) (Bock et al., 2003). PKB suppresses GSK3β activity resulting in decreased hyperphosphorylation of the microtubule associated protein tau (τ) and thus preserving microtubule integrity (Beffert et al., 2002). Hyperphosphorylated tau is subject to aggregation into intracellular tangles, a pathological hallmark of Alzheimer's Disease (Alonso et al., 2001). Phospho-Dab1 also binds the adaptor proteins CRK and CRK-like (CRKL) (Park and Curran, 2008) and promotes the phosphorylation and activation C3G, which acts as a guanine nucleotide exchange factor for RAP1, a modulator of the actin cytoskeleton (Ballif et al., 2004; Bos et al., 2001). Lastly, phosphorylated Dab1 can also bind Lis1 (Pafah1b1) (Assadi et al., 2003). Mutations in *LIS1* are the cause of some forms of human lissencephaly, a brain disorder in which the cortex appears smooth due to the lack of gyri because of defects in neuronal migration during early development (Dobyns et al., 1993; Reiner et al., 1993). Thus, Lis1 is thought to play a large role in regulating neuronal migration through its interaction with the cytoplasmic dynein heavy chain and NUDEL (Nuclear Distribution Element-Like) (Feng et al., 2000; Sasaki et al., 2000). Lis1 is also the regulatory subunit, along with two alpha catalytic subunits, of the

trimeric platelet activating factor acetylhydrolase 1b (Pafah1b) complex (Sweeney et al., 2000). Coming full circle, the alpha subunits of the Pafah1b complex have been recently found to also selectively interact with the Vldlr cytoplasmic tail (Zhang et al., 2007). This link between Lis1 and the Reelin signaling pathway, through the interaction between Vldlr and the Pafah1b complex, will be discussed in depth in the second chapter.

In mice, the deletion of any of the three main functional parts of the Reelin signaling pathway, Reelin, Dab1 or both Vldlr and Apoer2, results in identical *reeler* phenotypes (D'Arcangelo et al., 1995; Falconer, 1951; Frykman et al., 1995; Howell et al., 1997; Trommsdorff et al., 1999). *Reeler* animals are smaller than wild-type (WT), suffer from muscle atrophy, are ataxic with a reeling gait, and morphologically show a completely disorganized cortex with virtually no cerebellum. The mice generally live only to about 3 weeks of age. Because the animals have such severe phenotypes and only live a short time, it is more challenging to discern the role that Reelin signaling plays in adulthood. However, even though both receptors (Vldlr and Apoer2) need to be knocked out in order recapitulate the *reeler* phenotype, Reelin signaling and receptor function has been studied through single receptor KOs. Fortunately, the single receptor null animals still have phenotypes, although they are much more subtle than the double knockouts. Using the single receptor knockout mice we can at least gain some insight into their function during adulthood as well as the role they may play in Reelin signaling.

The Vldlr KO mice have disrupted organization of Purkinje cells in the cerebellum along with missing folia (Trommsdorff et al., 1999). The Apoer2 KO mice have a less severe cerebellar phenotype with only some disruption in foliation. The cortex and hippocampus of both single knockouts are generally intact with only minor

neuronal dispersion in the dentate gyrus and CA1 regions of the hippocampus. Neither KO mouse line seems to have any motor coordination or locomotor defects reminiscent of the *reeler* mouse, but they have been found to display deficits in associative learning as assessed through associative-fear conditioning tasks (Weeber et al., 2002). Vldlr KO mice also have a slight defect in the initial induction of long term potentiation (Weeber et al., 2002). Apoer2 KO mice, have a more severe LTP phenotype because their potentiation decays almost to baseline in the span of 60 minutes. Taken together, the results of the fear conditioning tasks and the LTP data suggest that both receptors, and in turn Reelin, may play a role in the formation and storage of memories.

Reelin does indeed play a role in the stimulation of long term potentiation. Wild-type brain slices treated with recombinant Reelin show almost a 50% increase in LTP induction over untreated slices (Weeber et al., 2002). Reelin is unable to show this same increase in potentiation in either of the two single receptor knockout mouse lines, confirming that Reelin can affect synaptic function by interacting with both Vldlr and Apoer2 (Weeber et al., 2002).

The phenotypes of mice expressing mutations or deletions of Reelin signaling pathway components are well documented (Sheldon et al., 1997; Trommsdorff et al., 1999; Weeber et al., 2002). The molecular mechanism of Reelin signal transduction across the plasma membrane, along with many downstream signaling pathways, has also been explored in great detail (Herz and Chen, 2006). However, the way in which Reelin guides neurons to their correct places in the developing brain still remains a mystery (Ogawa et al., 1995). Initially, two very simple hypotheses were proposed to explain the mechanism of how Reelin regulates neuronal migration in the cortex. First, it may act as

an attractant to guide the neurons, or the alternative, Reelin may give a "Stop" signal to migrating cells (Rice and Curran, 2001). The "Stop" signal hypothesis was supported by the observation that Reelin knockouts, which lack this "Stop" signal, show many neurons intermixed with the Cajal-Retzius cells in layer I of the cortex (Derer, 1985; Trommsdorff et al., 1999). Generally, migrating neurons do not invaded layer I, a neuron free layer save for the Reelin expressing Cajal-Retzius cells during development (Marin-Padilla, 1998; Meyer and Goffinet, 1998). Thus, Reelin could be stopping the neurons just underneath the marginal zone in the cortical plate. When Reelin is absent the neurons do not get the "Stop" signal and continue to migrate into the marginal zone.

Normal cortical lamination occurs in an inside-out fashion. Neurons are born in the ventricular zone and migrate past older neurons out towards the pial surface guided by radial glial cells (Figure 1.3) (Angevine and Sidman, 1961; Bielas et al., 2004). More specifically, at around embryonic day 13 (E13), the preplate (pp) is invaded by the first wave of newborn neurons which splits it into the marginal zone (mz) and the subplate (sp) (Figure 1.4). The marginal zone is the location of the Reelin expressing Cajal-Retzius cells that eventually will become layer I in the adult brain. These new neurons, along with subsequent waves of newborn neurons migrating past older generations, form the cortical plate (cp) consisting of cortical layers II-VI. By tracing the birth date and final location of new neurons in the developing *reeler* mutants, it has been established that the layering of the cortex is generally inverted in these mutants. The disruption of normal cortical lamination in the *reeler* mice begins as the first wave of neurons are

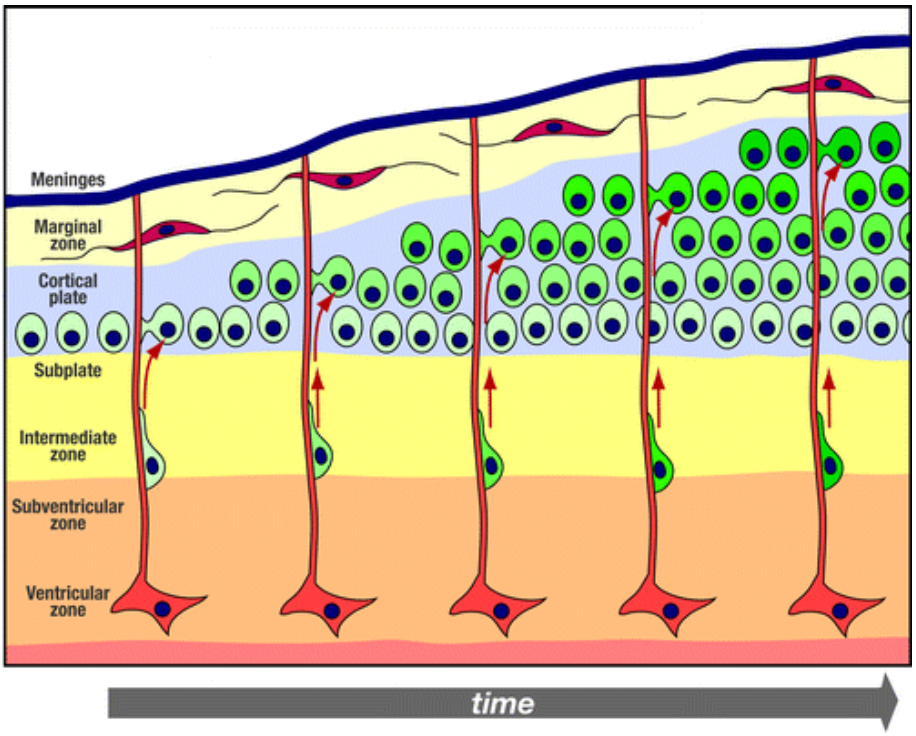

Figure 1.3: Cortical Neuronal Migration. During inside-out cortical development, young neurons (darker green) are born in the ventricular zone, migrate past older neurons (light green) along the processes of radial glial cells (red), to take their position just beneath the marginal zone in the cortical plate. (Bielas et al., 2004)

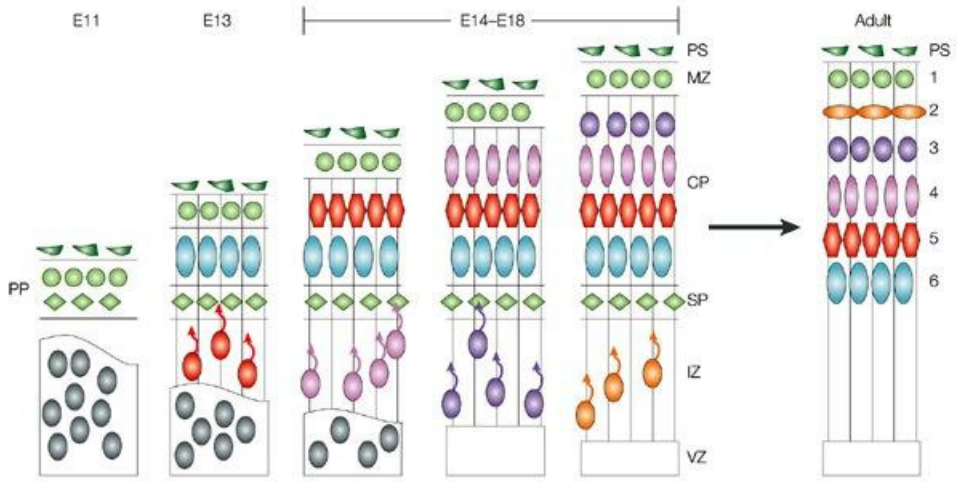

Figure 1.4: Cortical Lamination. At day E13 the first wave of newborn neurons migrates into the preplate (pp) and splits it into the marginal zone (mz) and the subplate (sp). Subsequent generations of neurons follow this same path and migrate past their predecessors until they reach the Cajal-Retzius cells in the marginal zone, thus, creating the inner layers (II-VI) in an inside-out manner. (Gupta et al., 2002)

unable to make their way into the preplate to split it into the marginal zone and subplate (Ogawa et al., 1995; Sheppard and Pearlman, 1997). Instead, they form a disorganized cortical plate as the newborn neurons are unable to migrate past older neurons and the result is an inverted cortex (Caviness and Sidman, 1973). These observations contradict the "Stop" signal hypothesis because the new neurons never even make it past older generations as would be expected if the migrating cells were simply missing an inhibitory signal.

Other hypotheses have included a role for Reelin signaling in neuron/radial glia interaction because some migrating neurons in *reeler* mice are unable to detach from the glial processes as they ascend into the cortical plate (Pinto-Lord et al., 1982). It has also been suggested that Reelin plays a role in neuron/neuron interactions, as early born

neurons from *reeler* animals aggregate more readily *in vitro* and may actually form a barrier preventing new neurons from getting past them (Hoffarth et al., 1995). Another hypothesis involves Reelin acting on the existing subplate neurons, instead of newborn migrating neurons. If the function of Reelin was to push away the subplate neurons, extra room would be created for newborn neurons to migrate into the cortical plate (D'Arcangelo and Curran, 1998).

One of the most recent hypotheses, from the laboratory of J.A. Cooper (Cooper, 2008), proposes a "detach and go" model for Reelin involvement in neuronal migration. This model proposes that Reelin affects the initial phase of glial cell dependent neuronal migration involving the splitting of the preplate and localization of layer VI neurons. This is supported by data from Magdaleno et al. showing that addition of exogenous Reelin rescues the preplate splitting and normal localization of layer VI neurons, but not the inside-out lamination of the other layers of the cortex (Magdaleno et al., 2002). Cooper suggests that as neurons migrate, they extend long processes ahead of the cell soma. Once the process reaches the marginal zone rich in Reelin, the Reelin signal is activated within the process, telling the neuron to detach from the radial glial cell. The soma of the neuron then continues to migrate up towards the tip of its process independent of glial cell assistance, a phenomena called somal translocation. The soma moves past older neurons until it catches up with its process and reaches the top most layer of the cortex just beneath the Cajal-Retzius cells. This is a valid and highly probable hypothesis that takes into account approximately three decades of Reelin signaling and neuronal migration research. As convincing as this model may be, we still have many more questions to answer before we can be certain of the role that Reelin

plays in the organization and function of the most complex organ in the body, the brain, both in the healthy and diseased states.

Reelin signaling and disease

Reelin signaling has been linked to various neuropsychiatric diseases such as autism, schizophrenia, bipolar disorder, and major depression (Fatemi, 2005). Many studies have confirmed that patients suffering from these disorders have decreased Reelin mRNA and protein levels in the cerebellum, hippocampus, and frontal cortices (Guidotti et al., 2000; Impagnatiello et al., 1998).

In schizophrenia, the direct role that Reelin plays remains unclear. However, hypermethylation of the Reelin promoter may be involved in decreasing Reelin expression levels (Costa et al., 2003b). Increased expression of a DNA methyltransferase in GABAergic neurons of the prefrontal cortex in schizophrenia patients supports this hypothesis (Costa et al., 2003a). Schizophrenia patients also have impaired sensorimotor gating as determined by defects in prepulse inhibition (PPI), a phenomenon frequently explored in both human patients and mouse models of the disease. Apoer2 and Vldlr null mice also show abnormal PPI, indicating that the Reelin receptors may indeed play an important role in schizophrenia (Barr et al., 2007).

In autism, not only is Reelin expression altered, so is the expression of Dab1 and Vldlr. In a study by Fatemi et al., Dab1 expression was decreased, whereas Vldlr expression was increased in the superior frontal and cerebellar cortices of autistic patients examined post mortem (Fatemi et al., 2005). In support of the studies showing decreased Reelin expression in autism patients, many reports indicate a genetic link between autism

and Reelin. A few Reelin polymorphisms are suggested to be linked to autism in select human populations (Persico et al., 2001; Zhang et al., 2002). However, there have also been studies that have been unable to link any polymorphisms or other Reelin mutations to autism (Fatemi, 2005).

Reelin signaling has also been implicated in the pathogenesis of neurodegenerative diseases such as frontotemporal dementia (FTD) and Alzheimer's disease (Fatemi, 2005). Frontotemporal dementia is caused by neuronal degeneration and atrophy of the frontal and temporal lobes of the cortex. Patients suffering from FTD as well as AD have increased Reelin protein in the cerebrospinal fluid (CSF) (Saez-Valero et al., 2003).

AD is one of the most prominent neurodegenerative diseases in the current human population, affecting 5.3 million American's in 2009 (www.alz.org). Alzheimer's disease was first described by the German psychiatrist Alois Alzheimer in 1906. Although the disease can only be confirmed postmortem, patients diagnosed with AD suffer from symptoms such as memory loss, confusion, and mood-swings that eventually lead to severe cognitive decline and loss of bodily functions. The cause of the disease has been under investigation for many decades with no single prevailing hypothesis. However, two pathological hallmarks of AD have been identified: extracellular amyloid beta (Aβ) plaques and intracellular neurofibrillary Tau tangles. The Aβ plaques form when the amyloid precursor protein (APP) is proteolytically processed by two different proteases, β-secretase and γ-secretase, to yield the amyloidogenic Aβ peptide which aggregates to form plaques (Zheng and Koo, 2006). However, recent findings show that Aβ dimers and not the plaques, function in memory impairment and cognitive decline

(Shankar et al., 2008). Tau neurofibrillary tangles, the other pathological hallmark of AD, form when the microtubule associated Tau protein is hyperphosphorylated, promoting aggregation and intraneuronal tangle formation (Brion et al., 1993).

Reelin receptors, Apoer2 and Vldlr, have been linked to Alzheimer's disease in three different ways. First of all, the receptors bind the only known risk factor for late-onset AD. Unlike early-onset AD (before the age of 65), which is sometimes linked to mutations in the APP gene itself or presenilins which encode subunits of the γ-secretase involved in APP proteolytic processing, late-onset AD (after the age of 65) is associated with a single genetic risk factor, the Apolipoprotein E (ApoE) (Roses et al., 1995). Human ApoE is present in three different isoforms – ApoE2, ApoE3, and ApoE4 – of which E3 is the most common (Singh et al., 2006). The isoforms differ only in amino acid positions 112 and 158. Even with such minute differences between isoforms, the expression of the ApoE4 isoform in various ethnic backgrounds is an increased risk factor for the development of Alzheimer's disease. However, not all humans expressing ApoE4 develop AD, and only 40-65% of AD patients express at least one allele of E4.

The second and third links between the Reelin signaling pathway and AD involve both pathological hallmarks of AD: Aβ plaques and hyperphosphorylated Tau neurofibrillary tangles. Data from Fuentealba et al. concluded that Apoer2 directly interacts with APP, increasing its expression at the cell surface and enhancing Aβ formation (Fuentealba et al., 2007). This is attributed to the guidance of APP, by Apoer2, into lipid rafts, enriched in β-secretase (Cordy et al., 2003). Thus, Apoer2 promotes the production of the Aβ peptide over the non-amyloidogenic peptide p3 which is initially cleaved by α-secretase, a protease selectively excluded from lipid rafts.

Reelin signaling has the ability to regulate Tau phosphorylation. The signaling pathway promotes PI3K and PKB activation through Dab1 phosphorylation. Activated PKB subsequently inhibits GSK-3β which normally functions in Tau phosphorylation (Utton et al., 1997). Vldlr and Apoer2 KO mice show increased Tau phosphorylation in the brain, supporting the role of Reelin signaling in the regulation of Tau protein hyperphosphorylation and potential involvement in AD pathogenesis (Hiesberger et al., 1999).

All of this evidence points towards a significant involvement of Reelin signaling in a diverse array of neurological diseases and thus, it is imperative that we keep exploring the molecular mechanisms involved in the Reelin signaling pathway in order to better understand its role in the pathogenesis of disease. As such, my thesis focuses on the exploration of the regulation and function of the two Reelin receptors, Apoer2 and Vldlr, in the central nervous system as wells as an extension into the reproductive system.

CHAPTER TWO

THE INTERACTION BETWEEN VLDLR AND THE PAFAH1B COMPLEX AND ITS ROLE IN NEURONAL MIGRATION AND SYNAPTIC FUNCTION

Introduction

Vldlr and Apoer2 are both involved in Reelin signaling and compensate for each other when either receptor is missing. This compensation is apparent as neither of the single knockout mouse lines recapitulates the *reeler* phenotype. However, the single knockout animals do have more subtle neuronal migration defects along with deficits in learning and memory (Trommsdorff et al., 1999; Weeber et al., 2002). The appearance of independent phenotypes in these mutant animals supports the hypothesis that although Vldlr and Apoer2 share common domains and sequence similarity, there have to be domains or sequences with unique functions in each of the receptors. In Apoer2, a prime example of such a domain is the alternatively spliced exon 19 expressing part of the cytoplasmic tail of the receptor. The amino acid sequence encoded by this exon is absent in all other LDL receptor family members, including Vldlr. This domain is responsible for regulating the increase in NMDA receptor dependent LTP after Reelin stimulation and will be explored in greater depth in Chapter 3.

For many years, no unique functional domains had been identified in the VLDL receptor. However, clinical observations that loss of function mutations in either *RELN* or *LIS1* result in lissencephaly, suggested that perhaps the functions of Reelin and Lis1 merge somewhere in the various branches of signaling that regulate neuronal migration (Hong et al., 2000; Reiner et al., 1993). Clark et al. were interested to see whether this

hypothesis was true, and if Lis1 might somehow fit into the Reelin signaling schematic. They looked for genetic interactions between Reelin signaling components and Lis1 mutant mice. Lis1 homozygous KO animals are embryonic lethal so breeding was limited to Lis1 heterozygotes. Lis1 +/- mice were crossed to other mouse lines null for various proteins involved in the Reelin signaling pathway, and prevalence of progressive hydrocephalus was observed (Assadi et al., 2003; Hirotsune et al., 1998). Hydrocephalus is a disorder which is characterized by an abnormal accumulation of cerebrospinal fluid in the brain leading to increased intracranial pressure causing convulsions and mental retardation. In the Lis1 mutant mice, the progressive hydrocephalus results from defective ependymal lining which causes blockage of the ventricular system (Assadi et al., 2003). Mice suffering from hydrocephalus have an enlarged, dome-like shaped skull, an easily identifiable external phenotype. Lis1 heterozygotes have a 5-7% occurrence of progressive hydrocephalus. If Lis1 heterozygotes are crossed to Vldlr heterozygous or Vldlr KO mice, the incidence of hydrocephalus increases to 60% and 70%, respectively. On the other hand, Lis1 hets crossed to Apoer2 mutants results only in a 10% incidence in Lis1+/-;Apoer2+/- mice and 40% in Lis1+/-;Apoer2-/- animals. This is not nearly as drastic of an increase as that seen in crosses with Vldlr mutants, substantiating the suggestion that Vldlr embodies unique function in its ability to genetically interact with Lis1 and affect brain development.

Lis1 is also a subunit of the PAF (platelet-activating factor) acetylhydrolase 1b (PAF-AH) 1b enzyme, which is a member of the phospholipase A_2 superfamily (Six and Dennis, 2000). PAF-AH is involved in the inactivation/hydrolysis of the platelet-activating factor (PAF), a potent phospholipid mediator of inflammation (Prescott et al.,

2000). Currently, there are three identified isoforms of PAF-AH: one plasma and two intracellular forms. The Pafah1b complex is one of the intracellular isoforms and is expressed mainly in the brain. Pafah1b is unique compared to the other two isoforms as it resembles a G-protein like complex which is made up of two alpha catalytic subunits, Pafah1b2 and Pafah1b3, and a beta regulatory subunit, Lis1 (Pafah1b1) (Arai, 2002; Hattori et al., 1994b). Pafah1b function in the brain is still unclear, although there is some data suggesting involvement of PAF and the Pafah1b complex itself, in brain development and neuronal migration (Albrecht et al., 1996; Hattori et al., 1994a). In addition, PAF or PAF derivatives may be involved in the regulation of presynaptic neurotransmitter release during induction of hippocampal LTP (Kato et al., 1994).

Although little is know about the CNS function of the Pafah1b complex as a whole, protein interaction studies have revealed that the β regulatory subunit, Lis1, binds to phospho-Dab1 (Assadi et al., 2003). Also, recent data suggest that the alpha subunit Pafah1b2, has the ability to bind Disabled independent of the adaptor protein's phosphorylation state (Zhang et al., 2009). Most interestingly, Zhang and colleagues were able to support the hypothesis, that Vldlr does contain unique functional domains, by biochemically confirming that Vldlr binds to the alpha subunits of the Pafah1b complex *in vitro*. They were able to conclude that there is a single amino acid difference between the cytoplasmic tails of Apoer2 and Vldlr that allows Vldlr, but not Apoer2, to bind to the alpha catalytic subunits of the complex (Zhang et al., 2007). This single amino acid is the lysine immediately following the NPxY motif in the cytoplasmic tail of Vldlr. Although Apoer2 shares some sequence homology with Vldlr in the cytoplasmic tail, at this particular amino acid position it expresses an arginine instead of the lysine. It

is because of this small difference that Apoer2 is unable to bind Pafah1b2 or Pafah1b3 *in vitro*.

This single amino acid difference, conferring novel abilities to the Vldlr, is the first example of a functional region within Vldlr that confers unique capability to the receptor. The significance of this specific interaction *in vivo* is not yet known, however its exploration has the potential to yield new insights into the role of Vldlr in neuronal migration and synaptic function. It has been postulated that by binding to Vldlr, the alpha subunits may act as scaffolding proteins, bringing Lis1 into closer proximity to phospho-Dab1 (Zhang et al., 2007). Lis1 and Dab1 are both involved in regulating neuronal migration during development (Feng et al., 2000; Sheldon et al., 1997). This unique interaction brings Lis1 even deeper into the Reelin signaling pathway and adds a new branch to the multifaceted pathway and its role in the organization of the developing brain. Finally, it is possible that loss of the interaction between Vldlr and the Pafah1b complex may be the explanation for the morphological or electrophysiological phenotypes seen in the Vldlr KO animals. If loss of the interaction between Vldlr and the Pafah1b complex is responsible for the electrophysiological Vldlr KO phenotypes, it would be the first example of the Pafah1b complex and Reelin signaling playing a concerted role in synaptic function and not solely in neuronal migration.

Based on these data, I propose that the unique lysine in the cytoplasmic tail of Vldlr confers function to the receptor, independent of Apoer2. These functions include the modulation of neuronal migration, brain development, and perhaps synaptic function, all mediated through interaction with the Pafah1b complex and Lis1. To explore this hypothesis, it was vital to disrupt the interaction *in vivo*. Therefore, mouse models were

created that introduce a single amino acid substitution in the Vldlr tail so that it resembles the Apoer2 tail which is unable to bind the alpha subunits of the complex. Creation of these mouse models was attempted using two separate methods: ES cell homologous recombination and BAC genome integration. Each method presented separate hurdles; however, a usable model was finally achieved.

VLDLR L838R BAC TRANSGENIC MICE

Materials and Methods

BAC Selection and DNA Isolation – The www.ensembl.org website was used to search for BACs containing *Vldlr* with equal amounts of genomic sequences both up- and downstream of the gene. BAC PR24-210E24 contains *Vldlr* along with approximately 50-75 kb of genomic sequence up- and downstream of the gene. The PR24-210E24 BAC was ordered from www.bacpac.chori.org. DNA was isolated from 250 ml overnight cultures grown in Luria Broth (LB) media (supplemented with 20 μg/mL of chloramphenicol (Sigma)) using the Large-Construct DNA purification kit (Qiagen).

BAC Cassette Cloning:

Vldlr Sequence Cloning – The BAC *Vldlr* sequences containing intron 17 through the 3' untranslated region (UTR) after exon 19 were amplified via PCR from the BAC PR24-210E24 using the primers:

Exon18 and part of exon 19

IM274 (5'-CGAATTCTGGAACTGTTGTTAGTGTTAATTCC-3', EcoRI)

IM300 (5'-GGATCCAGCCAGATCATCATCTGTGCTTAC-3', BamHI)

Part of exon19 and the 3' UTR

IM303 (5'-GGATCCGTTCTGAACAAATCTTGGTCTATG-3', BamHI)

IM304 (5'-AGATCTGACTTCAGCACTGGCTCTGTTACC-3', BglII)

The two amplified *Vldlr* fragments were ligated into the multiple cloning site (MLS) of the pBluescript II KS(+) vector (pBSKS, Stratagene) using the EcoRI and BglII restriction sites.

EGFP Sequence Cloning – The EGFP sequence was amplified by PCR from the vector pUB385 containing EGFP using the primers: IM301 (5'-GGATCCATGGTGAGCA AGGGCGAGGAGCTG-3', BamHI) and IM302 (5'-GGATCCTTACTTGTACAGCT CGTCCATGCCG-3', BamHI). The amplified EGFP sequence was ligated into the pBSKS-Vldlr cassette digested with BamHI. This ligation deletes the natural *Vldlr* stop codon and replaces it with the EGFP sequence followed by a new stop codon.

floxed Tn5-neomycin Cloning – The Tn5-neo sequence was amplified from the PCR template contained in the Quick and Easy BAC Modification Kit (Gene Bridges) using the primers IM294 (5'-CATATG ACCGGTTGGACAGCAAGCGAACCGGAATTGC-3', NdeI, AgeI) and IM295 (5'-CATATG GGCCGGCCTCAGAAGAACTCGTCAA GAAGGCG-3', NdeI, FseI). The Tn5-neo fragment and the pBSKS-Vldlr-EGFP vector were digested with NdeI (an endogenous restriction site that exists within intron 18) and the Tn5-neo fragment was ligated into the pBSKS-Vldlr-EGFP plasmid. The loxP sequences were synthesized as complimentary oligonucleotides: 5' loxP, IM296 (5'-

AACGTAACCGGTATAACTTCGTATAGCATACATTATACGAAGTTATACC-3', AgeI), IM297 (5'-TATTAAACCGGTATAACTTCGTATAATGTATGCTATACGAA GTTATACC-3', AgeI) and 3' loxP IM298 (5'-TACGAAGGCCGGCCATAACT TCGTATAGCATACATTATACGAAGTTATG-3', FseI), IM299 (5'-ATAAGC GGCCGGCCATAACTTCGTATAATGTATGCTATACGAAGTTATG-3', FseI). 55 µg of each primer were combined and the ends were filled in using Taq polymerase. The double stranded fragments were digested with their respective restriction enzymes and ligated into the pBSKS-*Vldlr*-EGFP plasmid to complete the pBSKS- Vldlr-floxed Tn5-neo-EGFP cassette plasmid.

Cassette mutagenesis – For the mutant L838R VLDLR BAC, the cassette was mutated from TT to AG at the amino acid position 838 such that the amino acid is changed from a leucine to an arginine. The mutation was performed using the QuickChange Site-Directed Mutagenesis Kit (Stratagene). The mutagenesis primers used were IM222 (5'-CTTTGACAATCCTGTGTACAGGAAGACCACTGAAGAGGAC-3') and IM223 (5'-GTCCTCTTCAGTGGTCTTCCTGTACACAGGATTGTCAAAG-3').

BAC Recombination – The BAC cassette was linearized by digesting it from the pBSKS backbone using the restriction enzyme EcoRI. The 1647 bp band containing the cassette is purified from an agarose gel using phenol/chloroform extraction. The purified cassette and BAC PR24-210E24 are used with the Quick and Easy BAC Modification Kit; By Red/ET Recombination (Stratagene) to achieve a BAC expressing the WT or L838R

mutant version of *Vldlr* containing a neomycin/kanamycin resistance gene and fused to EGFP.

BAC Recombination Verification – After homologous recombination, the resultant bacterial colonies were cultured and DNA was prepared using the QIAprep Spin Miniprep Kit (Qiagen). The BACs were verified for the presence of the neomycin selectable marker by PCR using the primers IM275 (5'-CGAATTCTCTATCCACAA TTCTCATGTGTCC-3') and IM315 (5'-GGAACTGTTGTTAGTGTTAATTCCCA TAG-3'). The BACs were verified for the presence of the EGFP sequence by PCR using the primers IM312 (5'-GATCTGACTTCAGCGCTGGCTCTGTTACC-3') and IM313 (5'-CCGTAGAGTAACCGCCAAGCTCACCTGA-3'). The BACs were screened for proper recombination by restriction digest using the FspI restriction enzyme. A 7,164 bp band is seen in homologously recombined BACs but absent in the unmodified PR24-210E24 BAC.

BAEC BAC Transfection – Bovine aortic endothelial cells were grown on coverslips in 6 well dishes at a density of 75,000 cells per well in high glucose (4500 mg) DMEM media (Cellgro) supplemented with 15% FCS, 2 mM L-glutamine, 1x MEM Non-essential amino acids (Cellgro), 1 mM sodium pyruvate (Cellgro), and 1.8% HEPES. Cells were transfected with either the WT or L838R mutant Vldlr BACs using the Lipofectamine (Invitrogen) Transfection Reagent after seven days in culture. Coverslips were washed three times in PBS before mounting them on slides using ProLong Gold with DAPI

mounting medium (Invitrogen). Pictures were taken with a Zeiss Axioplan 2 fluorescence microscope.

BAC Blastocyst Injection – In collaboration with Dr. Robert Hammer (UTSW Department of Biochemistry) circular WT and L838R mutant BACs were injected into SJL mouse blastocysts.

Animals – All BAC mice (SJL/SV129/BL6 hybrids) were housed under a 12 h: 12 h light dark cycle and fed a normal chow diet. All animals were euthanized via inhalation of isoflurane according to the National Institutes of Health's Guide for the Care and Use of Laboratory Animals and the UT Southwestern Animal Care and Use Committee.

BAC mouse DNA sequencing – Tails from BAC expressing animals were cut and digested with DirectPCR tail reagent (Viagen Biotech) and 0.5 mg/ml Proteinase K at 55ºC overnight. A part of exon 18 was amplified by PCR using the primers IM314 (5'-AATGCTTATTAACTGACTGCTCTCATGG- 3') and IM315. The PCR product was purified using the QIAquick PCR purification kit (Qiagen) and sent for sequencing (UTSW McDermott Center Core) using the primer IM315.

Simple Repeat Screening for Vldlr Genotyping – The www.ensembl.org website was used to find microsatellite marker repeats close to the *Vldlr* genomic sequence. Primers were designed around four different simple repeats: #1 D19Mit30 marker, #2 (TG)n at position Chr19:27,197,984, #3 (TG)n at position Chr19:27,384,809, and #4(TCC)n at position

Chr19:27,184,133. All genomic locations are from the *mus musculus* version 43.36d, NCBIM36, strain C57BL/6J sequence. PCR products were run on a 5% agarose gel (1/3 standard melting temperature agarose, 2/3 low melting temperature agarose). Tails were cut and digested as described previously. DNA isolated from the tails was used in the PCR reactions using the following primers:

#1	D19Mit30 fwd (5'-GGTGGCTTAGAAATAGTATCGAAA-3')
	D19Mit30 rev (5'-CCAGCTCTAGGCAGGCATAT-3')
#2	IM362 (5'-TTCAGAATATAAATGTGTTCAGAAACC-3')
	IM363 (5'-CACCAAGGAAGTTGTTATCAAGAAG-3')
#3	IM364 (5'-AGCTCCTTTCTCTGTGATAACTCC-3')
	IM365 (5'-AAAGATCCAGATCAATGGTAGAATG-3')
#4	IM366 (5'-GTTCCTCATTCTCTGCCATATTTC-3')
	IM367 (5'-TCTGTCCTAGACTTTGGAAGAACAG-3')

BAC Mouse Genotyping – DNA was prepared as before with the DirectPCR tail reagent and Proteinase K digestion. PCR genotyping from tail DNA, for confirmation of BAC containing genomes, utilized primers IM312 and IM313, which are located in the Vldlr gene locus on either side of the EGFP sequence. The WT band without EGFP is 165bps and the BAC positive band with EGFP is 896bps. PCR genotyping for endogenous *Vldlr* utilized the primers IM362 from the second simple repeat PCR and were run on a 5% agarose gel.

Generation of Vldlr mid-tail antibody – The peptide NH_2-CTEEDLSIDIGRHSASVG HTY-COOH (underlined portion located within the cytoplasmic tail of Vldlr) was produced by UTSouthwestern Peptide Chemistry Lab. This particular peptide sequence was selected in an attempt to prevent cross-reactivity with other receptors in the LDL receptor family as it was the most unique region within the tail. The peptide was conjugated to Imject Maleimide Activated KLH (Pierce) and rabbits were given an initial immunization of 500 µg of conjugated peptide followed by 250 µg boosts every two weeks. Serum was collected every two weeks to check for antibody specificity via western blotting.

Membrane Fraction Preparation – Selected tissue was homogenized using a polytron tissue grinder in 1 ml of Buffer I (20 mM Tris-HCl, pH 8.0, 120 mM NaCl, 1 mM $CaCl_2$, EDTA-free protease inhibitor cocktail (Complete, mini, protease Inhibitor Cocktail Tablets, Roche)) per mg of tissue. Homogenate was spun down at 800 rpm (rotor JS-5.2, Beckman J-6B centrifuge) for 5 minutes at 4ºC. Supernatant was spun again for 10 minutes at 10,000 x g, 4ºC. The supernatant of the intermediate spin was spun in an ultracentrifuge (TLA110 rotor, Beckman Optima TLX ultracentrifuge) at 55,000 rpm for 30 minutes at 4ºC. The resulting pellet was resuspended in Buffer II (50 mM Tris-HCl, pH 8.0, 80 mM NaCl, 2 mM $CaCl_2$, 1% Triton X-100, 0.1% SDS, EDTA-free protease inhibitor cocktail) and homogenized by forcing the suspension 15-20 times through a 23 gauge needle. The homogenate was solubilized on ice for 10 minutes and spun again at 55,000 rpm for 30 minutes at 4ºC. The supernatant after the last high speed spin contained the membrane enriched fraction.

Western blotting for Vldlr-GFP expression – Brain membrane fractions from each founder line were prepared. Protein concentration was measured using the Lowry assay (D_C Protein Assay, Bio-Rad) and 40 μg of protein were loaded on an 8% SDS-PAGE gel. Proteins were transferred to a nitrocellulose membrane, blocked in LI-COR blocking buffer for one hour at 4ºC, and probed with a polyclonal anti-GFP antibody (rb, 1:5000) or the 431 Vldlr-midtail antibody (rb, 1:500), overnight (4ºC) in LI-COR blocking buffer supplemented with 0.2% Tween-20. The anti-GFP polyclonal antibody was a generous gift from Dr. Joachim Seeman (Department of Cell Biology, UTSouthwestern). Membranes were washed 4 times, 5 minutes each, with PBST. Infrared Dye labeled secondary antibody (gt anti-mouse IRDye 800CW or gt anti-rabbit IRDye 680CW, LI-COR) was diluted 1:10,000 in LI-COR blocking buffer supplemented with 0.2% Tween20 and 0.01% SDS. Membranes were incubated in secondary antibody solution for 1 hour at room temperature. Membranes were washed 4 times, 5 minutes each, in PBST, rinsed once in PBS and scanned and quantitated using the LI-COR Odyssey infrared imaging system.

Immunohistochemistry – Mice were perfused first with 1xPBS followed by 4% paraformaldehyde/PBS. Brains were removed and postfixed in 4% paraformaldehyde at room temperature for 45 minutes. Brains were rinsed in 1xPBS and cryoprotected in 25% sucrose dissolved in PBS overnight at room temperature. The tissue was imbedded in OCT medium (Tissue-Tek, Sakura) and frozen on a block of dry ice. Coronal brain sections (10 μm) were sliced using a cryostat (Leica CM1900) and mounted onto slides

(Fisherbrand Superfrost/Plus, Fisher Scientific). Slides were kept frozen at -20ºC until processed. Frozen sections were allowed to thaw, rinsed in 1xPBS and permeabilized in methanol at -20ºC for 10 minutes. Slides were washed 3 times in PBS and blocked for 1 hour on ice in blocking buffer (10% serum, 0.1% BSA in PBS). Slices were incubated overnight in a 4ºC humid chamber with the polyclonal anti-GFP antibody diluted (rb, 1:100) in blocking buffer. Slides were washed 4 times, 10 minutes each, with PBS and incubated with the Alexa Fluor 488 goat anti-rabbit fluorescently labeled secondary antibody (Invitrogen, 1:200 in blocking buffer) for one hour at room temperature in a humid chamber. Slides were washed again 4 times, 10 minutes each, in 1x PBS. Coverslips were mounted using ProLong Gold with DAPI mounting medium (Invitrogen). Pictures were taken with a Zeiss Axioplan 2 fluorescence microscope.

Hematoxylin and eosin Staining – Mice were perfused as described previously. Brains were removed and postfixed in 4% paraformaldehyde overnight at 4 ºC. The tissue was transferred to 70% ethanol and submitted to the Pathology Department (UT Southwestern) for paraffin embedding, slicing, and H&E staining. Bright field pictures were taken using a Nikon eclipse E1000M microscope at 2x and 10x magnifications.

Hippocampal slice preparation and NMDA receptor dependent LTP recordings – Established protocols for slice preparation and electrophysiological recordings were used from Weeber et al., 2002. Two to three month old animals were deeply anesthetized and euthanized by cervical dislocation. The brain was quickly removed and immersed in an ice-slush of oxygenated (95% O_2, 5% CO_2) sucrose cutting solution (110 mM sucrose, 60

mM NaCl, 3 mM KCl, 1.25 mM NaH_2PO_4, 28 mM $NaHCO_3$, 0.5 mM $CaCl_2$, 5 mM D-glucose, 0.6 mM ascorbic acid, 7 mM $MgCl_2$). Using a vibratome, 400μm transverse hippocampal slices were cut and allowed to recover at least one hour, at 30°C, in oxygenated artificial cerebrospinal fluid (ACSF: 124 mM NaCl, 3 mM KCl, 1.25 mM NaH_2PO_4, 26 mM $NaHCO_3$, 10 mM D-glucose, 2 mM $CaCl_2$, 1 mM $MgCl_2$). Slices were then transferred to an interface recording chamber and were kept at 31°C at an ACSF flow rate of 2-3 ml/min. In the Reelin treated conditions, slices were treated with purified Reelin (2μg/ml) for at least 30 minutes prior to theta burst stimulation and subsequently for the rest of the recording time. The slices were stimulated with platinum/iridium concentric bipolar electrodes (CBBRC75, FHC Inc.) using the theta-burst stimulation (TBS) method to evoke LTP. The TBS consists of a sequence of 4 100Hz pulses at 200 ms intervals repeated 10 times; repeated 5 times at 10 second intervals. Extracellular field recordings were measured (using a custom written program for Labview 7.0 by Dr. Jay Gibson) from the CA1 stratum radiatum using ACSF filled pulled glass microelectrodes. Input/output curves were first measured for each slice and 40-60% of the maximal stimulus intensity was used to stimulate the slices during the recording using an Isolated Pulse Stimulator (A-M Systems). The potentiation of the responses (slope fEPSP) after TBS was normalized to the pre-TBS baseline responses (slope fEPSP). LTP recordings were performed by both Irene Masiulis Bowen and Murat Durakoglugil, M.D., Ph.D. One-way ANOVA and Tukey's post hoc tests were used for statistical analyses.

Results

WT and L838R mutant Vldlr BAC construction

The sequences of the mouse Apoer2 and Vldlr cytoplasmic tails were compared and it was determined that in order to change the amino acid at position 838 from a leucine to an arginine, a two base pair substitution needed to be made. The Vldlr amino acid sequence N P V Y **L** is encoded by the DNA sequence "aat cct gtg tac **ttg**". The Apoer2 amino acid sequence N P V Y **R** is encoded by the DNA sequence "aac cca gtg tac **agg**". The first two bases in the fifth codon of the DNA sequence would need to be mutated from "tt" to "ag" in order to simulate the Apoer2 sequence in the Vldlr tail.

One of the methods used to introduce the L838R Vldlr mutation into mice was the generation of BAC transgenic animals. The goal was to create mice which express the L838R Vldlr from the BAC and cross them to endogenous Vldlr KO mice so that the only Vldlr expressed would be that encoded by the BAC. The PR24-210E24 BAC was found to contain the entire *mus musculus Vldlr* genomic sequence which is about 32 kilobases in length. The BAC was large enough to also contain 50-75 kb of endogenous genomic sequence on either side of Vldlr, which should encode any regulatory and promoter regions necessary for normal expression of the gene. A DNA cassette was cloned and used to introduce the L838R mutation, neomycin selection marker, and EGFP sequence into the *Vldlr* coding region via homologous recombination (Figure 2.1).

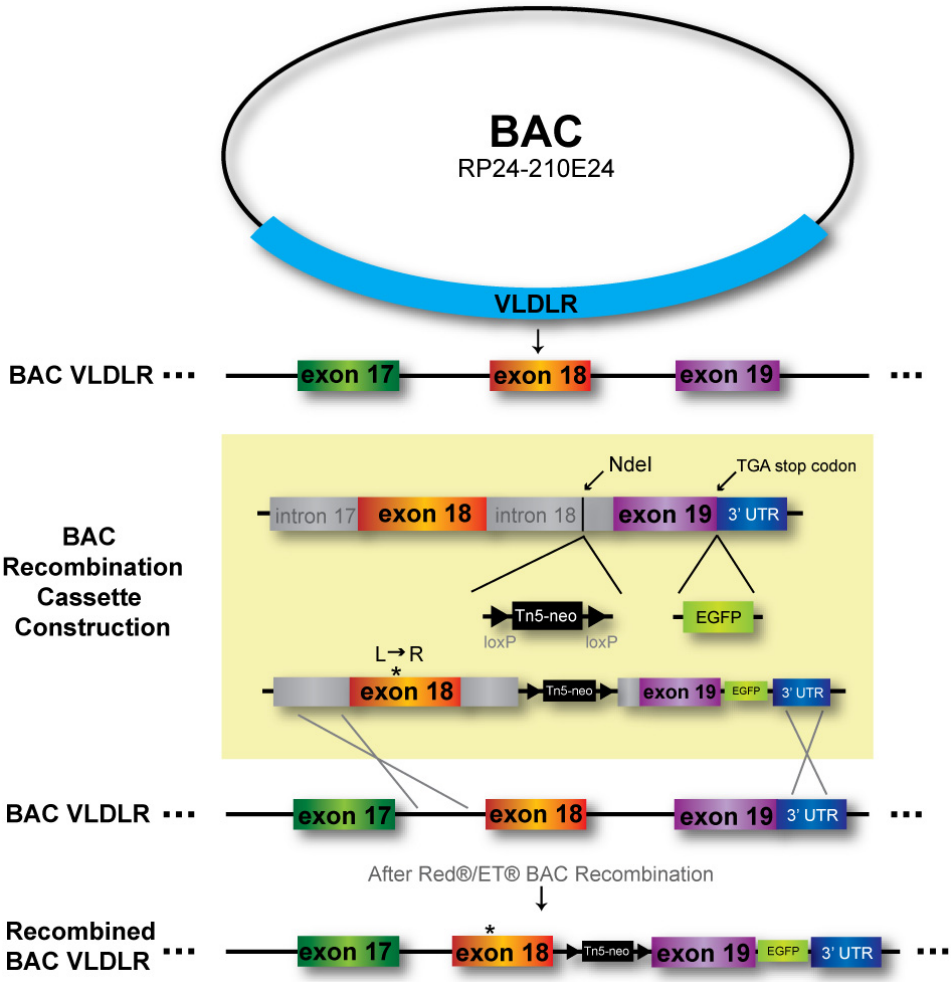

Figure 2.1: BAC Homologous Recombination Strategy. The BAC PR24-210E24 contains *Vldlr* along with sequences up- and downstream of the gene. A cassette encoding *Vldlr* exons 18, 19, surrounding intronic sequence and the 3' untranslated region (UTR) was cloned from the BAC into a Bluescript vector in two separate fragments. This cassette was modified by the addition of the Tn5-neo selection marker, flanked by loxP sites, into an endogenous NdeI restriction site in intron 18. The EGFP sequence was inserted using a BamHI site that was generated during the initial cloning of the two genomic fragments. The BamHI site replaced the endogenous STOP codon, thus allowing for the transcription of the EGFP sequence after the VLDLR gene. The cassette sequence was also mutated such that the amino acid following the NPVY motif within exon 18 was changed from a lysine to an arginine to mimic the ApoER2 protein sequence. After completion of the cassette, it was cut from the plasmid and used in

Red®/ET® BAC Recombination to achieve a BAC encoding the complete VLDLR sequence mutated to express an L → R mutation at residue 838, containing a neomycin resistance gene within intron 18 and linked c-terminally to EGFP. Two recombined BACs were generated, one with the L → R mutation and one without. [Not drawn to scale]

The BAC was designed so that the L838R Vldlr would express c-terminally fused EGFP to ease in the detection of the Vldlr expressed from the BAC. Two BACs were created, one encoding the original lysine at the 838 amino acid position and another encoding the arginine mutation at that same position. It was important to create the WT BAC mice as a control not only for the neomycin and EGFP, but also as a control for the expression of Vldlr from the BAC. The experimenter has no control over where the BAC integrates or how it functions once it is incorporated into the mouse genome. I first needed to show that expression of Vldlr from the BAC is comparable to endogenous Vldlr expression and when the BAC Vldlr mice are crossed to endogenous Vldlr KOs, expression of Vldlr from the BAC can rescue the Vldlr KO phenotypes. Once this is achieved, the WT BAC animals can serve as controls for the mice expressing the L838R Vldlr mutation.

BAC homologous recombination confirmation

BAC clones were verified for the presence of the neomycin resistance gene as well as the EGFP sequence by PCR (Figure 2.2A, B). It was also imperative to assess whether any unwanted secondary recombination events may have taken place during the cloning process that may affect normal expression of the Vldlr. BAC clones were

screened by restriction digests to confirm the expected recombination events (Figure 2.2C).

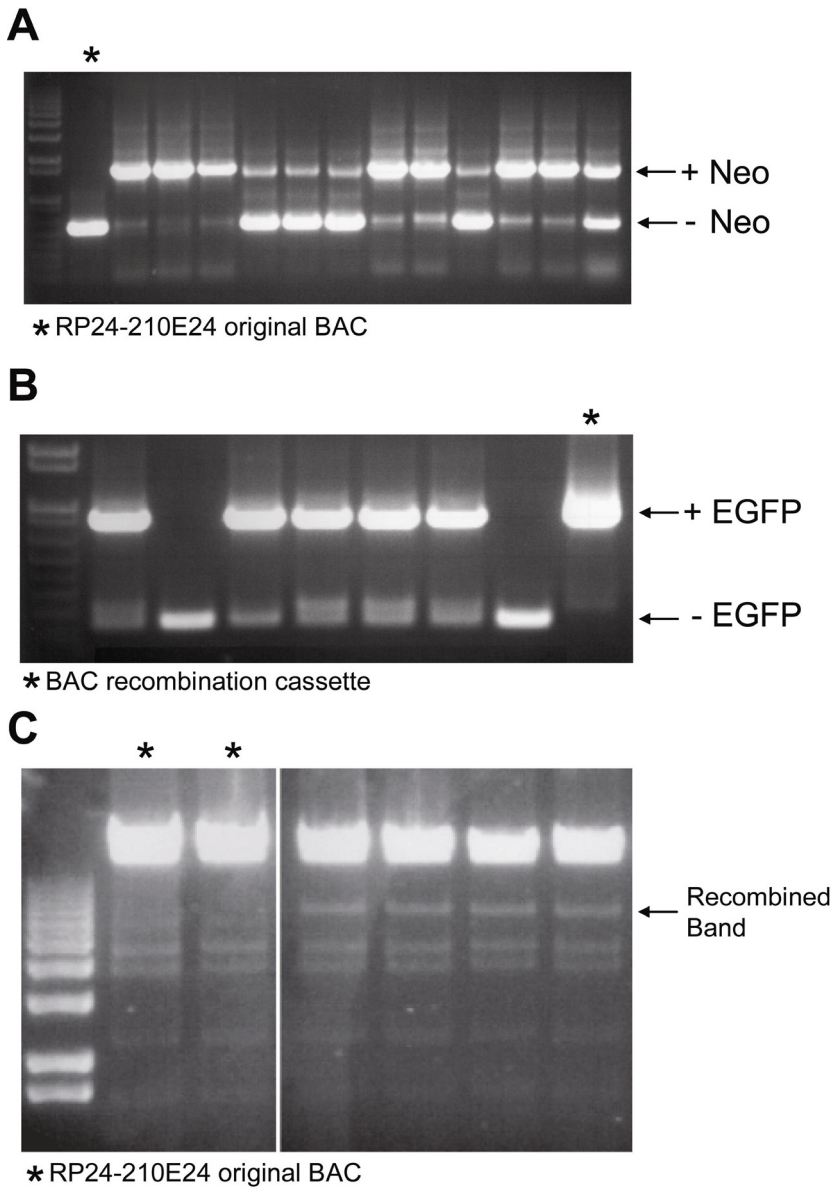

Figure 2.2: PCR and Restriction Digest BAC Confirmation. Resulting recombined BACs were analyzed by PCR to confirm the presence of the neomycin resistance gene (A), the presence of the EGFP gene (B), and finally, restriction digests were used to confirm that the selected BACs contained the expected recombination bands (C).

Confirmation of Vldlr-EGFP expression from mutated BACs

Before blastocyst injection of the BACs, Vldlr-EGFP fusion protein expression was confirmed by transfection of the BAC into bovine aortic endothelial cells (BAEC). BAEC were chosen because Vldlr is expressed in vascular endothelial cells. Expression of the BAC Vldlr, containing endogenous promoters and enhancers, may be improved in an endothelial cell line which normally expresses Vldlr as opposed to cells that do not express the protein. Indeed, both the WT and L838R Vldlr-BAC mutants were successfully transfected and expressed in about 10% of aortic endothelial cells as assessed by EGFP fluorescence (Figure 2.3).

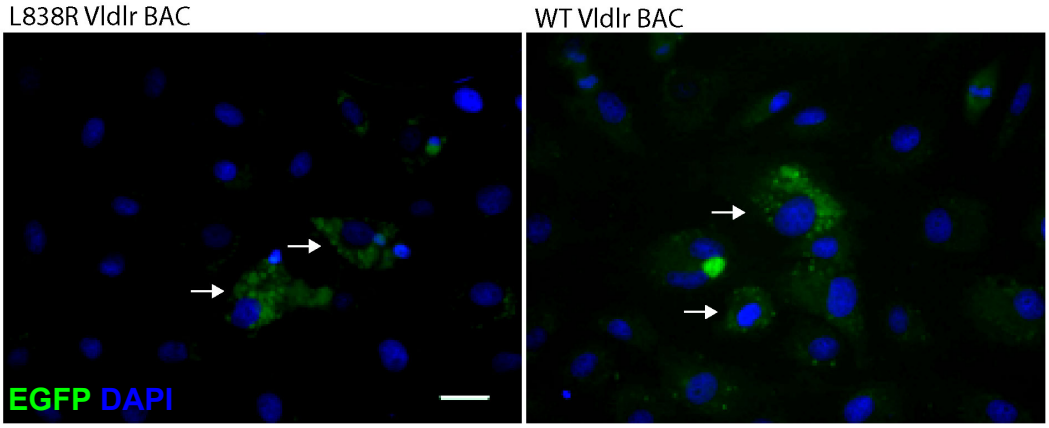

Figure 2.3: Expression of BAC-Vldlr-EGFP in endothelial cells. Bovine aortic endothelial cells were transfected with the Vldlr-EGFP BACs to confirm expression of the Vldlr-EGFP fusion protein via fluorescence of the GFP. Arrows show BAC transfected cells expressing the BAC Vldlr-EGFP protein. Scale bar = 20μM.

BAC transgenic mouse screening and genotyping

The verified WT and L838R Vldlr-BAC clones were injected into SJL mouse blastocysts. There were a total of 33 offspring from the WT BAC injection pregnancies and 21 from the L383R BAC mutant injections. All of these animals were screen by PCR for the presence of the EGFP coding sequence as this was one of the only unique sequences differentiating the BAC Vldlr from the endogenous Vldlr sequence. Six WT and five mutant BAC mice tested positive for the BAC EGFP sequence (Figure 2.4A). These were given founder line names based on the founder's identification number. Verifying the presence of the EGFP sequence confirms the presence of the BAC but it does not differentiate between the WT Vldlr BAC and the L838R Vldlr BAC. To validate that the correct founder lines contained the WT or L838R mutant Vldlr-BACs, the sequence in exon 18 surrounding the 838 amino acid codon position was amplified by PCR and sequenced. As expected, the WT-Vldlr-BAC animals encoded the lysine "TTG" codon and the L838R-Vldlr-BAC animals showed two peaks for the first two base pairs of the codon (Figure 2.4B). The mutant animals expressed the lysine "TTG" codon from the endogenous Vldlr locus as well as the mutant arginine codon "AGG" encoded in the L838R-Vldlr-BAC.

The founder animals had the potential not only to express Vldlr from the BAC but also from the endogenous *Vldlr* gene. To eliminate Vldlr expression from the endogenous locus so that Vldlr was solely expressed from the BAC, the BAC transgenic animals were crossed to Vldlr KO animals previously created and characterized in the lab (Frykman et al., 1995). Existing Vldlr KO mouse line genotyping strategies were no

longer useful in genotyping the endogenous *Vldlr* locus. The previously designed PCR primers would amplify DNA from the BAC as well as the endogenous locus because the

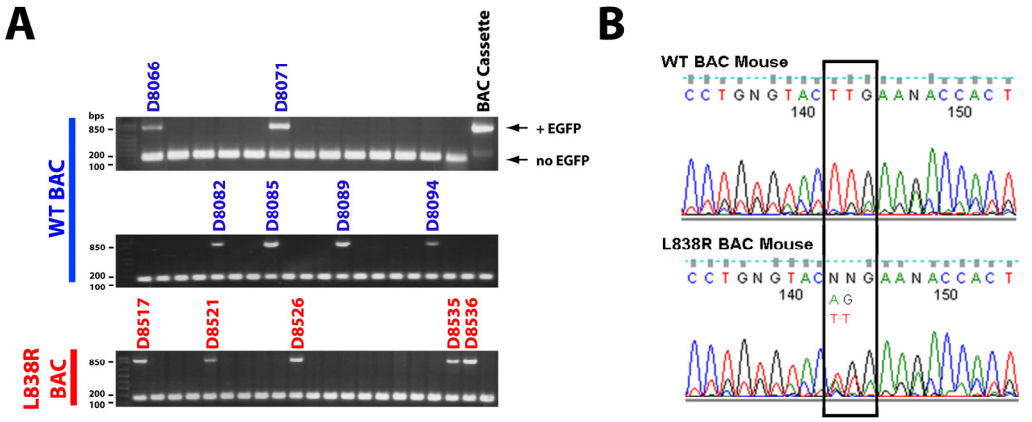

Figure 2.4: Vldlr BAC transgenic animal screening. (A) All animals resulting from the WT and L838R BAC blastocyst injection were screened to assess for BAC presence in the genome. The "+EGFP" band denoting the presence of the BAC is approximately 896 bps in size and the "no EGFP" band marking the Vldlr sequence without EGFP (endogenous Vldlr) is approximately 165 bps in size. There were six WT BAC mice and five L838R BAC mutant mice that were confirmed as positive for their respective BAC. (B) The sequencing of exon 18 shows the "T, T, G" sequence in the WT BAC and the double peak "AorT, GorT, G" sequence of those mice containing both the mutant BAC and the endogenous Vldlr genomic sequence.

endogenous *Vldlr* contained no unique sequence that would separate it from the Vldlr encoded by the BAC. To solve this problem I utilized differences in simple repeat lengths between mouse strains. Because the BAC mice were on an SJL background whereas the Vldlr KO mice were hybrid SV129/BL6, there was a chance that simple repeats close to the endogenous locus (but outside the reach of the BAC) would differ between the two backgrounds and allow for the determination of which endogenous Vldlr allele came from which strain (BAC or Vldlr KO). I proceeded to screen four candidate

simple repeats from mouse genomic DNA found close to the start or end of the BAC sequence but not encoded directly by the BAC. PCR primers were designed to amplify the simple repeat loci in search of a repeat that would have varying lengths in each of the different genetic backgrounds. Two of the four repeats (2 and 4) gave visibly different sized bands between the SV129/BL6 and SJL backgrounds on a 5% agarose gel (Figure 2.5A). Repeat 2 was selected for all further genotyping reactions as it gave a larger difference in band sizes and thus the heterozygote (one WT endogenous Vldlr allele and one KO endogenous Vldlr allele) could be easily identified (Figure 2.5B). For the rest of the study all of the BAC mice used express Vldlr only from the BAC locus and not the endogenous Vldlr locus (BAC+ Vldlr KO).

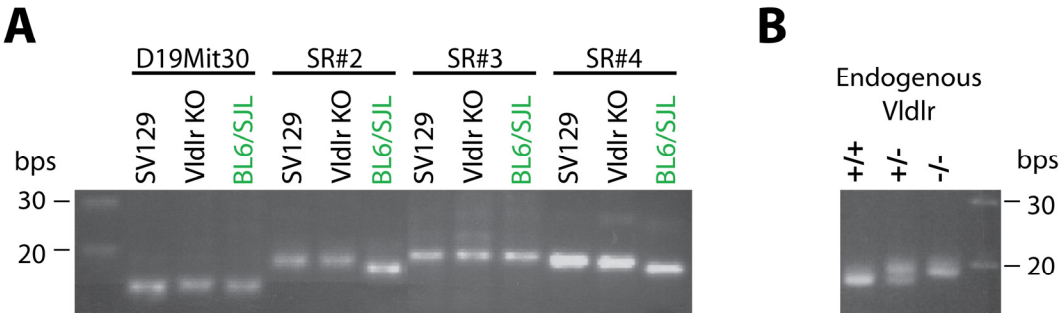

Figure 2.5: Simple repeat differences allow for endogenous Vldlr genotyping. (A) Four different simple repeats (SR) were amplified by PCR to identify differences in band size between animals of different backgrounds. SR#2 gave the biggest band size difference and allowed for endogenous Vldlr genotyping. (B) Sample genotyping of the endogenous Vldlr locus in the BAC+ Vldlr KO transgenic animals.

Confirmation of Vldlr-EGFP expression in BAC transgenic mice

Once the founder lines were all bred to an endogenous Vldlr KO background, the expression of BAC Vldlr from the founder animals needed to be confirmed. The readily available Vldlr polyclonal antibody was unfortunately directed against the c-terminal end

of the protein. The c-terminal end of the BAC-Vldlr is occupied by EGFP and not accessible for recognition by the c-terminal antibody (Figure 2.6). Thus, a new peptide from the middle of the Vldlr cytoplasmic tail was selected for the creation of a new mid-tail Vldlr antibody. This newly generated mid-tail antibody was able to specifically recognize both the WT Vldlr protein as well as the Vldlr-EGFP expressed by the BAC mice (Figure 2.6).

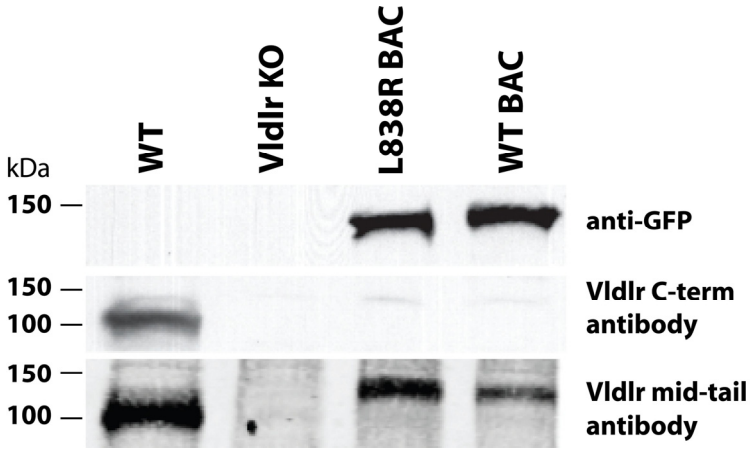

Figure 2.6: Vldlr mid-tail antibody recognizes endogenous and BAC Vldlr. Brain membrane fractions from WT, Vldlr KO, L838R BAC Vldlr, and WT BAC Vldlr animals were probed with three different antibodies. The anti-GFP antibody only recognizes the BAC transgenic animals with GFP fused to the c-terminal end of Vldlr. The Vldlr c-terminal antibody recognizes only the endogenous Vldlr as the fused GFP blocks recognition of the c-terminal end of the BAC Vldlr. The mid-tail antibody is able to recognize all forms of Vldlr and is a highly specific antibody.

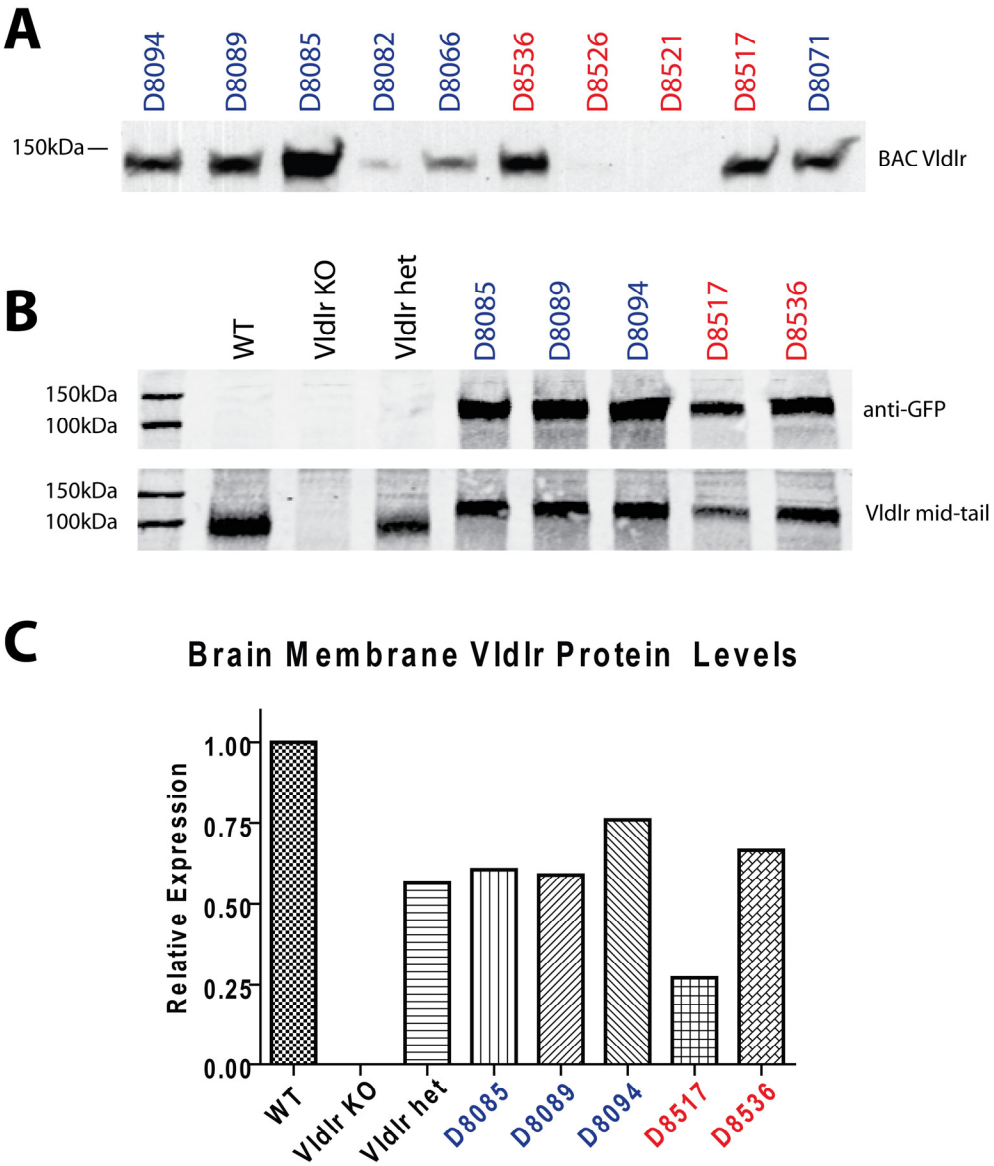

Figure 2.7: BAC Vldlr protein expression levels. (A) Brain membrane fractions from all BAC founder lines were analyzed for BAC Vldlr expression. Four WT BAC (blue) lines and two L838R BAC (red) founder lines expressed high levels of the Vldlr-EGFP. (B) Highly expressing BAC transgenic founder lines were compared to WT and heterozygous Vldlr expression levels. All founder lines expressed at least heterozygous levels of Vldlr except for L838R Vldlr BAC line D8517 which only expressed a quarter of the WT levels as quantified in (C).

levels from BAC transgenic animals (either heterozygous or homozygous) were compared to WT, Vldlr het, and Vldlr KO levels (Figure 2.7B, C). All of the BAC transgenic animals expressed Vldlr at similar levels compared to the Vldlr heterozygous mice, except for the L838R founder D8517 which only expressed about a quarter of the WT Vldlr levels. Unfortunately at this point in the breeding of these mouse lines, it was not possible to tell which mice had two BAC alleles and which had only one Vldlr BAC allele. Thus it may be possible that some of the founder lines would be able to express more Vldlr in the homozygote state if all animals in Figure 2.7B are assumed to be heterozygotes.

The EGFP sequence was attached to the c-terminal end of the VLDL receptor in the BAC construct to aid in the differentiation between Vldlr endogenously expressed and that expressed from the newly introduced BAC. Although Vldlr is expressed throughout the brain, expression levels are low and receptor detection in tissue via immunohistochemistry is virtually impossible using the polyclonal antibodies available. This was also true for visualizing the fluorescence of the EGFP expressed on the Vldlr-EGFP fusion protein. However, some success in observing Vldlr BAC expression was achieved using the strong affinity anti-GFP polyclonal antibody in immunohistochemical staining of cerebellar slices from the BAC transgenic animals. Vldlr expression is relatively high in the Purkinje cells of the cerebellar folia (Zhao et al., 2007) and this is where fluorescence was observed (Figure 2.8C).

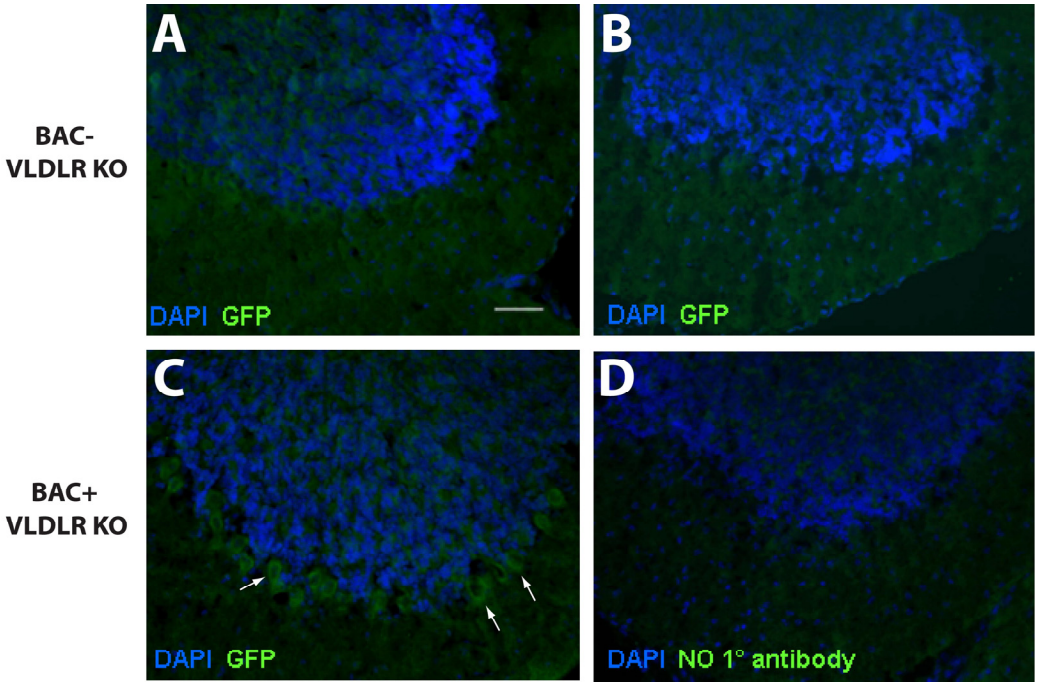

Figure 2.8: BAC Vldlr is expressed in Purkinje cells in the cerebellum. Sagittal sections through the cerebellum show localization of Vldlr-EGFP to the Purkinje cell (arrows) monolayer in BAC+ Vldlr KO (C) animals but not BAC-Vldlr KO (A)(B) animals. Controlling for autofluorescence and nonspecific secondary antibody staining in the brain, no primary antibody was used panel (D). Scale bar = 200 μm.

Once Vldlr expression from the BAC was confirmed in the transgenic animals, it was imperative to identify whether or not the WT Vldlr-EGFP fusion protein was able to rescue the Vldlr KO phenotypes. When working with BAC transgenic animals it is first crucial to confirm that the exogenously introduced WT gene can function normally and thus provide a control for the mutant version of the BAC. Rescue of two obvious phenotypes was assessed in each founder line: one morphological (cerebellar malformation) and the other functional (inhibition of long term potentiation upon Reelin stimulation).

Figure 2.9 summarizes the cerebellar phenotype rescue in the BAC mice. As seen in previous studies, the Vldlr KO animals have a smaller cerebellum with obvious disorganization of cells within the folia and also the absence of entire folia (Figure 2.9C, arrow). The Purkinje cell layer is generally found as a monolayer just above the darkly stained granule cell layer. However, in the Vldlr KO animals, the Purkinje cells are intermixed randomly throughout the granule cell layer. All of the BAC mutant animals, WT and L838R, were able to return the cerebellum to a normal size. All but one of the founder lines, D8094 (WT, Figure 2.9O), were able to restore normal gross organization of the folia. However, only one of the WT founder lines, D8089 (Figure 2.9M), was able to completely restore normal Purkinje cell monolayer organization. Vldlr heterozygotes were included in the morphological analysis because they only express half of the normal Vldlr levels and yet show normal cerebellar and hippocampal morphology. This is important because the BAC transgenic animals may also express half of the normal WT levels of Vldlr, however normal morphology should still be expected. It can be concluded that the inability of the BAC to rescue the Vldlr KO morphological phenotype is not a direct result of lower Vldlr expression in the entire brain.

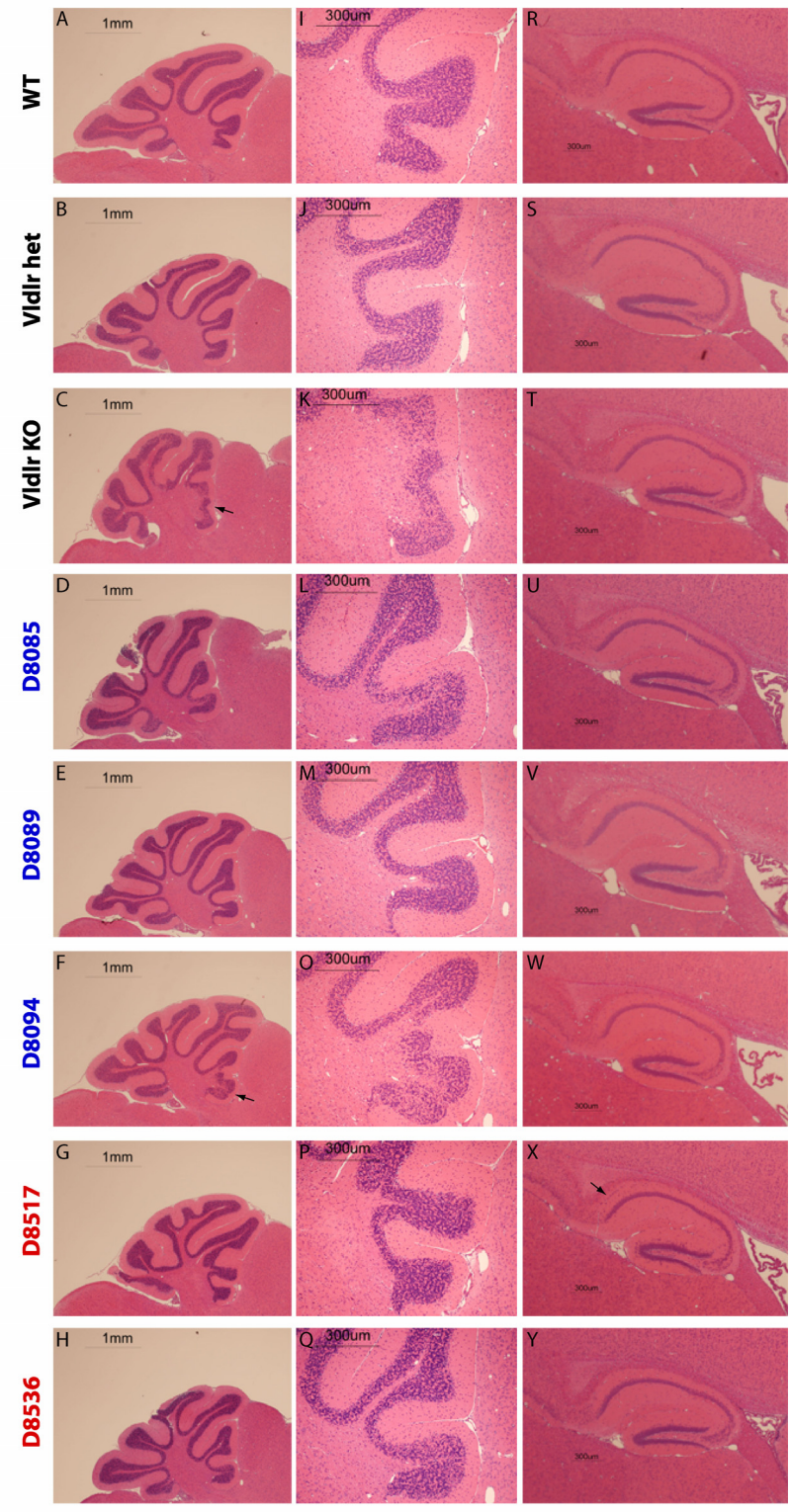
WT
Vldlr het
Vldlr KO
D8085
D8089
D8094
D8517
D8536
A
1mm
I
300um
R
B
1mm
J
300um
S
C
1mm
K
300um
T
D
1mm
L
300um
U
E
1mm
M
300um
V
F
1mm
O
300um
W
G
1mm
P
300um
X
H
1mm
Q
300um
Y

Figure 2.9: BAC founder line cerebellar and hippocampal morphology. Cerebellar and hippocampal morphology of WT, Vldlr het, Vldlr KO and WT BAC (blue) and L838R mutant (red) BAC transgenic animals was observed in sectioned, H&E stained sagittal brain slices. (A-H) Missing folia and disorganization of granule cells (arrows) are apparent in the Vldlr KO animals (C) and WT founder line D8094 (F). (I-Q) High power magnification of the first two anterior folia shows that only one of the WT (D8089, M) and none of L838R mutant BAC animals have completely restored organization of the Purkinje cell monolayer. (R-Y) Hippocampal morphology is generally normal save for occasional splitting in the CA1 region in the D8517 founder line (X, arrow). Vldlr KO animals also show mild dispersion of dentate granule cells (T) which is recapitulated in some of the transgenic animals as well (W, X).

Because the second phenotype of interest was the rescue of the hippocampal LTP deficit, gross morphology of the hippocampus was first analyzed. The Vldlr KO animals have a subtle hippocampal phenotype: an occasional split in the CA1 region and a slight dispersion of the granule cells of the dentate gyrus. Only one animal, founder line D8517 (Figure 2.9X), was observed with a split in the CA1 region. The dispersion of granule cells was more prevalent, and seen in founder lines D8094 and D8517 (Figure 2.9W, X). To summarize the morphological data, only the D8089 founder line resulted in complete rescue of the cerebellar phenotype and exhibited normal gross hippocampal morphology.

Results from the electrophysiology recordings gave different results from the morphological data. Using the theta burst model to induce LTP, we see approximately a 40-50% increase in potentiation after Reelin stimulation in normal WT slices (Weeber et al., 2002). Reelin is unable to induce this increase in potentiation in Vldlr KO hippocampal slices (Figure 2.10, (Weeber et al., 2002)). Control and Reelin stimulated LTP was recorded for mice from each founder line to confirm whether or not the BAC is able to rescue the functional Vldlr KO phenotype. Only one BAC founder line, WT D8094, was able to partially rescue the Reelin stimulation LTP deficit (Figure 2.10).

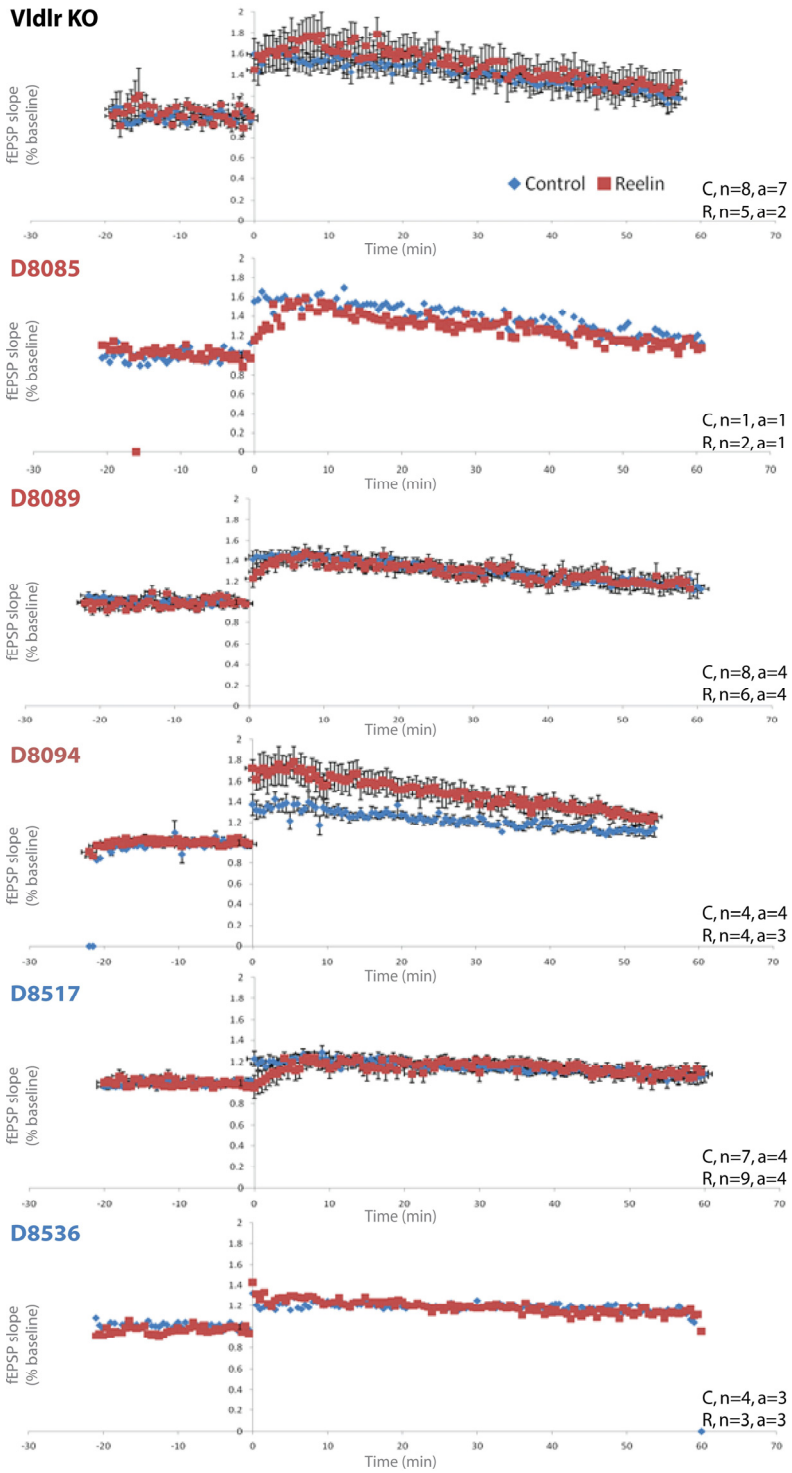
Vldlr KO
fEPSP slope (% baseline)
Control
Reelin
C, n=8, a=7
R, n=5, a=2
Time (min)
D8085
C, n=1, a=1
R, n=2, a=1
D8089
C, n=8, a=4
R, n=6, a=4
D8094
C, n=4, a=4
R, n=4, a=3
D8517
C, n=7, a=4
R, n=9, a=4
D8536
C, n=4, a=3
R, n=3, a=3

Figure 2.10: LTP induction after Reelin stimulation in BAC mutants. The theta burst paradigm was used to induce LTP (at time 0) in the presence or absence of Reelin in hippocampal slices from Vldlr KO, WT BAC (blue), and L838R mutant BAC (red) animals. The slices were stimulated with Reelin least 30 minutes prior to theta burst and Reelin remained in the perfusion ACSF throughout the remainder of the experiment.

This particular founder line, however, was the one WT founder line that was unable to completely rescue the Vldlr KO cerebellar morphology phenotype and thus the conclusion must be drawn that founder line D8094 gives an incomplete rescue of the null phenotype. This is also true for the only WT founder line that completely rescued the cerebellar morphology phenotype, D8089 (Figure 2.9E, M), as it was unable to rescue the Reelin stimulation LTP defect found in the Vldlr KO animals.

Discussion

In conclusion, we were able to successfully make transgenic mice that expressed Vldlr solely from an exogenously introduced BAC. Multiple founder lines were obtained for both the WT and L838R Vldlr mutant BAC constructs. Examining cerebellar as well as gross hippocampal morphology it was concluded that only one of the Vldlr BAC expressing mouse lines, D8089, was able to completely rescue the morphological Vldlr KO phenotype. Analyzing LTP induction results, only one Vldlr BAC founder line, D8094, was able to rescue the Reelin stimulated LTP phenotype seen in Vldlr KO mice. Unfortunately, the same BAC transgenic mouse line could not rescue both the morphological and electrophysiological Vldlr KO phenotypes. I must conclude that none of the BAC transgenic mice generated in this study show Vldlr expression from the BAC that is identical to endogenous Vldlr expression.

The difference for the inconsistent Vldlr KO phenotype rescue could be attributed to ectopic or mosaic expression of the Vldlr from the exogenous BAC, thus explaining why some founder lines are able to rescue cerebellar morphology and others the LTP defects. It would be necessary to perform *in situ* hybridization studies on the Vldlr BAC mice to confirm an abnormal expression pattern of the exogenous Vldlr. Vldlr is important during development and if the BAC Vldlr expression pattern changed temporally in some of the founder lines, it could also explain for the varied results in phenotype rescue.

Without proof of principle that Vldlr expressed from the WT BAC can function as expected in WT animals, it is impossible to make any assessments of the effects of the L838R Vldlr mutation on brain development and function in the mutant BAC transgenic animals. There is however, one interesting finding regarding LTP induction in the L838R mutant BAC founder lines. Both of the mouse lines expressing the mutated BAC Vldlr showed a decrease in baseline LTP induction. The Vldlr-EGFP protein expressed in these animals may be acting as a dominant negative to inhibit normal LTP induction. Both the neomycin gene and EGFP can be excluded as the causes of the reduction in baseline LTP because the WT BAC Vldlr animals, which also contain the neomycin gene and express EGFP, exhibit normal baseline LTP. These BAC transgenic mice alone will not be useful in the investigation of the significance of the binding between the alpha catalytic subunits of Pafah1b and the cytoplasmic tail of Vldlr. However, in the future, they may provide a model with which to confirm the results collected from the L838R Vldlr knockin mouse line generated by ES cell homologous recombination.

Although not much can be concluded about the L838R Vldlr mutation from the BAC transgenic mouse lines, I can assess this particular method of making mutant mouse models. The introduction of a mutated bacterial artificial chromosome is a simpler way of introducing mutated genes into the mouse genome as opposed to all of the tedious cell culture work needed to create and screen for homologous recombination in embryonic stem cells. However, the BAC technique has its own caveats.

First, there is no guarantee that the injected BAC will incorporate into the host genome without disrupting endogenous genes or regulatory elements. Because of this, it is imperative that more than one founder line be analyzed and result in identical phenotypes to confirm that the phenotypes observed are indeed a result of the purposely mutated exogenous gene and not a result of the disruption of an endogenous gene locus. This ends up doubling and tripling the required number of experiments. Circumventing this problem might be possible if the BAC allele can be kept at the hemizygous state. This may prevent unwanted phenotypes due to disrupted endogenous genes as they would still be present in a hemizygous state. However, in the hemizygous state, gene expression levels maybe affected for either the introduced gene or the endogenous disrupted gene and may be enough to induce phenotypic changes.

Second, it is possible that only part of the BAC will recombine into the host genome. The larger the regulatory and coding region of the gene is, the greater chance that truncation of the sequence will occur during integration into endogenous genomic sequences. The coding region of the gene may be intact but regulatory domains may be lost and thus disrupt normal expression of the exogenous gene. In the generation of the WT and L838R Vldlr BAC transgenic animals, circularized BAC DNA was injected into

fertilized embryos. Although there may be complete BAC integration sites, the location where the break occurred to allow for BAC insertion into the genome may separate some of the regulatory domains from the coding region, again potentially disrupting normal gene expression and regulation. This may have been the reason for the varied phenotypes seen in the Vldlr BAC transgenic animals.

If expression of a particular gene, solely from the BAC locus is desired, the endogenous gene needs to be suppressed. Breeding to null animals may be difficult if none are available. Luckily, for this study Vldlr KO animals were available, however creative genotyping strategies needed to be developed in order to genotype the endogenous gene locus.

Lastly, quite often the BAC will integrate into multiple sites within the genome. These sites may segregate separately from one another during breeding and form subclones from the main founder lines. This phenomenon has the possibility to create variability in phenotypes even in mice from the same original founder, thus making it difficult to arrive at any concrete conclusions. Not only is there a potential for multiple insertion sites but also for multiple BACs inserted into the same locus. Head-to-tail repeats, or concatmers, can number from a few to a few hundred (Yang and Gong, 2005). This again may increase gene expression, a potentially unwanted side effect that has little to do with the induced mutation.

In summary, expression of the BAC Vldlr-EGFP protein was successfully achieved in the transgenic animals although with variable results. Unfortunately, because I was not able to confirm that any of the WT BAC founder lines can fully rescue the Vldlr KO phenotypes, no conclusions can be made regarding the phenotypes that we see

in the L838R mutant BAC mice. I have thus concluded that it would be more relevant, physiologically to analyze the L838R mutation introduced into the genome by ES cell homologous recombination. The creation of the L838R Vldlr knockin mouse line will be described in the next section of this chapter.

VLDLR L838R KNOCKIN MICE

Materials and Methods

Targeting vector cloning – The Vldlr L838R targeting vector (#2) long and short arms of homology were cloned into the pJB1 (Gotthardt et al., 2003) targeting vector backbone in three pieces. All fragments were amplified from SV129 ES cell DNA. The short arm (911 bps) containing exon 16 was amplified using the primers IM316 (5'-CTCGAGT ACTAGCCTCAGTAGATGACACAAG-3', XhoI) and IM317 (5'-CTCGAGCGAAT TAGGTAGAGATCCTTATACCTTTG-3', XhoI). The first piece of the long arm (1638 bps) containing exon 18 and the location of the desired mutation was amplified using the primers IM318 (5'-GCGGCCGCTAGATGTCTAAGTCTTAATTCAAATCC-3', NotI) and IM319 (5'-GCGGCCGCTCATGTTCATCATGGTTCAGTCAG-3', NotI). The remainder of the long arm (8041 bps) was amplified using the primers IM320 (5'-GCGGCCGCACAGTGTCCTTGCATGATCTCTGGTG-3', NotI) and IM321 (5'-CGGCCGTCTATTGTCATAGTCCTCTAACTCACAC-3', NotI). The short arm was directly cloned into the pJB-1 vector upstream of the floxed neomycin cassette. The first section of the long arm containing exon 18 was cloned into the pBSKS plasmid and mutated using the QuickChange Site-Directed Mutagenesis Kit (Stratagene) and the

primers IM222 and IM223. The second long arm fragment was cloned into pJB1+SA (on the opposite side of the floxed neomycin) followed by the first mutated long arm fragment which was digested from the pBSKS vector after mutagenesis.

ES cell targeting – Detailed protocols established in the lab were closely followed (Willnow and Herz, 1994). Briefly, mouse ES cells (SV129, clone SM-1) were cultured on irradiated STO fibroblast (SNL 76 clone) feeder layers. Near confluent ES cell cultures (approximately 3 x 10^7 cells) were trypsinized, washed in 1x PBS, and mixed with 100μg of linearized targeting vector DNA. The cell suspension was electroporated (330μF, 275V, low Ω, Cell-Porator, BRL) and replated onto fresh STO cell feeder layers. The day of electroporation was designated day 0 of the experiment. Two-thirds of the media was changed every day and LIF (leukemia inhibitory factor, ESGRO, Chemicon) was added to the media from electroporation through ES cell blastocyst injection. On day 1, 2/3 of the media was changed with the addition of G418, final active concentration of 250 μg/ml (positive selection). G418 was included in the media through day 6. On day 5, media was changed to the same final concentration of G418 and with the addition of 2.5 μM Ganciclovir. On Day 6 the ES cells remained in the media with both G418 and Ganciclovir. From Day 7 and on, cells were switched to regular ES cell media without G418 or Ganciclovir (LIF still present). Colonies began appearing around day 9 and were ready for picking, expansion, and screening on days 10-12.

ES cell screening – ES cells were lysed in lysis buffer (1x Soriano PCR buffer, 1.7 μM SDS, 50 ng/ml Proteinase K) at 37°C for 2 hours, after which the Proteinase K was inactivated at 94°C for 15 minutes. The lysate was added directly to the PCR reaction.

Primer IM345 (5'-ACCAGTATATGAAGGCACTTGAGTAAG-3'), located in the genomic sequence just outside the short arm of the targeting vector, and primer IM348 (5'-AAGTTCCTATTCCGAAGTTCCTATTC-3'), located in the targeting vector sequence between the short arm and the neo gene, were used to find clones positive for homologous recombination. Location of these primers is marked in Figure 2.11E by purple arrows.

L838R ES cell southern blot – DNA from positive ES cell clones was digested with the AlwNI restriction enzyme and run on a 0.8% agarose gel for 8 hours at 45 volts. The southern transfer was set up overnight. The DNA was crosslinked to the membrane in a UV Stratalinker (Stratagene) and incubated with Rapid-hyb buffer (Amersham) for 2 hours at 65°C. The probe was amplified by PCR from genomic ES cell DNA using primers IM368 (5'-TGGTACATGTTTGTACCCATAGTTC-3') and IM 369 (5'-TTTAAAGGTTAGCCACAACAGAGTC-3'). The probe (100ng) was combined with 2µl of Random Hexamers (Roche) and boiled for 5 minutes. The probe was immediately incubated on ice for 5 minutes followed by the addition of the reaction cocktail: 1x oligo labeling buffer (10x = 0.5 M Tris pH 7.4, 0.1 M $MgSO_4$, 1 mM DTT, 0.5 mM each dATP, dTTP, dGTP), 3 µl Easy Tide [^{32}P] dCTP (10mCi/ml, Perkin Elmer), and 5 units Klenow enzyme (Roche). The reaction was incubated at room temperature for 1 hour. Before adding it to the membrane in Rapid-hyb buffer, the labeled probe was boiled for 5 minutes. The membrane was incubated with the probe overnight at 65°C, washed 4 times with 0.1xSSC and 0.1% SDS at 65°C, and exposed to x-ray film at -80°C.

Animals – All L838R knockin mice (SV129/BL6 hybrid) were housed under a 12 h: 12 h light dark cycle and fed a normal chow diet unless otherwise stated. All animals were euthanized via inhalation of isoflurane according to the National Institutes of Health's Guide for the Care and Use of Laboratory Animals and the UT Southwestern Animal Care and Use Committee.

L838R knockin animal genotyping – Tail DNA was prepared from animals as previously described. Three primers were used to amplify WT and KI products. The common primer IM378 (5'-GCAAACTGTTAATCTCAACTAACTGC-3') is located in the short arm just downstream of exon 16. The WT primer IM379 (5'-AATTCAGTGT CACATGTGTTAGGAC-3') is just downstream of exon 17 and yields a 380 bp band. The KI primer IM380 (5'-TTCCTATTCCGAAGTTCCTATTCTC-3') is located in the targeting vector between the short arm and neo sequence and yields a 600 bp band.

Results

The first attempt to introduce the L838R mutation into the murine *Vldlr* gene locus employed the embryonic stem (ES) cell homologous recombination method. A targeting vector was designed with the short arm of homology containing exon 17 of the gene, a floxed neomycin selection marker in intron 17, and the long arm of homology spanning exons 18 (expressing the L838R mutation, Figure 2.11A) and 19 (Figure 2.11B). The targeting vector was introduced into ES cells and homologous recombination was anticipated to give the recombined Vldlr locus depicted in Figure 2.11C. Multiple electroporations were performed and over 2,000 clones were screened

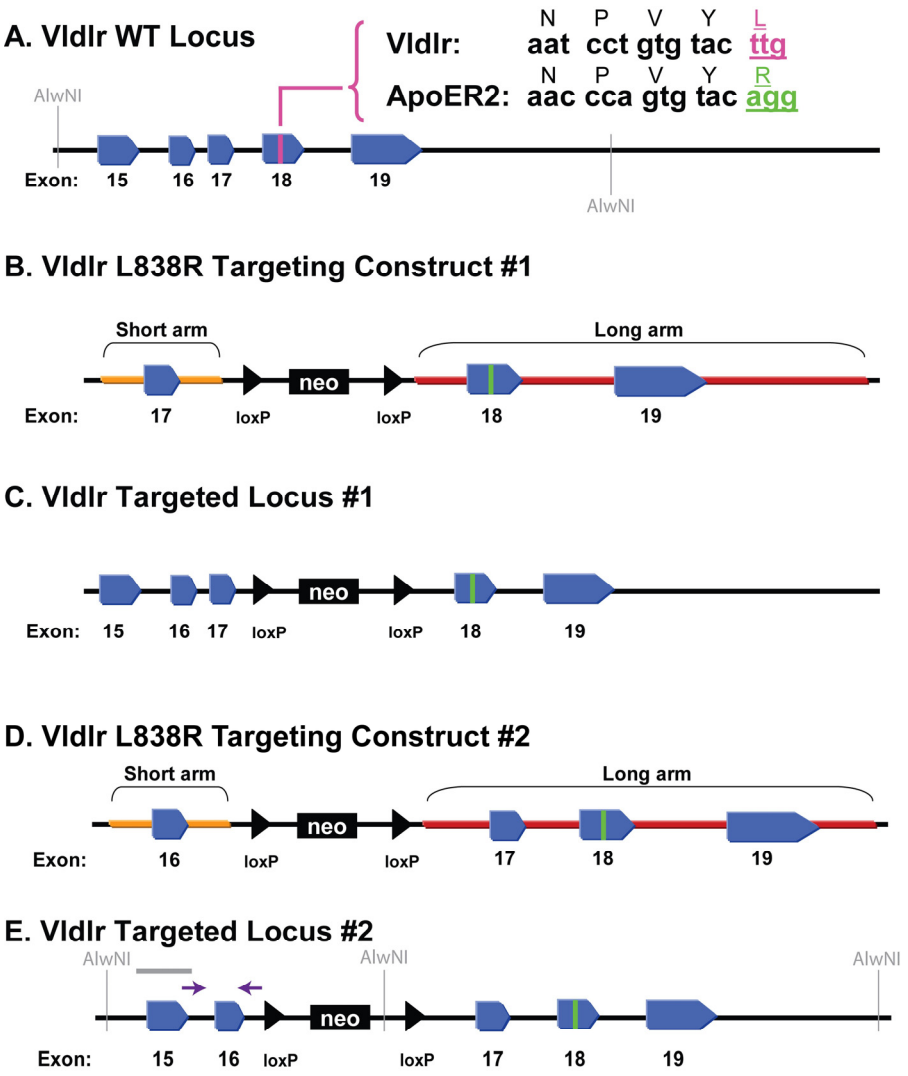

Figure 2.11: ES cell targeting vector strategies. (A) Diagram of the endogenous *Vldlr* locus from intron 14 through 19. AlwNI sites were used in the restriction digest for Southern blotting. Exon 18 is the location of the L838R mutation and both the Vldlr and Apoer2 DNA and amino acid sequences are illustrated. (B) Diagram of the first targeting vector highlighting regions of homology. (C) Diagram of the expected targeted locus using targeting vector one. (D) Diagram of the second, successful, targeting vector with short and long arms of homology shifted upstream by one exon. (E) Diagram of the expected targeted locus using targeting vector two. AlwNI sites used in the restriction digest for Southern blotting are included for reference. Purple arrows indicate primers used for ES cell screening to confirm homologous recombination. The left most arrow is outside of the short arm of homology.

by PCR or Southern blotting, however, none of them gave a positive result for homologous recombination.

At this point, it was concluded that this particular location within the *Vldlr* gene was not a "hotspot" for recombination and that the ES cell strategy for introducing the L838R mutation may not be feasible. This is when the BAC Vldlr mice were generated as described in the previous section. The BAC transgenic animals did not provide an ideal model for exploring the effects of the L838R mutation and therefore, the ES cell homologous recombination strategy was revisited.

It was proposed that perhaps by moving the arms of homology, better recombination efficiency could be achieved. A new targeting vector was constructed which shifted the floxed neomycin selection marker upstream to intron 16 and resulted in an upstream shift in the sequence of the short and long arms of homology as well (Figure 2.11D). This second targeting vector was also introduced into ES cells and resulted in approximately 2% recombination efficiency, giving the expected recombined Vldlr locus (Figure 2.11E).

Before injection, homologous recombination was confirmed in the ES cell clones by Southern blot. All of the positive clones exhibited the expected WT and KI bands, 6 kb and 3.5 kb respectively (Figure 2.12A). The L838R knockin animals have been bred successfully to achieve L838R Vldlr homozygous knockin mice (Figure 2.12B).

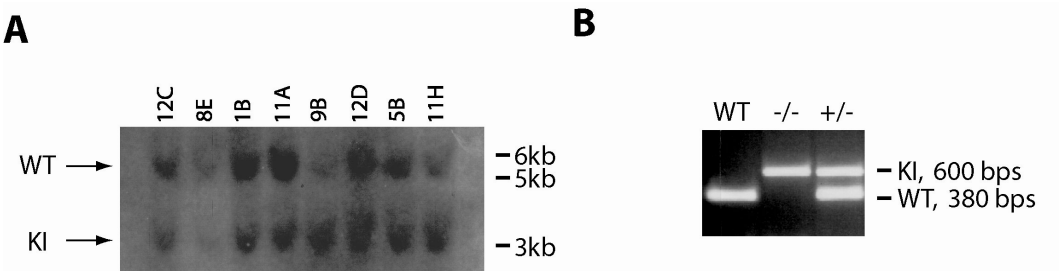

Figure 2.12: Targeted ES cell Southern blot and mouse genotyping. (A) DNA from each ES cell clone that tested positive for homologous recombination via PCR was digested using the AlwNI restriction enzyme and used for Southern blotting. The probe consisted of the sequence surrounding and including exon 15. The probe is marked in Figure 2.11E and did not contain any overlapping sequence with the short arm of homology. All clones were heterozygous for the KI allele as both the WT (6 kb) and KI (3.5 kb) bands were present in the Southern blot as expected. (B) PCR results from mouse tail DNA confirming the generation of homozygous KI L838R Vldlr mice.

Discussion

We were able to achieve germline transmission of the Vldlr L838R mutation in knockin mice. This mutation was introduced into mice using ES cell homologous recombination techniques. Two different targeting vectors were constructed. The first targeting vector, spanning exons 17 to 19, yielded no positive clones which had successfully undergone homologous recombination to replace the endogenous Vldlr sequence with the mutated sequence introduced by the targeting vector. In the second targeting vector, the short arm of homology and intronic location of the neomycin resistance gene were shifted upstream by 500 bps. This new targeting vector spanned across exons 16 to 19 and resulted in a 2% homologous recombination efficiency.

Significance of the Vldlr Pafah1b Interaction

Although, a successful knockin mouse model has been achieved, I cannot make any conclusions regarding the significance of the Vldlr/Pafah1b interaction. However, experiments using the newly created L838R knockin mice that will address the importance of the interaction include the following projects. Brains from homozygous KI animals will be sliced and stained to observe any morphological phenotypes. I would not expect to see any phenotypes more severe than those in the Apoer2 KO animals. Also, the D8536 L838R Vldlr founder line showed a normal sized cerebellum with normal foliation. The only discrepancy between this L838R Vldlr BAC mutant and the WT brain was the dispersion of the Purkinje cells. The D8536 hippocampus looked normal. The mutant Vldlr that was expressed in this BAC transgenic animal founder line was able to rescue almost all of the Vldlr KO phenotypes. Thus, it would not be surprising to see normal brain morphology in the L838R KI animals, or at the most, dispersion of the Purkinje cells within the granule cell layer.

The L838R KI animals will also be bred to Lis1 heterozygotes. If an increase in progressive hydrocephalus, comparable to VldlrKO;Lis1+/- animals, is observed, it will be clear that the genetic interaction between Vldlr and Lis1 can potentially be translated to the protein interaction between Vldlr and the Pafah1b complex. This will strengthen the hypothesis that Lis1 function can be considered a new branch of the Reelin Signaling pathway.

Lastly, LTP, both with and without Reelin stimulation will be recorded in the L838R Vldlr KI mice. It must not be overlooked that the two L838R BAC Vldlr founder lines produced lower than normal baseline LTP. It is possible that the L838R mutation is

a dominant negative mutation which may result from the sequestration of Disabled at the receptor or downregulation of SFK activation. Regardless, the LTP results should be analyzed carefully. As such, I suggest that the interaction between Vldlr and the Pafah1b complex may mediate the Reelin stimulated LTP induction that relies partially on Vldlr. Recall that Vldlr KO animals are unable to induce the increased potentiation after Reelin stimulation even though Apoer2 is normally expressed and Dab1 is phosphorylated. There must be a Vldlr dependent component to the increased LTP induction upon Reelin stimulation and the interaction with the Pafah1b complex could be the answer. As previously mentioned, this would be the first example of Lis1 involvement in synaptic function.

Analyzing Successful vs. Failed Targeting Vector Recombination Events

Although no conclusions can currently be made from the L838R knockin animals regarding the importance of the interaction between Vldlr and the Pafah1b complex, the difficulties in generating these knockin animals brings up some interesting findings involving homologous recombination strategies and the creation of knockin animals. The only difference between the first targeting vector and the second was an approximately 500 bp upstream shift in the sequence of the short and long arms of homology and the location of the neomycin resistance gene. This minor shift made a big difference in whether or not homologous recombination successfully took place.

As reviewed in Koren et al., recombination hotspots exist in the genomes of all organisms, from yeast to humans (Myers et al., 2005). These hotspots enhance meiotic recombination as a means to create genetic diversity which is crucial for the survival of

species and evolution. As many as 25,000 hotspots have been identified in the human genome (Koren et al., 2002). Hotspots generally have an increased propensity for double strand DNA breaks (DSB) (Gerton et al., 2000) and are frequently found in transcription start sites where increased transcription factor binding allows for access to chromatin in the "open" conformation (Petes, 2001). Hotspots may even depend on high GC rich regions where it is proposed that transcriptional machinery has a greater chance of stalling and requiring histone modification, thus also allowing easier access to the DNA by endonucleases (Petes, 2001).

Although the ES cells used to create the knockin mouse models are not undergoing meiosis, it is still probable that genomic sequences and environments can alter the recombination frequency of one genetic locus versus another. The first targeting vector attempt is a good example of reduced homologous recombination efficiency at a particular site within a gene. Moving the arms of homology over a few hundred base pairs made the difference between 0% recombination efficiency and 2%. This is a minute difference, however, when one is trying to make a knockin mouse line, it makes all the difference in the world. I would attribute this difference to the actual sequence of the area of homology or the location within a chromosome. The sequence is found in the middle of the coding region and should not be influenced by transcription factor binding. There must be a particular characteristic embodied by the genomic sequence containing and surrounding exon 16 that makes it a more favorable recombination "hotspot" than the exon 17 region.

Genetic modification of animals to create models of disease and to study molecular mechanisms *in vivo* is an indispensible scientific tool. The introduction of the

L838R Vldlr mutation into the mouse genome has not been easy, however, the process has given insight into the challenges scientists face not only in the investigation of the pathogenesis of disease but also in the creation of models need for this exploration.

CHAPTER THREE

THE ALTERNATIVELY SPLICED O-LINKED SUGAR DOMAIN REGULATES APOER2 PROCESSING

Introduction

Apoer2 is a developmentally and functionally important receptor in the central nervous system and it comes as no surprise that it is a highly regulated and modified protein as well. To date, it has been established that Apoer2 is regulated by three different processes: alternative splicing, glycosylation, and proteolytic processing.

Alternative splicing of Apoer2

The coding region of Apoer2 is highly similar between mice and men. There is only one large difference between the two species, an extra ligand binding repeat in the mouse ligand binding domain. This extra murine ligand binding repeat is encoded by a separate exon (#7) and causes the exon numbering to change between mice and humans after exon 6 (Figure 3.1).

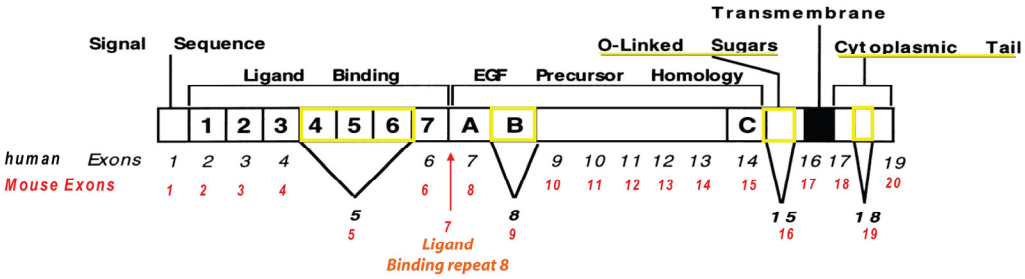

Figure 3.1: Alternative splicing of Apoer2. This diagram shows the domains of Apoer2 and the exons that encode them in both mice and humans. The four domains highlighted in yellow are encoded by the most commonly spliced exons. Modified from (Clatworthy et al., 1999).

In both mammals, there are four exons which are most commonly alternatively spliced: exon 5 encoding ligand binding repeats 4 through 6, exon 9 (8 in humans) encoding the second EGF repeat, exon 16 (15 in humans) encoding the O-linked sugar domain, and finally, exon 19 (18 in humans) encoding the unique cytoplasmic insert not found in any other protein, let alone member of the LDL receptor gene family (Figure 3.1).

Our laboratory and others have found that most of the splice variants cloned from WT mice lack exon 5 (our unpublished data) (Clatworthy et al., 1999; Kim et al., 1997). The significance of this particular splice variant and why it is preferred over the full length ligand binding domain is still unclear. Kim et al., showed that lack of ligand binding repeats 4-6 did not alter the binding of Apoer2 to Apolipoprotein E containing lipid particles (Kim et al., 1997).

Nothing is known about the reason for the splicing of the EGF repeat B. The EGF precursor homology domain contains a β-propeller between repeats B and C, which mediates the pH dependent release of ligands from the ligand binding domain of the receptor (Rudenko et al., 2002). It has been suggested that alternative splicing of the second EGF repeat may alter the ligand releasing properties of the receptor (Clatworthy et al., 1999).

The Apoer2 O-linked sugar domain, encoded by the alternatively spliced exon 16, provides attachment sites for O-linked sugars (Kim et al., 1996). The significance of glycosylation in proteolytic processing of Apoer2 is discussed in a later section of this chapter. However, in this thesis I suggest a novel characteristic of this domain; not only does it contain many serine, threonine, and arginine residues needed for glycosylation but

it also encodes a protease recognition/cleavage site important for specific proteolytic processing of the receptor.

Lastly, exon 19 encodes a proline rich 59 amino acid cytoplasmic insert that, as previously stated, is unique to Apoer2. We have determined that this particular insert plays vital roles in both synaptic plasticity and neuronal survival (Beffert et al., 2006b; Beffert et al., 2005).

Initially, the function of the insert was explored by searching for proteins that bound to this particular domain. Yeast two hybrid assays were employed which uncovered a few adaptor proteins that bound only to Apoer2 expressing exon 19. The proteins that gave the strongest responses were the postsynaptic density protein of 95 kDa (PSD95) and the JNK-interacting proteins (JIPs). I was able to confirm this specific interaction between the cytoplasmic insert of Apoer2 and the adaptor/scaffolding proteins PSD95 (Figure 3.2) and three different isoforms of the JNK-interacting proteins (JIP1, JIP1b, and JIP2) (Figure 3.3) by performing co-immunoprecipitation assays from transfected cells (Beffert et al., 2006b; Beffert et al., 2005).

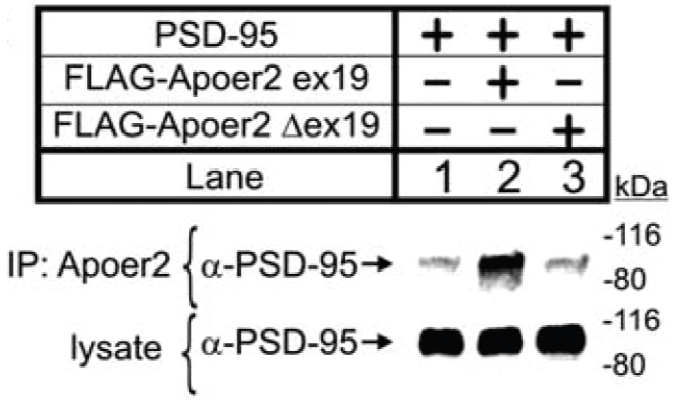

Figure 3.2: Exon 19 is required for PSD95 binding to Apoer2. FLAG-tagged Apoer2 constructs expressing or lacking exon 19 were co-transfected with PSD95 in HEK 293 cells. PSD95 specifically co-precipitated only with Apoer2 expressing exon 19. (Beffert et al., 2005)

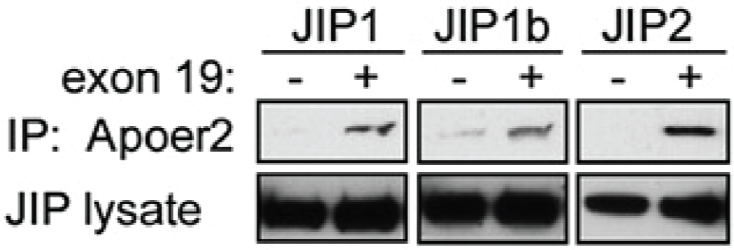

Figure 3.3: Exon 19 is required for JIP binding to Apoer2. All three JIP isoforms co-precipitated only with Apoer2 expressing exon 19 from lysates of HEK 293 cells co-transfected with both Apoer2 and any one of the JIP isoforms. (Beffert et al., 2006b)

Functions of the insert encoded by Apoer2 exon 19

Functions of this alternatively spliced insert were explored through the creation of knockin animals constitutively expressing or lacking exon 19 (Beffert et al., 2005). Using WT animals along with the Apoer2 KI mutants, our laboratory was able to show activity dependent splicing of the exon and requirement of the insert in Reelin dependent

phosphorylation of NMDA receptor subunits and regulation of synaptic plasticity. In WT hippocampal slices, Reelin significantly enhances NMDA receptor mediated LTP. This increase is dependent on the presence of the cytoplasmic tail insert of Apoer2 as hippocampal slices from Apoer2*[Δ19]* animals fail to show the expected increase in LTP after Reelin stimulation. Strengthening these results, data from Apoer2*[+19]* and *[Δ19]* animals which were subjected to two different behavioral tasks illustrates that in the absence of exon 19 mice perform poorly in selected learning and memory tests. Apoer2*[Δ19]* animals exhibited less freezing in the hippocampus dependent contextual fear conditioning task. Also, the Morris Water maze task was used to address spatial learning abilities in the Apoer2 knockin animals. Apoer2*[Δ19]* animals spent less time, compared to WT and Apoer2*[+19]* mice, in the goal quadrant where the escape platform is expected to be during the probe test. This suggests an inability of the mice lacking the alternatively spliced exon 19 to learn/remember/use spatial clues.

The amino acid sequence encoded by exon 19 was also found to be important in neuronal survival during aging (Beffert et al., 2006b). Corticospinal neurons (CSNs), labeled by injecting mice with the retrograde tracer True Blue (TB), were counted in WT, Apoer2*[Δ19]*, and Apoer2*[+19]* 8 month old mice. The Apoer2*[Δ19]* mice showed approximately a 36% reduction in the number of CSN compared to WT and Apoer2*[+19]*. On the other hand, the unique cytoplasmic insert has also been implicated in promoting neuronal degeneration after lesion induction (Beffert et al., 2006b). Mice injected with TB were subjected to stereotaxic lesioning of the CSN tract before corticospinal neuron counting. Apoer2*[+19]* animals showed a 40% reduction in CSN numbers after lesioning whereas the corticospinal neurons from Apoer2*[Δ19]* animals

were spared. The conclusion was made that the cytoplasmic insert may be involved in the JNK-signaling pathway mediating neurodegeneration through specific interaction with the JIP scaffolding proteins.

Glycosylation of Apoer2

Protein glycosylation mediates processes such as protein trafficking, turnover, stability, and function (Rademacher et al., 1988). Most proteins synthesized in the rough endoplasmic reticulum (ER) undergo glycosylation during their transit through the ER and Golgi apparatus. There are two main types of glycosylation. N-linked glycosylation modifies arginine residues, whereas O-linked glycosylation takes place on serine and threonine residues. The three smallest LDL receptor family members, LDL receptor, VLDL receptor, and Apoer2, all contain O-linked sugar domains which encode multiple serine and threonine residues available for glycosylation.

A mutant CHO-K1 cell line exists (*ldl*D) which is unable to glycosylate the LDL receptor due to a deficiency in the enzyme UDP-N-acetylgalactosamine 4-epimerase (Kingsley et al., 1986a). This enzyme is necessary for the production of sugars used in protein glycosylation. The *ldl*D cell line has been used in many studies, including those in this thesis, to explore the function of protein glycosylation. The LDL receptor in these cells is rapidly degraded and shows defective O-linked glycosylation, substantiating that the addition of sugars increases LDL receptor stability (Kingsley et al., 1986b). This same *ldl*D cell line has been used to assess the stability of Vldlr, which also contains an alternatively spliced O-linked sugar domain and shows increased protein stability in the glycosylated form (Magrane et al., 1999).

Finally, Apoer2 is the third receptor in the family to express the O-linked sugar domain and is modified by both O- and N-linked sugars (Figure 3.7 and 3.12A). Our laboratory has previously observed that hypoglycosylated Apoer2 expressed from transfected *ldl*D cells has decreased stability and is more susceptible to proteolytic cleavage (May et al., 2003).

Lrp1, one of the largest members of the LDL receptor family, does not express an O-linked sugar domain, however, it is still highly modified by N-linked sugars. Interestingly, LRP1 glycosylation is tissue specific as the receptor from mouse liver migrates slower than brain Lrp1 in Western blots (May et al., 2003). Even without a specific region dedicated to glycosylation of the receptor, the addition of sugar residues to Lrp1 helps protect it from proteolytic processing. Sequential cleavage of Lrp1 is akin to APP, Notch, as well as Apoer2 processing which will be discussed in the next section (May et al., 2002).

Proteolytic processing of Apoer2

Indeed, Apoer2 is proteolytically processed in a manner similar to APP, Notch, and its relative Lrp1. For example, APP, a membrane spanning protein, is first cleaved by a protease within its extracellular domain. This cleavage is performed by either α- or β-secretase and releases the Lrp1 extracellular domain, providing the necessary membrane bound N-terminal stub which is proposed to be necessary for substrate recognition by the γ-secretase subunit nicastrin (Shah et al., 2005). Upon γ-secretase intramembrane cleavage, both the extracellular peptide (p3 or Aβ) as well as the intracellular domain (ICD) are released from the membrane (Zheng and Koo, 2006).

The large Lrp1 protein is first cleaved by furin (similar to Notch (Logeat et al., 1998)) to form an extracellular fragment non-covalently bound to the smaller transmembrane spanning segment (Willnow et al., 1996b). The smaller 85 kDa fragment is then cleaved by a metalloprotease thus releasing the extracellular portion of the membrane bound protein (Quinn et al., 1997; Quinn et al., 1999). As with APP, this cleavage also creates a substrate for γ-secretase mediated intramembrane cleavage releasing the ICD which is free to translocate to the nucleus (May et al., 2003; May et al., 2002). Further studies have revealed that the Lrp1 ICD, once in the nucleus, regulates transcription of lipopolysaccharide (LPS)-inducible genes (Zurhove et al., 2008).

It has been established that metalloproteases, for example ADAM10, cleave the extracellular domain of Apoer2 (Hoe et al., 2007; Hoe and Rebeck, 2005) again leaving a substrate for γ-secretase which then releases the Apoer2 ICD via intramembrane cleavage. However, as there are many metalloproteases and most metalloprotease inhibitors are not specific for a single enzyme, it has been difficult to deduce exactly which enzyme(s) is responsible for Apoer2 extracellular cleavage *in vivo*. Lastly, Apoer2 proteolytic processing seems to be ligand binding mediated as ApoE peptide treatment *in vitro* shows increase CTF accumulation (Hoe and Rebeck, 2005). The release of the ICD from the accumulated CTF fragment could be significant if it functions in transcriptional gene regulation similarly to the cytoplasmic tail of Lrp1. However, the function of the released Apoer2 ICD is still unclear.

The multifaceted Apoer2 exon 16

Taking together all of the complex mechanisms involved in the regulation of Apoer2, it is clear that exon 16, encoding the O-linked sugar domain, is not only glycosylated but also alternatively spliced and involved in the proteolytic processing of the receptor. No other exon in Apoer2 is subjected to all three modifications. For this reason I chose to explore why Apoer2 regulates glycosylation and proteolytic processing by alternative splicing. I initially proposed that glycosylation of exon 16 protects the receptor from proteolytic processing and that this is important in the normal functioning of the receptor in terms of Reelin signaling and synaptic function. Most of the previous studies regarding cleavage of the receptor had been performed *in vitro*, generally in transfected cells. In order to study the function of exon 16 *in vivo*, I made a mouse model constitutively expressing the alternatively spliced variant of the receptor lacking exon 16 (Δ16). Previous data utilizing a luciferase reporter gene assay resulted in the conclusion that deletion of exon 16 from Apoer2 increases intracellular domain release and translocation to the nucleus in transfected cells (May et al., 2003). Increased release of the ICD could potentially alter gene transcriptional regulation. Because the released ICD encompasses the alternatively spliced exon 19, it is possible to have two different forms of the ICD with two completely different functions. Thus, I created two differed Δ16 mouse lines. One mouse line constitutively lacking exon 16 but still expressing exon 19 (Apoer2*[Δ16+19]*) and the other constitutively lacking both exons (Apoer2*[Δ16 Δ19]*). Using these mice and some *in vitro* experiments I was able to conclude that exon 16 is glycosylated and that the absence of the exon contradicts previous data by, preventing specific proteolytic cleavage of the receptor. This misregulation of the Apoer2 receptor

increases the Apoer2 levels in the brain and affects LTP stimulation in an exon 19 dependent manner. However, preliminary PPF data suggest no presynaptic effects of the exon 16 deletion in either of the Δ16 mouse lines. Morris water maze, open field, startle response, and PPI behavioral testing of the Apoer2 Δ16 mouse lines also did not reveal any significant differences between the KI mutants and WT mice.

Materials and Methods

Apoer2 and adaptor protein co-immunoprecipitation – HEK 293 cells were transiently transfected with Apoer2 lacking or expressing exon 19 (p3XFLAG-CMV-9), PSD95 (pCMV-Sport6), and JIP (JIP1; pcDNA3, JIP1b; pcDNA3, JIP2; pCMV-5Xmyc) isoform constructs using the FuGENE 6 transfection reagent (Roche). 24 hours after transfection cells were lysed in 1% TritonX-100 lysis buffer (50 mM Tris pH 7.4, 150 mM NaCl, 1 mM $MgCl_2$, 1 mM $CaCl_2$, 1% Triton X-100, EDTA-free protease inhibitor cocktail). Lysates were precleared using rabbit non-immune serum and Apoer2 was immunoprecipitated using the c-terminal end polyclonal antibody (rb serum, 8 μl). Immunoprecipitated proteins were run on an SDS-PAGE gel and transferred to nitrocellulose membranes. Membranes were blotted in 5% milk in PBST. Membranes were probed with one of the following antibodies α-PSD95 (clone K28/43, Upstate), JIP1 (recognizes both JIP1 and 1b; Santa Cruz Biotechnology), or α-myc (for myc tagged JIP2; Invitrogen).

Human brain RT-PCR – Human brain cDNA was used to amplify exon 15 and exon 18 splice variant transcripts using the following primers: 1 = IM160 (5'-TTGTACTGGG

TAGACTCCAAGCTACAC-3'), 2 = IM161 (5'-TAGACATGGCCAATCTGAGCAGT TCTC-3'), and 3 = IM162 (5'-GCACGAAGGGGGTGATCCCATCCTCAG-3'). For primers 1 and 2, expected bands are: +ex15 = 877 bps and Δex15 = 652 bps. For primers 1 and 3, expected bands are: +ex15+ex18 = 1123 bps, +ex15Δex18 = 946 bps, Δex15+ex18 = 898 bps, and Δex15Δex18 = 721 bps.

Targeting vector cloning – The previously described targeting vectors used to create the Apoer2*[±19]* knockin animals (Beffert et al., 2005) were modified to create the Apoer2*[Δ16±19]* targeting vectors. Briefly, exon 16 and some surrounding intronic sequences were deleted from the targeting vectors by using the endogenous BamHI and PmeI restriction sites. The ends were filled in using the Klenow enzyme and blunt end ligated.

ES cell Targeting – See Chapter 2: Materials and Methods

ES cell screening – ES cells were lysed in lysis buffer (1x Soriano PCR buffer, 1.7 μM SDS, 50 ng/ml Proteinase K) at 37°C for 2 hours and the Proteinase K was inactivated at 94°C for 15 minutes. The lysate was added directly to the PCR reaction. Primer IM166 (5'-GAGTTGGTGAAGCTGTGACCTTG-3'), located in the genomic sequence just outside the short arm of the targeting vector, and primer IM108 (5'- TGAAAACCACA CTGCTCGATCCGGAAC-3'), located in the targeting vector sequence between the short arm and the neo gene, were used to find clones positive for homologous recombination.

Animals – Generation of Apoer2*[+19]* and Apoer2*[Δ19]* mice has been previously described (Beffert et al., 2005). These mice as well as the Apoer2 Δ16 mice were housed under a 12 h: 12 h light dark cycle and fed a normal chow diet unless otherwise stated. All animals were euthanized via inhalation of isoflurane according to the National Institutes of Health's Guide for the Care and Use of Laboratory Animals and the UT Southwestern Animal Care and Use Committee.

Apoer2Δ16 knockin animal genotyping – Tail DNA was prepared from animals as previously described. Three primers were used to amplify WT and KI products. The common primer IM305 (5'-CTTCCCTGAGACACCTGTACAGCACTAG-3') is located in the short arm just downstream of exon 16. The WT primer IM379 (5'-AATTCA GTGTCACATGTGTTAGGAC-3') is just downstream of exon 17 and yields a 380 bp band. The KI primer IM380 (5'-TTCCTATTCCGAAGTTCCTATTCTC-3') is located in the targeting vector between the short arm and neo sequence and yields a 600 bp band.

Apoer2Δ16 knockin RT-PCR – Brain tissue was homogenized in 4 ml RNA STAT-60 (1ml/1mg tissue, TEL-TEST, Inc.) using a polytron and incubated for 5 minutes at room temperature. 800 µl of chloroform were added to the homogenate, the sample was shaken vigorously for 15 seconds and incubated at room temperature for 3 minutes. The sample was spun down at 5,200 rpm (rotor JS-5.2, Beckman J-6B centrifuge) for 30 minutes at 4°C. The aqueous phase was removed, added to 2 ml of isopropanol, and incubated at room temperature for 10 minutes. The RNA was precipitated by spinning at 20,000 x g for 20 minutes at 4°C. The pellet was washed with ethanol and dissolved in

RNase free water. DNA was digested from the RNA sample using the DNA-*free*™ Kit (Applied Biosystems). cDNA was prepared using the TaqMan Reverse Transcription Reagents Kit (Applied Biosystems). PCR was used to amplify the region encompassing exon 16 to visualize the lack of expression of exon 16 in the Apoer2Δ16 animals. The primers used were IM372 (5'-ACATGACATTGTAATCTTCCACGAG-3') in exon 14 and IM373 (5'-CTATGTGAAGCTCATCTTCCTCTTC-3') in exon 18. Expected band with exon 16 was 626 bps and expected band without exon 16 was 401 bps.

Membrane fraction preparation – Brain membrane fractions were prepared as described in Chapter 2. 30 μg of protein were run on 8% SDS-PAGE gels and transferred to nitrocellulose membranes. Membranes were blocked with blocking buffer (LI-COR) for one hour at 4ºC. Membranes were probed with the polyclonal rabbit Apoer2 c-terminal antibody (2561) and a monoclonal βIII-tubulin (clone 2G10, Millipore) antibody overnight (4ºC) in LI-COR blocking buffer supplemented with 0.2% Tween-20. Membranes were washed 4 times, 5 minutes each, with PBST. Infrared Dye labeled secondary antibody (gt anti-mouse IRDye 800CW and gt anti-rabbit IRDye 680CW, LI-COR) was diluted 1:10,000 in LI-COR blocking buffer supplemented with 0.2% Tween20 and 0.01% SDS. Membranes were incubated in secondary antibody solution for 1 hour at room temperature. Membranes were washed 4 times, 5 minutes each, in PBST, rinsed once in PBS, scanned and quantitated using the LI-COR Odyssey infrared imaging system. Apoer2 intensity was normalized to βIII-tubulin. At least four animals were used per genotype to assess the Apoer2 brain membrane fraction protein levels. Each genotype was statistically compared to WT using the Student's t-test.

Apoer2 qRT-PCR – mRNA and cDNA was prepared from ½ of a mouse brain using the protocol described above. Real-Time PCR reactions were set up in triplicate using SYBR Green PCR Master Mix (Applied Biosystems). The real time PCR reaction used primers in exon 18 (which is not alternatively spliced and should account for all Apoer2 splice variants): mApoER2ex18-2F (5'-GGTAATAGCCCTGCTATGTATGAGTG-3') and mApoER2ex18-71R (5'-GCTCTTGGTGTTCTTCCGCTT-3'). The resulting Apoer2 CT values were normalized to cyclophilin CT values using the Delta-Delta CT method. At least three animals per genotype were analyzed.

Cell lysate and membrane protein glycosidase treatment – 20 μg of brain membrane fractions or 10 μg of transfected cell lysate were incubated overnight at 37ºC with neuraminidase (New England Biolabs), O-glycosidase (Roche), or PNGaseF (New England Biolabs) according to manufacturer provided protocols. Reactions were then directly used for Western blotting by adding SDS sample buffer and running on an 8% SDS-PAGE gel. Membranes were probed with the rabbit polyclonal Apoer2 c-terminal antibody (2561) and visualized using the LI-COR system. Cell lysate proteins were probed with the rabbit polyclonal Apoer2 exon 19 antibody (204) and visualized using the LI-COR system.

Primary neuron cultures – Timed matings were set up and the pregnant females were euthanized via isoflurane on embryonic day 16 (E16). Five embryo brains were used per preparation. The brain was removed and the cortex and hippocampus were dissected free

from other brain tissue and meninges. All of the cortical and hippocampal tissue from all five brains was place into Hanks' Balanced Salt Solution (HBSS, Gibco). 1/10 volume of trypsin was added and the tissue was incubated at 37ºC for 15 minutes. Trypsin was inactivated by the addition of 1/20 volume of fetal calf serum and the tissue was spun down in a clinical centrifuge. The supernatant was removed and the tissue was incubated in 450 µl of dissociation buffer (12 mM $MgSO_4$, 0.025% DNase (Sigma), 0.4 mg/ml trypsin inhibitor (Roche), and 2 mg/ml BSA (Sigma) in HBSS) at 37ºC for 5 minutes. The tissue was triturated 40 times using a P200 pipette. Complete neurobasal media (5ml, Neurobasal media (Gibco), 1 mM L-glutamine, 2% B27 supplement (Gibco), and 1% Pen/Strep) was added to the cell suspension. Cells were spun down and resuspended in fresh complete neurobasal media**.** Neurons were plated on poly-D-lysine (Sigma) coated 6cm dishes (Corning, Inc.) at a density of $1.5x10^6$ cells per dish and cultured at 37ºC in a 5% CO_2 incubator. Half of the neuron media was changed every four days.

Neuron culture biotinylation – Primary neuron cultures were prepared as described above. The neurons were kept in culture for 7 days before treatment. 1 mg/ml of biotin (Sulfo-NHS-LC-Biotin, Pierce) was dissolved in Wash Buffer I (1x PBS, 0.1 mM $CaCl_2$, 0.1 mM $MgCl_2$). Neurons were washed with ice-cold Wash Buffer I twice on ice and incubated with the dissolved biotin for 30 minutes at 4ºC with gentle shaking. Dishes were washed twice with cold Wash Buffer II (1x PBS, 0.1 mM $CaCl_2$, 0.1 mM $MgCl_2$, 100 mM glycine). 300 µl of 1% TritonX-100 lysis buffer (50 mM Tris pH 7.4, 150 mM NaCl, 1 mM $MgCl_2$, 1 mM $CaCl_2$, 1% Triton X-100, EDTA-free protease inhibitor cocktail) was added to each dish, cells were scraped off, and cellular debris was spun

down at 20,000 x g for 15 minutes at 4ºC. 250 µl of lysate were incubated with 50 µl of NeutrAvidin beads (Thermo Scientific) overnight, rotating at 4ºC. Beads were washed three times with lysis buffer. SDS sample buffer was added to the beads, the beads were boiled and the sample was loaded onto an 8% SDS-PAGE gel.

Primary neuron culture DAPT treatment – Primary neuron cultures prepared as outlined above and were grown in culture for one week. A 20 mM stock of DAPT (*N*-[N-(3,5-difluorophenacetyl)-L-alanyl]-S-phenylglycine t-butyl ester) was prepared in DMSO. DAPT was added to the culture media at a final concentration of 10 µM. After incubation with DAPT for 24hrs, the dishes were washed twice with ice-cold PBS, collected in 1 ml of PBS, spun down and lysed in 50 µl of 1% TritonX-100 lysis buffer (50 mM Tris pH 7.4, 150 mM NaCl, 1 mM $MgCl_2$, 1 mM $CaCl_2$, 1% Triton X-100, EDTA-free protease inhibitor cocktail). Protein concentrations were measured using the Lowry method and 30 µg of protein were run on a 4-15% gradient gel. Membranes were probed with the Apoer2 polyclonal antibody 2561 and visualized using the LI-COR system.

Generation of the Apoer2 extracellular antibody (582) – The Apoer2 ligand binding domain was amplified from mouse cDNA using primers IM423 (5'-GAATTCGGACCA GTCAAGGAGTGTGAAGAG-3', EcoRI) and IM424 (5'-GGATCCTCAAT TTAGCCCACACACTTTCTGAGGCTC-3', BamHI) and cloned into the pMAL-p4x plasmid (New England Biolabs). The Apoer2 maltose binding protein (MBP) fusion protein vector was transformed into E. coli (BL21). 10 ml overnight cultures in Luria

Broth (LB), supplemented with 100 μg/ml ampicillin and 2 g/L glucose, were grown at 37ºC. 5 mls of the overnight culture were used to inoculate 1 L (LB+Amp+glucose) cultures which were grown at 37ºC for approximately 3 hours or until the culture reached an OD of 0.5-0.6. The cultures were induced with the addition of IPTG (isopropyl thiogalactoside, Research Products International Corp.) to a final concentration of 1% and were grown for another 2 hours at 37ºC. Cultures were spun down at 4,000 rpm at 4ºC for 20 minutes (rotor JS-5.2, Beckman J-6B centrifuge). The cell pellet was resuspended in 80 ml buffer S (30 mM Tris pH 8, 20 % sucrose, 1 mM EDTA pH 8, EDTA-free protease inhibitor cocktail) per liter of culture media. The suspension was rotated at room temperature for 10 minutes and spun down at 10,000 rpm at 4ºC for 15 minutes. The pellet was resuspended in 15 ml of ice-cold 5 mM MgSO4, and left to shake on ice for 10 minutes. The suspension was spun down again at 10,000 rpm at 4ºC for 15 minutes and the supernatant was collected and incubated with 3 ml amylose resin (equilibrated in column buffer (20 mM Tris ph 7.4, 200 mM NaCl, 1 mM EDTA pH 7.4)) while rotating for 2 hours at 4ºC. The resin was washed with at least 30 ml of column buffer and the protein was eluted with elution buffer (column buffer supplemented with 10 mM maltose). 1 ml fractions were collected and run on an SDS-PAGE gel. High concentration fractions were pooled together and used for injections. Rabbits were given an initial injection of 500 μg of Apoer2 ligand binding domain-MBP purified fusion protein followed by 250 μg boosts every two weeks. The rabbits were bled every two weeks and serum was collected and tested via Western blotting. The antibody specificity is shown in Figure 3.4.

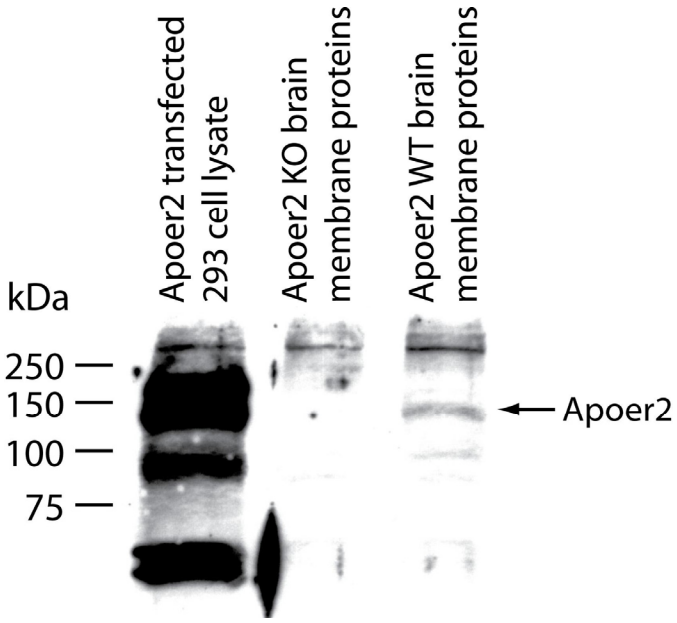

Figure 3.4: Apoer2 extracellular antibody specificity. Lysates from 293 cells transfected with full length Apoer2 constructs as well as brain membrane fractions from Apoer2 KO and WT animals were run on an SDS-PAGE gel, transferred to nitrocellulose and probed with serum (1:1000) from rabbits injected with the Apoer2 ligand binding domain-MBP purified fusion protein. The antibody strongly detects the Apoer2 from transfected cells as well as weaker bands for the endogenous Apoer2 from brain tissue.

Generation of the Apoer2 exon 19 specific antibody (204) – The peptide NH_2-QLPKNPLSELPVVKC-COOH was produced by the UTSouthwestern Peptide Chemistry Lab. This particular peptide sequence is the last 16 amino acids encoded by exon 19. The peptide was conjugated to Imject Maleimide Activated KLH (Pierce) and rabbits were given an initial immunization of 500 µg of conjugated peptide followed by 250 µg boosts every two weeks. Serum was collected every two weeks to check for antibody specificity via western blotting (Figure 3.5).

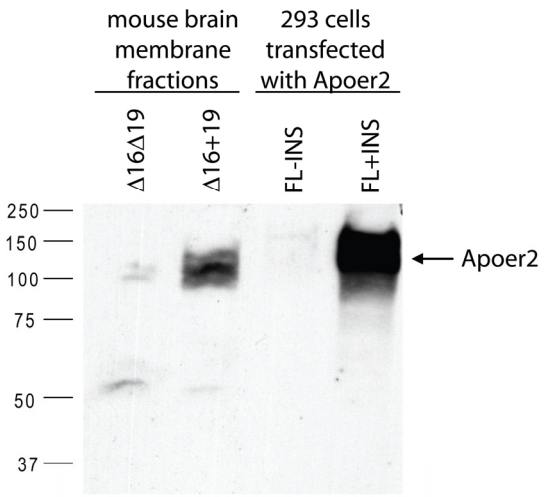

Figure 3.5: Apoer2 exon 19 antibody specificity. Lysates from 293 cells transfected with full length Apoer2(± exon19) constructs as well as brain membrane fractions from Apoer2[Δ16±19] animals were run on an SDS-PAGE gel, transferred to nitrocellulose and probed with serum (1:1000) from rabbits injected with the KLH conjugated Apoer2 exon 19 end peptide. The antibody strongly and specifically detects the Apoer2 splice variant containing exon 19 from both transfected cells and brain membrane fractions.

HEK 293, Neuro2A, CHO-KI, and ldlD cell: cell culture, transfection, and treatment – HEK 293 cells were cultured in DMEM (Sigma) supplemented with 10% FCS at 37°C, 8.8% CO_2. CHO-KI cells were cultured in DMEM/F-12 (50:50, Cellgro) supplemented with 5% FCS at 37°C, 8.8% CO_2. *ldl*D cells were cultured in Hams F-12 media supplemented with 5% FCS and 1% Pen/Strep at 37°C, 5% CO_2. Neuro2A cells were cultured in DMEM (Sigma) supplemented with 10% FCS at 37°C, 8.8% CO_2. All cells were plated on 6cm dishes at a density of 300,000 cells per dish. Cells were cultured for two days before transfection with FuGENE (Roche). Cells were switched to 0% FCS media for 1 hr prior to treatment and subsequently during the treatment. Cells were treated with DAPT (20 mM stock in DMSO, 10 μM final concentration in all

experiments, Sigma), DMSO (Sigma), or PMA (1 mM stock in DMSO, Sigma) 24 hrs after transfection. 24 hours after treatment the cells were washed twice with ice-cold PBS and scraped from the dish into 1ml of PBS. Cells were spun down at 10,000 x g for 3 minutes at 4°C. Cells were lysed in 5 cell volumes of 1% TritonX-100 lysis buffer (50 mM Tris pH 7.4, 150 mM NaCl, 1 mM $MgCl_2$, 1 mM $CaCl_2$, 1% Triton X-100, EDTA-free protease inhibitor cocktail). Cell debris was spun down at 20,000 x g for 15 minutes at 4°C.

Apoer2, ADAM10 and BirA vectors – Apoer2 expression plasmids were modified from the Apoer2 full length vector previously cloned and used in Beffert et al. 2005. In Figure 3.12 the "Apoer2" vector transfected was the original Apoer2 vector from Beffert et al. In all other figures the Apoer2+16+BLRP vector (aka: Apoer2, Apoer2+16, Apoer2+BLRP) was modified by the replacement of the endogenous STOP codon by a spacer region followed by the BLRP. Apoer2Δ16 was the Apoer2+16+BLRP vector with exon 16 deleted. The spacer and BLRP sequences were introduced as overlapping oligos IM428 (5'-AAAAAATTAATTAAGACACCGGTGGAGGAGGTTCAGGTGGTGGAG GATCCGGAATGGCCGGAGGCCTGAACGACATCTTCGAGGC-3') and IM 429 (5'-TTTTTTTTAATTAATCACTCGTGCCACTCGATCTTCTGGGCCTCGAAGATGT CGTTCAGGCCTCCGGCCATTCCGGATCCTCCACCAC-3', containing a new STOP codon after the BLRP). The ADAM10 vector was a gift from Dr. Stefan Lichtenthaler (Lichtenthaler et al., 2003). The BirA vector was a gift from Dr. Dies Meijer (Erasmus University Rotterdam, The Netherlands).

Antibodies – Apoer2 antibodies used: 2561 – rabbit polyclonal c-terminal (affinity purified, 1:500), 204 – rabbit polyclonal exon 19 (serum used to detect all FL and CTF transfected Apoer2 proteins, 1:1000), 582 – rabbit polyclonal extracellular domain (serum used to detect soluble Apoer2, 1:1000). Commercial antibodies used: βIII-tubulin monoclonal (1:10,000, Millipore), β-actin monoclonal (1:2,000, Abcam), anit-HA polyclonal (1:2,000, Sigma).

Cleavage assessment in ldlD cells vs. CHO-K1 cells – Cells were cultured, transfected, and treated as previously described. Results from 6 independent experiments were normalized and analyzed using the LI-COR Odyssey imaging system. Statistical analysis was done using the Student's t-test to compare the CTF fragment accumulation for each lane to the CTF from the CHO-K1 Apoer2+16 no DAPT treatment (lane 5).

NeutrAvidin bead pulldown – 293 cells were cultured, transfected, and lysates were collected as previously described. 300 µg of protein were incubated with 40 µl NeutrAvidin beads (Thermo Scientific) for 2 hours, rotating at 4°C. Beads were spun down at 2,500 rpm for 3 minutes at 4°C. Lysate was removed and beads were washed three times with cold 1% TritonX-100 lysis buffer. SDS sample buffer was added to the beads which were then boiled and used for Western blotting.

Electrophysiological recordings – Brain slices were prepared as described in Chapter 2. LTP recordings were measured as described in Chapter 2. LTP and PPF recordings were performed by Murat Durakoglugil Ph.D.

Morris Water Maze – An established laboratory protocol previously described was closely followed (Beffert et al., 2005). A Morris Water Maze station was set up with a 4 ft in diameter circular aluminum pool filled with 23°C water dyed with white, non-toxic, liquid tempera paint to make the water opaque. A plexiglass escape platform (circular, 10cm in diameter) was submerged in one of the quadrants of the pool (1cm below the level of the water). Various prominent visual cues were placed around the pool. 3-5 month old mice were subjected to four trials per day for 11 days. During each trial the mouse was placed into the pool in one of four starting locations (North, South, East, or West) and allowed to find the submerged platform. Once the mouse found the platform it was left there for 10 seconds before being removed and placed back into the holding cage. If the mouse did not find the platform within 60 seconds it was then guided to the platform and again left for 10 seconds before being removed. On days 5 and 9 the first of the four trials was a probe test (the mouse was allowed to free swim for 60 seconds with the submerged platform removed). On day 12 only the probe test was performed. The movements of the mouse were tracked by video camera and the HSVimage software. Latency to reach the platform and distance traveled to reach the platform were analyzed for each mouse during the 11 day training period. Percent time spent and distance traveled in the goal quadrant (quadrant where the submerged platform used to be) was analyzed for each of the three probe tests. The experimenter was blind to the genotype of the animals.

Results

Δ16 Knockin mouse model

In order to explore the function of exon 16, especially in terms of cytoplasmic tail release and the importance of exon 19, two different ES cell targeting strategies were devised. Before commencing with the knockin mouse line creation, it was important to establish whether the two targeting vectors designed were physiologically relevant in humans. As previously mentioned, both the O-linked sugar domain, encoded by exon 15, and the cytoplasmic insert, encoded by exon 18, are alternatively spliced in humans. cDNA prepared from human brain tissue was subjected to PCR using primers surrounding exons 15 and 18. Figure 3.6 confirms that the O-linked sugar domain is indeed alternatively spliced in human brain. The same is true for the alternatively spliced exon 18 and all four possible permutations of the two alternatively spliced exons (Figure 3.6). Based on the splice products found in human brain, two different targeting vectors

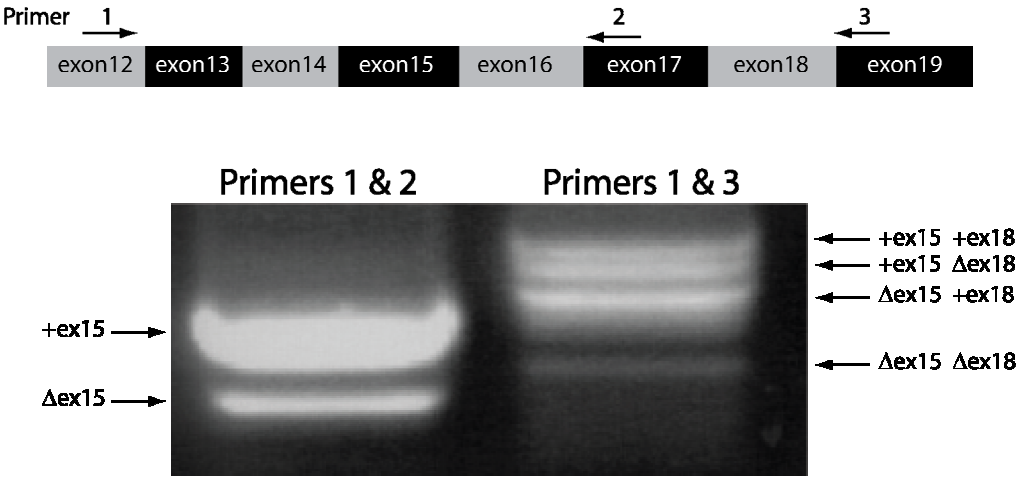

Figure 3.6: Human O-linked sugar domain and Apoer2 tail insert splice products. RT-PCR results confirm that splice products containing all possible permutations of the O-linked sugar domain (exon15) and the cytoplasmic tail insert (exon18) are found in human brain samples.

were created for ES cell homologous recombination knockin mouse generation. Both targeting vectors delete exon 16 from the endogenous Apoer2 locus, however, one vector constitutively expresses exon 19 and the other constitutively lacks the exon (Figure 3.7A).

Figure 3.7B illustrates the WT, full length Apoer2 receptor (Apoer2[*FL*]) domain organization compared to the two mutant Δ16 mouse lines. It should be noted that, the WT mice used for comparisons in the rest of the study are able to alternatively splice both exon 16 and exon 19 thus they do not constitutively express only the full length version of the receptor depicted in the figure. Δ16 animals from both +ex19 and Δex19 lines were bred to homozygosity (Figure 3.7C) and the absence of exon 16 in the transcribed mRNA was confirmed by RT-PCR (Figure 3.7D).

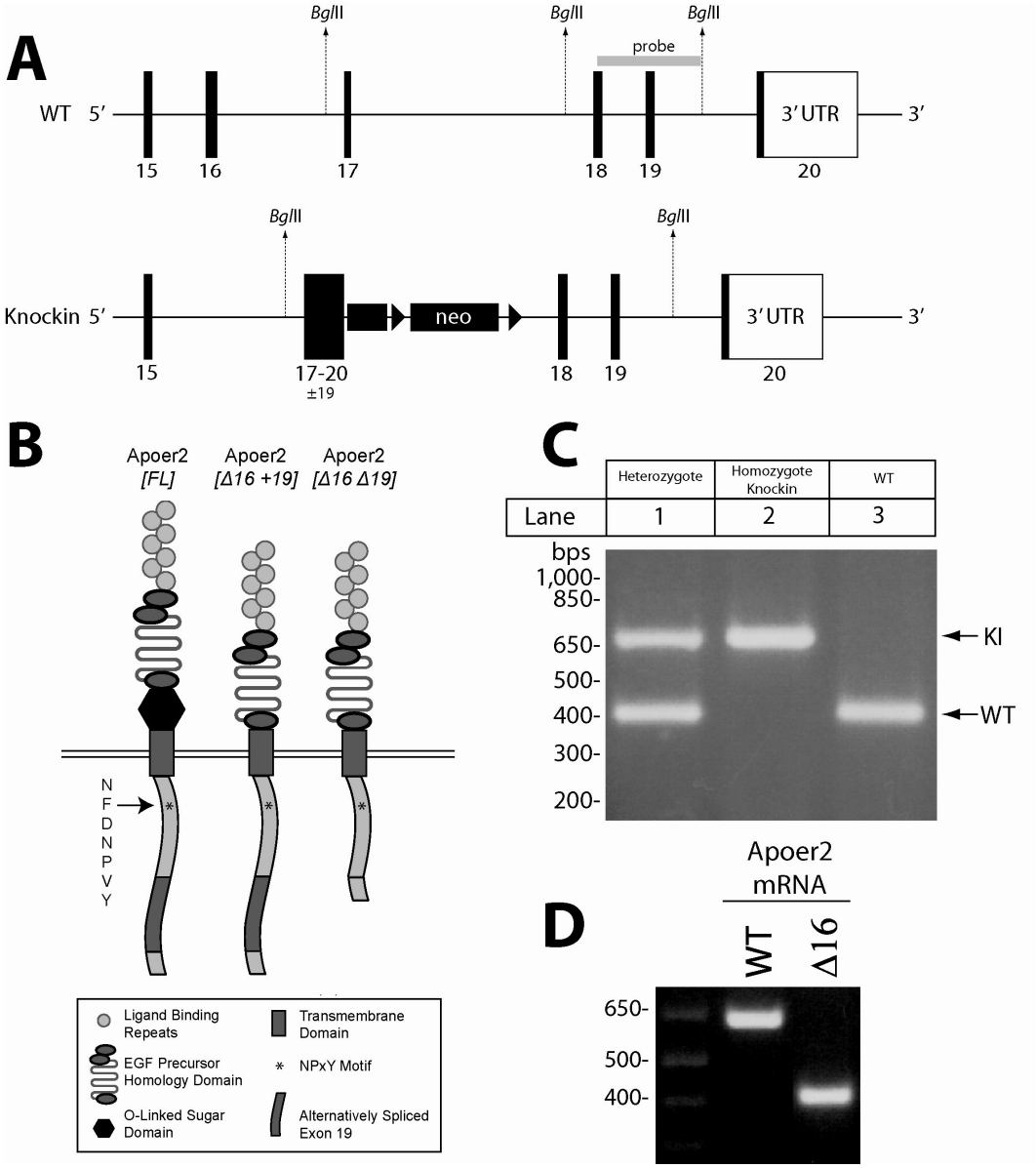

Figure 3.7: Apoer2 Δ16 knockin mutant animal generation. (A) Schematic of the WT and targeted Apoer2 locus with labeled exons. BglII restriction sites were used for Southern blotting using the designated probe to assess homologous recombination. (B) Diagram of Apoer2*[Δ16+19]* and Apoer2*[Δ16Δ19]* knockin mouse lines generated. Apoer2*[FL]* is the WT full length Apoer2 receptor included for comparison. (C) Genotyping example showing WT (400 bp) and KI (665 bp) bands and the achievement of homozygous KI animals. (D) Confirmation of mRNA product lacking exon 16 in the homozygous KI animals. The WT band was expected at 626 bps and the Δ16 knockin at 401 bps.

Hypoglycosylation of Δ16 Apoer2

The O-linked sugar domain, encoded by exon 16, contains multiple serine and threonine residues readily available for the addition of O-linked sugars. In order to confirm that deletion of exon 16 disrupts the O-linked glycosylation pattern of Apoer2, protein from brain membrane fractions was incubated with the glycosidases neuraminidase and O-glycosidase. The addition of sialic acid is a common modification of O-linked sugars and the enzyme O-glycosidase is unable to remove the glycans from the amino acids without prior removal of these sialic acids. Neuraminidase removes sialic acid from sugar chains and thus pretreatment with neuraminidase allows for O-glycosidase removal of O-linked core sugars. The WT Apoer2 protein treated with both glycosidases shows a slight decrease in molecular weight, while there is no band shift in the Δ16 forms of Apoer2 (Figure 3.8). This indicates that, as expected, Apoer2 is hypoglycosylated when lacking the O-linked sugar domain.

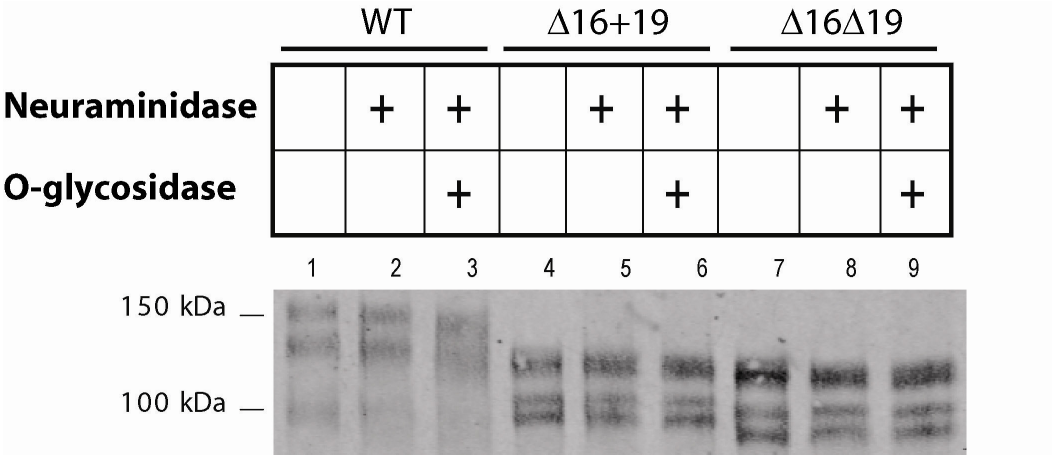

Figure 3.8: Hypoglycosylation of Δ16 Apoer2. Brain membrane fractions from WT animals treated with both neuraminidase and O-glycosidase show a band shift corresponding to the removal of O-linked sugars. Apoer2 protein from either of the Δ16 knockin strains shows no band shift, confirming the requirement of the exon16 coding region for O-linked glycosylation.

Δ16 Apoer2 reaches the cell surface

Glycosylation is important in protein trafficking, folding, and stability (Delacour and Jacob, 2006; Helenius and Aebi, 2004; Watanabe et al., 2004). Thus, it was imperative to confirm that the exon 16 deficient Apoer2, which lacks its usual O-linked sugars, has the ability to make it to the cell surface and is not sequestered in the ER or Golgi. Cell surface proteins in primary neuron cultures prepared from Apoer2*[Δ16±19]* knockin mice were labeled with soluble biotin. Labeled proteins were pulled down from cell lysates using NeutrAvidin beads and run on Western blots. Membranes probed for Apoer2 reveal surface expression of Δ16 Apoer2 (Figure 3.9). These data reveal that even without exon 16 and O-linked glycosylation, Apoer2 is trafficked to the cell surface and protein expression levels are not affected by accumulation of protein within the cell.

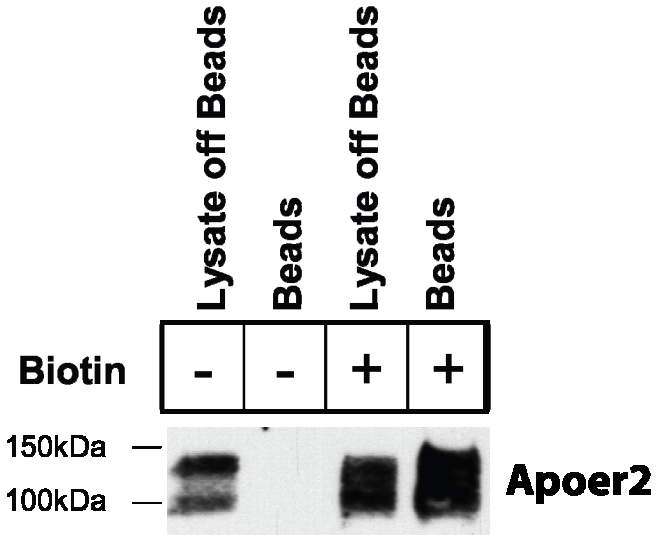

Figure 3.9: Δ16 Apoer2 reaches the plasma membrane in Δ16 KI mice. Surface proteins on primary neurons from Δ16 knockin animals were labeled with soluble biotin. Biotinylated proteins pulled down with NeutrAvidin beads were used in Western blots and probed for Apoer2, confirming Δ16 Apoer2 surface expression.

Brain Apoer2 protein level discrepancies during aging

In the process of working with the Apoer2*[Δ16]* mice, I discovered that Apoer2 protein levels seem to be high in embryonic brain membrane fractions and decrease after birth before leveling out at around three months (Figure 3.10). Apoer2 brain levels are approximately 4-5 fold higher in the embryonic brain at day E16 compared to adult three month old animals. It is still unclear whether or not this change in Apoer2 protein concentrations is physiologically relevant. The Apoer2 protein levels were normalized to the βIII-tubulin neuronal marker, which shows a slight decrease in protein levels with maturation as well, although not nearly as pronounced as Apoer2. It could be that the increase in myelination during the postnatal period may dilute the Apoer2 protein concentrations and give the appearance of Apoer2 downregulation when in fact there is no difference. It would be beneficial to compare the Apoer2 levels with MAP2 as well as Lrp1. However, if this change in Apoer2 expression levels is real, it echoes the decrease in Reelin levels after birth. It also generally correlates with the change in the Reelin expression pattern as well as the change in NMDA receptor subunit 2B expression during maturation (Monyer et al., 1994; Sinagra et al., 2005).

This observation is particularly important for the next section discussing Apoer2 levels in the various mutant mice. To avoid any misleading results in Apoer2 protein levels due to age differences, carefully age matched mice were used for the following experiments.

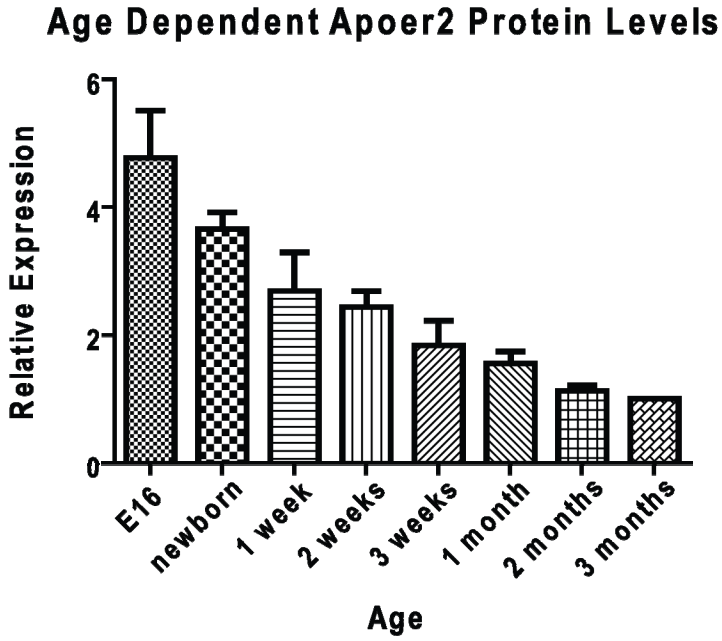

Figure 3.10: Brain Apoer2 protein level discrepancies during aging. Brain membrane fractions prepared from 4-7 mice of various ages were used in Western blots to determine Apoer2 protein expression levels. The protein levels were normalized first to βIII-tubulin and then compared to the three month old animal levels.

Increased mRNA and protein levels in Δ16 mice

I initially hypothesized that Apoer2*[Δ16]* mice would have less Apoer2 protein due to increased cleavage/processing of the receptor. If the protein lacks the O-linked sugar domain, it cannot be glycosylated. Without glycosylation, the receptor is not protected form proteolytic cleavage and the stability of the receptor is decreased. This hypothesis was based on previous *in vitro* data showing that lack of exon 16 increases Apoer2 cleavage as measured by the enhanced activation of a luciferase reporter gene by the released Apoer2 ICD in transfected cells (May et al., 2003).

Brain membrane fractions were prepared from WT, Apoer2*[Δ16+19]*, and Apoer2*[Δ16Δ19]* animals. Equal amount of protein from each genotype was run in Western blots and probed with an antibody against the cytoplasmic tail of Apoer2. Initial results revealed increased protein levels in both of the mutant mouse lines (Figure 3.11A). This increase in protein levels immediately contradicted the previous reporter gene data. Increased Apoer2 levels could be explained as a direct result of the elimination of a metalloprotease extracellular cleavage site by the deletion of exon 16. Thus, even when glycosylation of the receptor is prevented, if the cleavage site required for proteolytic processing is eliminated, the protein will become stabilized. This makes sense, if glycosylation does indeed protect the extracellular domain from cleavage, the cleavage site should be located close to glycosylation sites and the O-linked sugar domain would be a logical location. The difference between the increased cleavage seen with the luciferase *in vitro* data and the results from the knockin animals was initially attributed to cell specificity and environmental conditions. There are many different metalloproteases. Perhaps different proteases are produced in the HEK 293 cell cultures versus the heterogeneous cell populations in the intact brain. Different proteases may cleave at different locations and under different circumstances, thus in cultured 293 cells, deletion of exon 16 could enhance cleavage from a different cleavage site than that which is used in neurons.

The Apoer2*[+19]* and Apoer2*[Δ19]* animals are important controls for the Apoer2*[Δ16+19]* and Apoer2*[Δ16Δ19]* mice because it is critical to differentiate

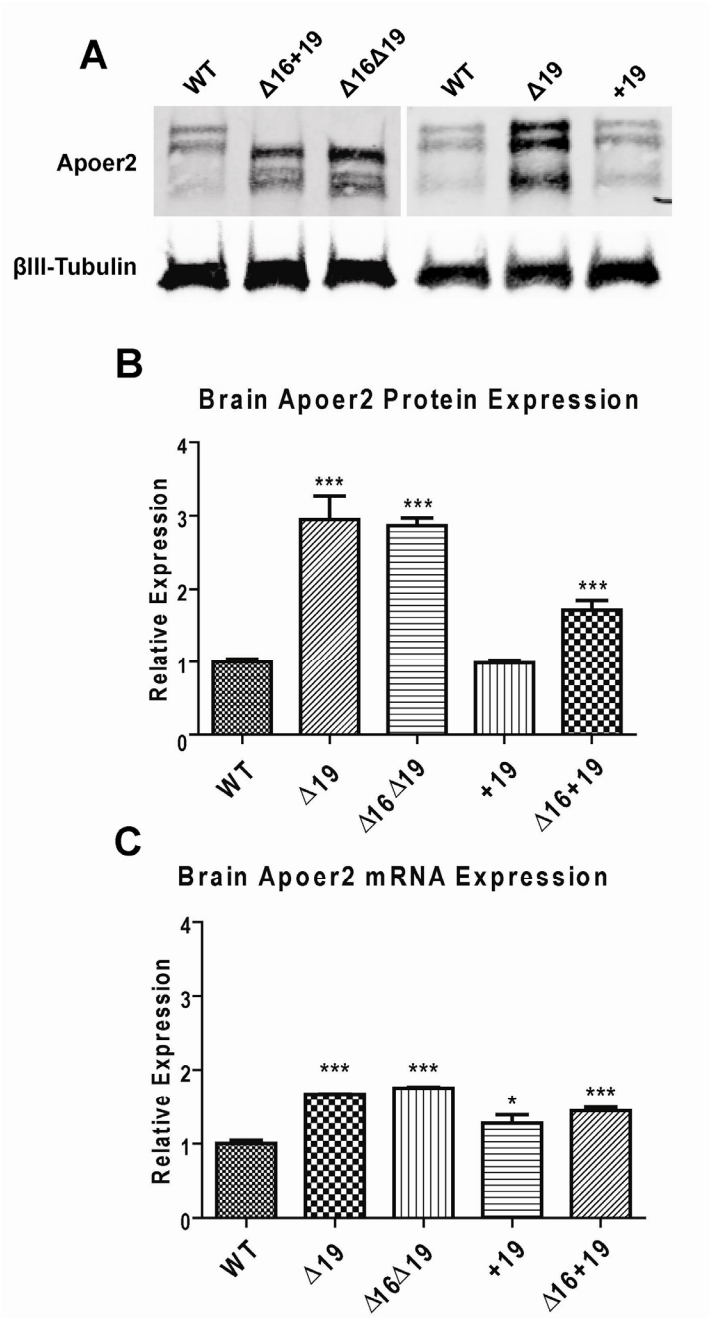

Figure 3.11: Increased protein and mRNA levels in Apoer2 KI mice. (A) Western blots of brain membrane fractions probed for Apoer2 and βIII-tubulin reveal increased Apoer2 protein levels in Apoer2*[Δ16+19]*, Apoer2*[Δ16Δ19]*, and Apoer2*[Δex19]* animals. (B) Quantification of brain membrane Apoer2 expression levels. (C) qRT-PCR results show increased mRNA levels of all splice variants of Apoer2 in knockin animals compared to WT. *** $p < 0.0001$, * $p < 0.05$

which phenotypes are mediated by exon 16 and which are regulated by exon 19. Thus, Apoer2 protein levels were also assessed in Apoer2*[+19]* and Apoer2*[Δ19]* mice (Figure 3.11A). The result was surprising. Not only do the Apoer2*[Δ16±19]* mice show a 2-3 fold increase in protein levels when compared to WT, the Apoer2*[Δ19]* mice do as well, even though they express exon 16 normally. The increase was just as high in the Apoer2*[Δ19]* mice as it was for the Apoer2*[Δ16Δ19]* mice (Figure 3.11B). This result was confirmed by a similar increase in mRNA levels in both the Apoer2*[Δ16Δ19]* and Apoer2*[Δ19]* mouse lines (Figure 3.11C). I conclude that the increase in Apoer2 protein levels in both Apoer2*[Δ16Δ19]* and Apoer2*[Δ19]* animals is not mediated by exon 16, but instead likely through the loss of function of exon 19. Mice lacking exon 19 can no longer mediate NMDAR phosphorylation/activation. Consequentially, the brain may upregulate Apoer2 production in an attempt to compensate for the loss of function. Therefore, in both lines which are missing exon 19, there is an equal increase in Apoer2 protein and mRNA levels.

Unlike the Apoer2*[Δ19]* mice, Apoer2 protein levels in the Apoer2*[+19]* are identical to WT. However, there is a 2 fold increase in Apoer2 protein expressed in the Apoer2*[Δ16+19]* mice. Interestingly, while there is a difference in protein levels, there is no significant difference in mRNA levels between the two mouse lines constitutively expressing exon 19. This suggests that the increase in Apoer2 protein in the Apoer2*[Δ16+19]* animals is mediated by exon 16. It is important to recognize that the increase in protein in the Apoer2*[Δ16+19]* mice is significantly less than that for either of the mouse lines lacking exon 19 ($p < 0.05$). Based on these data I would assume that different mechanisms are responsible for the increase in Apoer2 levels in the mice

lacking exon 19 verses the Apoer2*[Δ16+19]* animals. It was now important to figure out what properties the Δ16+19 splice variant embodied that would be responsible for this increase in protein levels.

Deletion of exon16 prevents specific extracellular Apoer2 cleavage in vivo

Although the Δ16 knockin mice show increased Apoer2 levels, it does not confirm that the receptor does not get cleaved *in vivo*. Data from previous studies revealed that the cleaved Apoer2 CTF is present in WT neuron cultures. However, it was still unclear whether the Apoer2 variant lacking exon 16 was sensitive to proteolytic cleavage *in vivo* as suggested by the luciferase assay (May et al., 2003). Primary neurons were cultured from WT, Apoer2 KO, Apoer2*[Δ16+19]*, Apoer2*[Δ16Δ19]*, and Apoer2*[Δ19]* mice. The neurons were kept in culture for one week before treatment with the γ-secretase inhibitor, DAPT, for 24hrs. DAPT was added to these cultures in order to get an accumulation of the CTF band that would be visible on Western blots and could give an indication as to whether or not the extracellular domain of Apoer2 was undergoing proteolytic processing. Also, DAPT sensitivity confirms that the band in question is a γ-secretase substrate, what we would expect for the Apoer2 CTF. The DAPT treated neuronal lysates were used in Western blots and were probed with the Apoer2 C-terminal antibody. WT neurons show a DAPT dependent increase in two bands, ~19kDa and ~15kDa, corresponding to the c-terminal fragment with and without the alternatively spliced exon 19 respectively (Figure 3.12). As expected Apoer2 null mice showed no bands reactive to the Apoer2 antibody. In lanes 9 and 10, the Apoer2*[Δ19]* neuron lysates show a DAPT dependent increase in the Δ19 form of the

CTF. Because the Apoer2*[Δ19]* mice do not express a variant containing the cytoplasmic exon, only the bottom band is present. Interestingly, in the lanes containing lysates from Apoer2*[Δ16+19]* and Apoer2*[Δ16Δ19]* neurons, there was only a faint laddering of bands in the 15-25 kDa range and the bands were not DAPT sensitive. This suggests that without exon 16, the specific extracellular cleavage of Apoer2 creating a γ-secretase substrate does not occur. There does seem to be some receptor processing because there are low molecular weight bands which are reactive to the Apoer2 antibody. However, due to the smearing/laddering effect this cleavage most likely does not take place at the preferred extracellular cleavage site and instead at some secondary and non-specific locations within the EGF precursor homology domain.

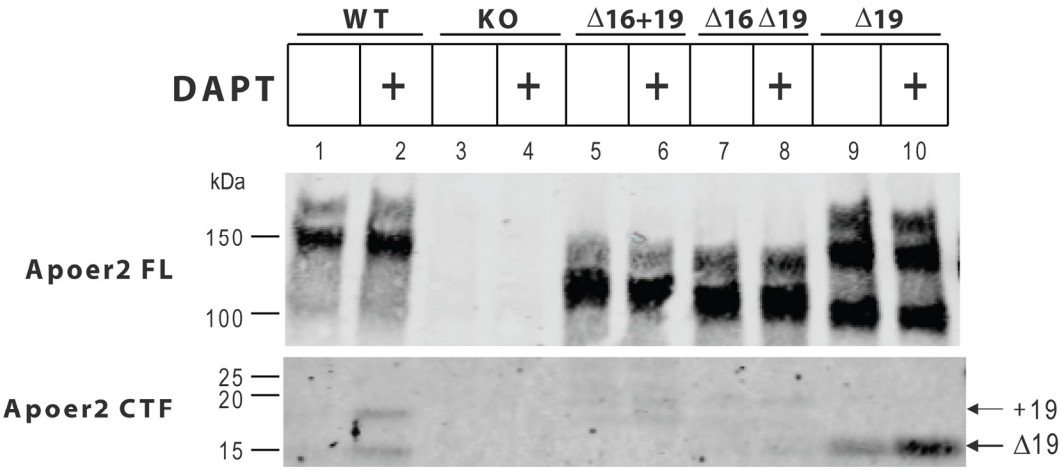

Figure 3.12: Lack of exon16 inhibits specific Apoer2 extracellular cleavage in neurons. Primary cortical neurons from Apoer2 WT, KO and KI mutant animals were treated with and without DAPT. WT neurons reveal accumulation of the CTF with and without exon19. Apoer2[Δ19] mice show only the CTF lacking exon19. The Δ16 mutants show weak laddering of bands suggesting nonspecific extracellular cleavage that is not sensitive to DAPT treatment.

Apoer2 is proteolytically processed in transiently transfected cells

Because the current *in vivo* data contradict previously published luciferase reporter assay results, I used transiently transfected 293 cells in an attempt to reproduce my primary neuron results. First I needed to confirm that proteolytic processing occurs in culture in non-neuronal cell lines by directly using Western blots instead of luciferase assays. HEK 293 cells were transfected with Apoer2 and the metalloprotease ADAM10. Using the newly generated antibodies against exon 19 and the extracellular ligand binding domain of Apoer2 (see Chapter 3: Materials and Methods), 293 cell lysates and media were assayed for accumulation of the CTF and extracellularly cleaved fragment of the receptor. Without any treatment, there was a band corresponding to the C-terminal fragment of Apoer2 at ~24kDa (Figure 3.13, lane 1). The size of this CTF is slightly larger than the endogenous Apoer2-CTF because it contains a biotin ligase recognition sequence at the C-terminal end whose function will be discussed later in this chapter. A band for the soluble Apoer2 was also apparent in the media using the extracellular Apoer2 antibody. ADAM10, the metalloprotease previously shown to cleave the extracellular domain of Apoer2, did indeed increase the accumulation of soluble Apoer2 (sApoer2) as well as the CTF (Figure 3.13A, lanes 1 and 2). This confirms that Apoer2 is a specific substrate for ADAM10 and that Apoer2 proteolytic processing functions as expected in transiently transfected 293 cells.

Previous data from the lab had shown that a fellow family member, Lrp1, is proteolytically processed in a similar manner as Apoer2 and that activation of PKC by phorbol esters stimulates Lrp1 ectodomain shedding (May et al., 2002). Similarly to Lrp1, Apoer2 extracellular cleavage is significantly enhanced by treatment with the

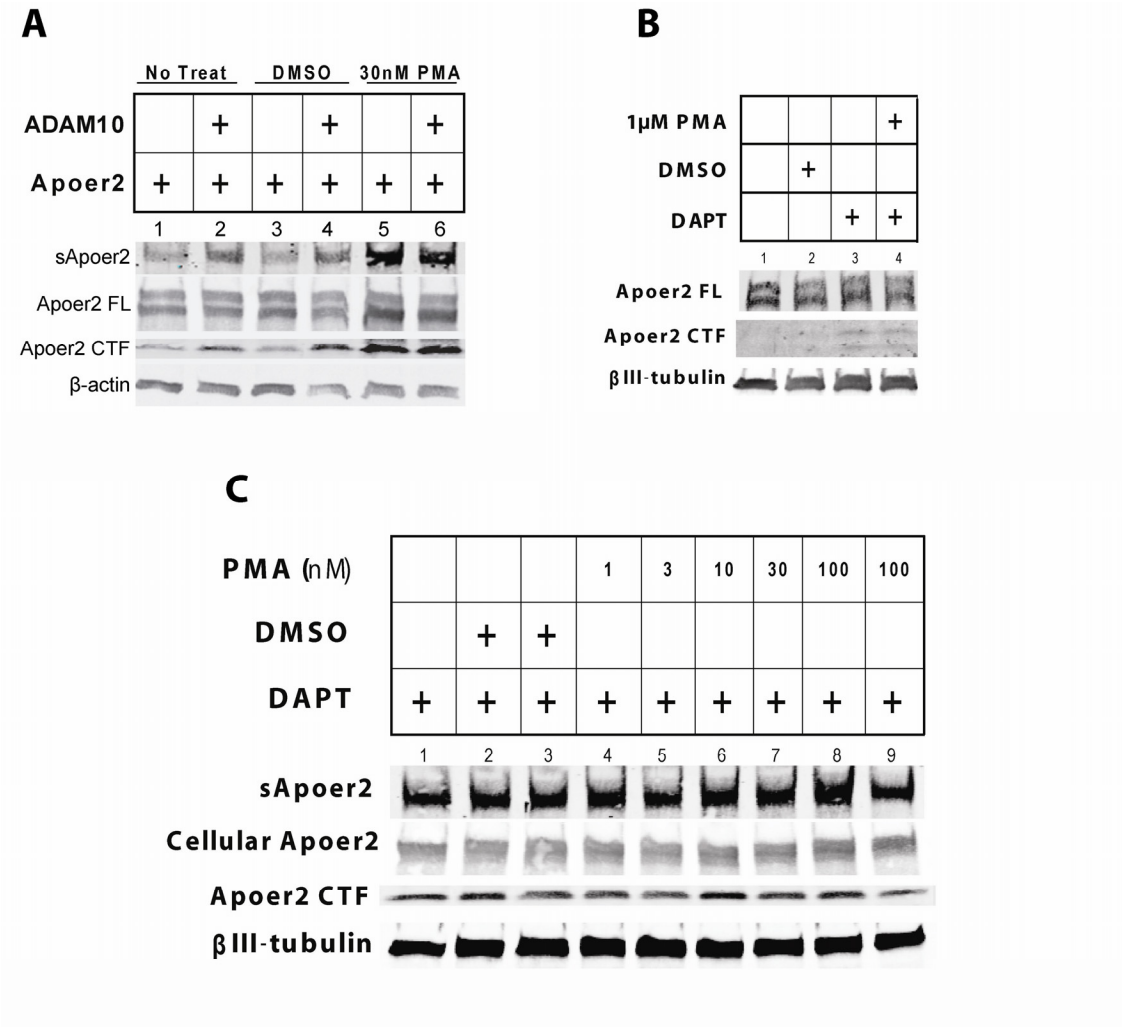

Figure 3.13: Extracellular cleavage of Apoer2 is mediated by PKC activation only in 293 cells. (A) 293 cells transfected with Apoer2 and ADAM10 were left untreated or were treated with vehicle (DMSO) or 30 nM PMA. PMA treatment increased both soluble Apoer2 levels and Apoer2 CTF accumulation. DAPT was present in all conditions. (B) Apeor2 processing in primary neurons was unaffected by PMA treatment. (C) Neuro2A cells were transiently transfected with Apoer2 and treated with PMA. Just as in the primary neurons, PMA had no effect on Apoer2 extracellular domain release or CTF accumulation.

phorbol ester PMA (phorbol 12-myristate 13-acetate) as is apparent by the increase in soluble Apoer2 and the production of the small γ-secretase substrate (Figure 3.13A, lanes 5 and 6). Vehicle (DMSO) control for PMA showed no increase in proteolytic processing (Figure 3.13A, lanes 3 and 4). This same result in transfected COS7 cells has been shown by Hoe et al., 2005. However, I attempted to reproduce the PMA stimulated CTF accumulation experiments in primary neuron cultures as well as the transiently transfected neuroblastoma cell line Neuro2A. PMA treatment did not affect extracellular cleavage or CTF accumulation in either of these cell types (3.13B, C). This leads to the conclusion that in the endogenous CNS environment, typical PKC activation may not play a role in increasing proteolytic processing as it had been assumed.

Deletion of exon16 prevents specific extracellular Apoer2 cleavage

Knowing that the Apoer2 CTF cleavage can be reproduced in transfected cells, an Apoer2 construct with exon 16 deleted was cloned that mimicked the Apoer2 produced by the Apoer2*[Δ16+19]* mice. This new Δ16 construct was also transfected into 293 cells to see if there is proteolytic processing of the receptor yielding increased extracellular domain cleavage and increased CTF accumulation as suggested by previous luciferase reporter assay results. However, the opposite result, no specific extracellular cleavage or CTF accumulation, would confirm *in vivo* data from the primary neuron cultures using the knockin animals. Apoer2 constructs with and without exon 16 were transfected into 293 cells and expressed in the presence or absence of DAPT. As see in Figure 3.14, Apoer2+16 showed an accumulation of the γ-secretase sensitive CTF fragment under DAPT treatment as expected (Figure 3.14, lane 3). However,

reproducing the primary neuron culture data, transfection of the Apoer2Δ16 construct resulted in a laddering of small molecular weight (35-25kDa) bands indicative of non-specific cleavage of the extracellular domain. It is also debatable that some of these products may be cleaved non-preferentially by γ-secretase and thus a very slight increase in the laddered bands can be seen when the cells are cultured in the presence of DAPT.

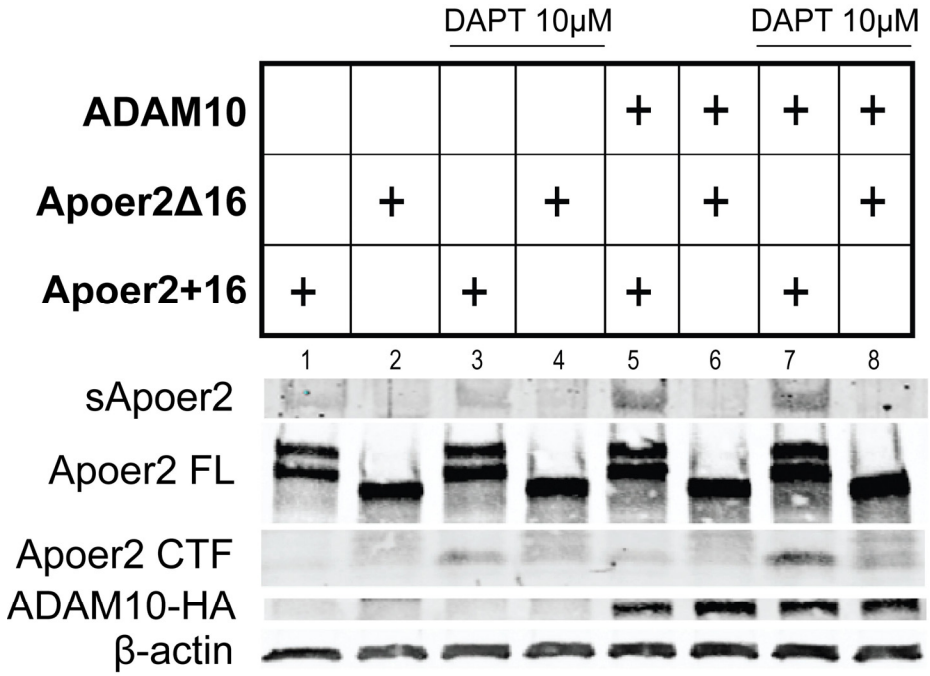

Figure 3.14: Deletion of exon 16 prevents specific extracellular Apoer2 cleavage. 293 cells transfected with Apoer2+16 show specific extracellular cleavage of the full length protein resulting in DAPT sensitive accumulation of the CTF as well as an increase in soluble Apoer2 independent of DAPT treatment. Cells transfected with Apoer2Δ16 show a smear suggesting multiple nonspecific cleavage products of the full length receptor. ADAM10 transfection increased the appearance of soluble Apoer2 (sApoer2) as well as the CTF.

I believe this accumulation to be non-specific as increased CTF accumulation is accompanied by increased extracellular cleavage and there is virtually no soluble Apoer2 cleavage product seen in lanes 2 and 4. Thus, the laddering of the small molecular weight bands is probably due to nonspecific degradation/processing of the receptor in the absence of regulated processing.

These data do not entirely contradict the conclusions previously published stating that deletion of exon 16 stimulates ICD release as measured by luciferase reporter gene activity. It is very likely that the low molecular weight laddered bands formed by non-specific cleavage of the receptor may still be released from the plasma membrane and have the ability to translocate to the nucleus and activate the reporter gene. This however, is not a measure of the specific proteolytic processing of the receptor and unlike the reporter gene assay, the Western blot analyses give more specific results that have now been duplicated in both transfected cells and primary neurons.

Glycosylation of Apoer2 protects against proteolytic processing

The study by May et al. (2003), used *ldl*D cells which are mutant CHO-K1 derived cells deficient in the enzyme UDP-N-acetylgalactosamine 4-epimerase. This enzyme is responsible for generating galactose which is used in N-acetylgalactosamine containing N- and O-linked sugars. N-acetylgalactosamine is commonly the first sugar residue found in O-linked sugar chains added to serine and threonine residues. May et al. again used the luciferase reporter gene assay to look for ICD release under the conditions of hypoglycosylation of the O-linked sugar domain in the *ldl*D cells. The luciferase reporter gene assay has proven to be somewhat misleading in the assessment of specific

proteolytic processing and thus Western blot analysis of cleavage of Apoer2 in these cells was performed (Figure 3.15).

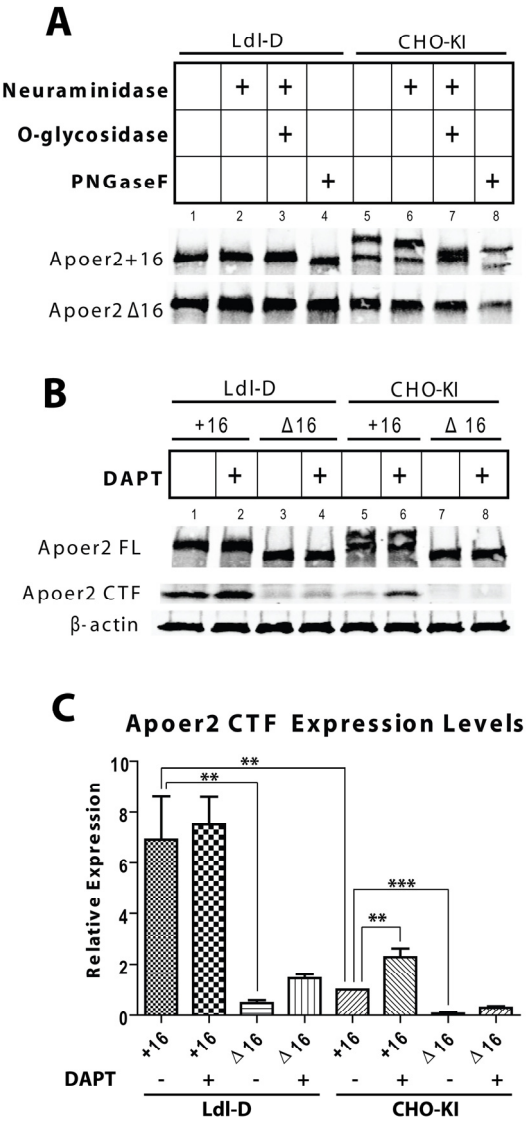

Figure 3.15: Glycosylation of Apoer2 protects against cleavage. (A) Lysates from *ldl*D cells transfected with Apoer2 and treated with various glycosidases confirm that Apoer2 glycosylation is severely impaired. Lysates from CHO-K1 cells transfected with Apoer2 and treated with various glycosidases show the removal of both N- and O-linked sugars. (B) Representative blot showing that decreased glycosylation of Apoer2 from transfected *ldl*D cells increases the accumulation of the C-terminal fragment when exon 16 is present. (C) Quantification of Western blot results in (B). ** $p<0.001$, *** $p<0.0001$

First, the Apoer2+16 and Δ16 constructs were expressed in both *ldl*D and WT CHO-K1 cells and glycosylation of the receptors was observed. Lysates were subjected to glycosidase treatments using the enzymes neuraminidase, O-glycosidase, and PNGaseF. PNGaseF is one of the most versatile glycosidases which can remove nearly all N-linked sugar chains. The Apoer2Δ16 protein expressed from either cell type was hypoglycosylated based on the results that there was no band shift after any of the glycosidase treatments (Figure 3.15A). This is expected and agrees with the results from the glycosidase treatment of brain membrane fractions from Apoer2*[Δ16]* animals. Conversely, the Apoer2+16 construct was highly glycosylated and contained both N- and O-linked sugars when expressed from the CHO cells. Various band shifts were observed in all treatment conditions (Figure 3.15A, Apoer2+16 lanes 5-8). On the other hand, even though Apoer2+16 contains the O-linked sugar domain, it was hypoglycosylated when expressed from *ldl*D cells. This was deduced by a lack of any band shifts when treated with neuraminidase and O-glycosidase. There is a small shift in mobility of the Apoer2+16 protein expressed from *ldl*D cells when treated with PNGaseF. This suggests that the 4 asparagines encoded by exon 16 are glycosylated, however, when expressed from the *ldl*D cells, the sugars do not contain any N-acetylgalactosamine monosaccharide components.

Hypoglycosylation of the Apoer2+16 protein expressed by *ldl*D cells led to a seven fold increase in the CTF accumulation (Figure 3.15B, C) when compared to the CTF levels in the CHO-K1 transfected cells which exhibit normal Apoer2+16 glycosylation. Apoer2Δ16 showed lower accumulation of low molecular weight bands compared to normally glycosylated Apoer2+16 when expressed from either cell line.

Again, this is most likely non-specific processing/degradation of the receptor. From these data I can conclude that in transfected cells, glycosylation of the O-linked sugar domain protects the extracellular domain from cleavage and the production of the γ-secretase CTF substrate. Because there was virtually no specific cleavage of the Apoer2Δ16 protein, even in the absence of glycosylation, suggests that there must be a specific cleavage site within exon 16 that is recognized by proteases such as ADAM10 which mediate ectodomain shedding and initiate proteolytic processing of the receptor.

Use of in vivo biotinylation to purify the Apoer2 CTF for N-terminal sequencing

An *in vivo* biotinylation system using the BirA biotin ligase cloned from *E. coli* and biotin ligase recognition peptide (BLRP) tagged proteins enables the specific biotin tagging of desired proteins inside a cell (Beckett et al., 1999; Tsao et al., 1996). I employed this *in vivo* biotinylation technique in an attempt to purify the Apoer2 CTF for sequencing of the N-terminal end. This would allow for the determination of whether the extracellular cleavage site of Apoer2 is indeed located in the region encoded by exon 16. A BLRP was fused to the C-terminal end of Apoer2+16. This Apoer2+BLRP construct was then transfected into 293 cells along with a plasmid encoding the BirA enzyme (Figure 3.16).

BirA-HA expression was detected by an anti-HA antibody. Both lanes transfected with BirA and the Apoer2+BLRP resulted in the biotinylation of the receptor as seen by the detection of the protein (both full length and the CTF) in the pulldown using NeutrAvidin beads. Specific labeling of the receptor with biotin along with high affinity binding of biotin to the NeutrAvidin beads made this technique highly desirable

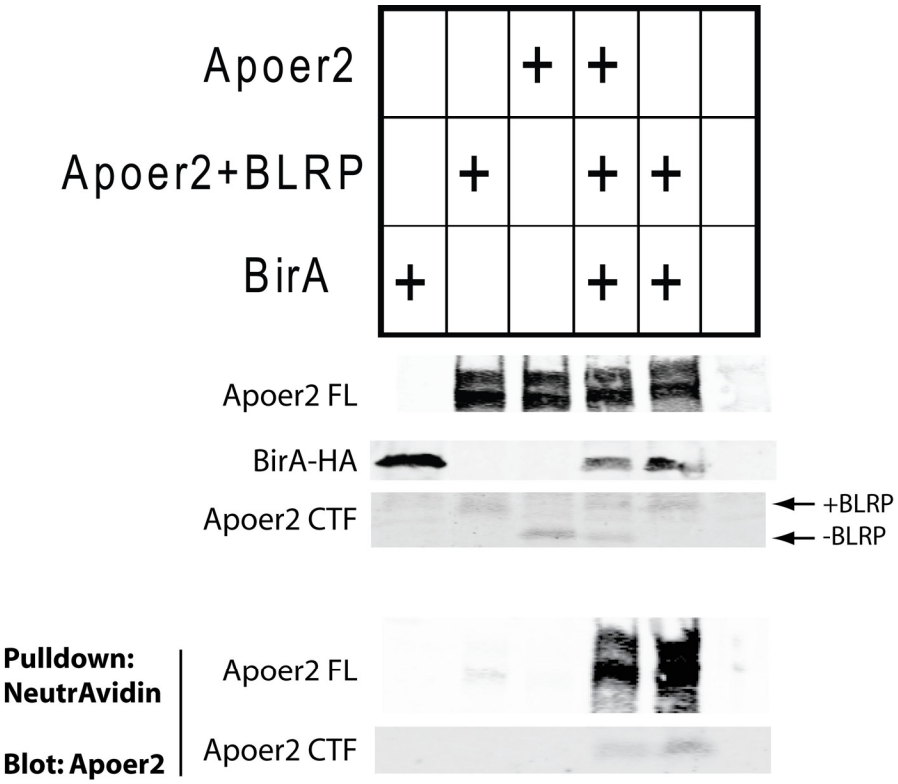

Figure 3.16: In vivo biotinylation of Apoer2 using the biotin ligase BirA. 293 cells were transfected with Apoer2+16 with and without the biotin ligase recognition peptide (BLRP) along with the BirA biotin ligase. The BirA protein is HA tagged and expression was detected by blotting with an antibody against HA. Full length Apoer2 and the CTF (higher band corresponds to Apoer2 with the BLRP and the lower without) were detected using the Apoer2 exon 19 specific antibody. The same lysates were incubated with NeutrAvidin beads which specifically pulled down biotinylated FL Apoer2 and CTF as detected using the Apoer2 exon 19 antibody.

for the purification of the C-terminal fragment. Previous attempts in using polyclonal Apoer2 antibodies to purify the C-terminal fragment failed due to low affinity binding of the antibody and low yields.

However, co-transfection of the Apoer2+BLRP and BirA into 293 cells did not yield sufficient protein and was neither detectable on the membrane using amido black

staining, or enough for sequencing. PMA treatment in 293 cells was also attempted but did not enhance the yield enough. I switched to using the *ldl*D cells which had previously shown an 8 fold increase in CTF production over regular CHO-KI cells in an attempt to enhance yield. Unfortunately this was not sufficient either. It seems as though the limiting step is a combination of incomplete biotinylation as well as insufficient receptor cleavage.

Apoer2Δ16 animals show defects in Reelin stimulated LTP induction

Results observed in our laboratory concerning the involvement of Apoer2 and Vldlr in Reelin signaling strongly suggest that stoichiometry of receptors in the synapses may be crucial for normal brain function (unpublished data). The Apoer2Δ16 animals showing a 2-3 fold increase in Apoer2 protein levels have the potential to severely affect receptor stoichiometry in the synapse. Thus, my next objective was to see how increased Apoer2 levels in the brain may affect synaptic function. Brain slices from Apoer2*[Δ16+19]* and Apoer2*[Δ16Δ19]* animals were used in the measurement of theta burst (TBS) induced NMDA receptor dependent CA1 region hippocampal LTP induction with and with out Reelin stimulation. Recall that in WT mice, Reelin stimulation increases LTP induction in this region of the hippocampus.

At the time of writing this thesis, electrophysiology results showed that slices from Apoer2*[Δ16Δ19]* animals had normal baseline LTP induction (Figure 3.17B). Upon Reelin treatment, the Apoer2*[Δ16Δ19]* slices were unable to induce the Reelin stimulated increase in LTP. This result is identical to the response that Apoer2*[Δ19]* slices have to Reelin stimulation.

Contrary to Apoer2*[Δ16Δ19]* slices and established WT data, Apoer2*[Δ16+19]* animals had increased baseline LTP without Reelin stimulation (Figure 3.17A). This was

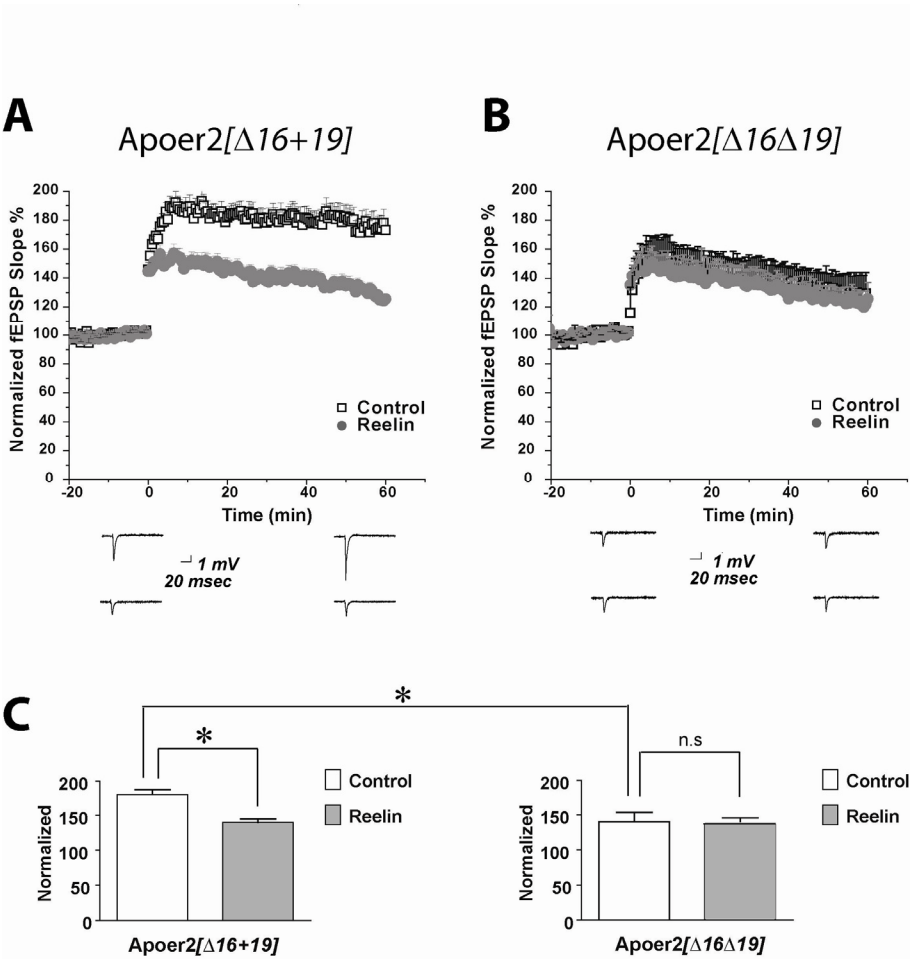

Figure 3.17: Apoer2Δ16 animals show defective Reelin-stimulated LTP induction. (A) Apoer2*[Δ16+19]* brain slices were used to measure CA1 hippocampal LTP induction (TBS induced at time 0) in the presence and absence of Reelin. These mice show increased baseline LTP which is brought to WT baseline levels after Reelin treatment. Upper traces are without Reelin, lower with Reelin. Left traces are before TBS, right traces, after TBS. (B) Apoer2*[Δ16Δ19]* brain slices were also used to measure CA1 hippocampal LTP induction in the presence and absence of Reelin. Baseline LTP was normal but Reelin failed to increase LTP induction just like in Apoer2*[Δ19]* slices. (C) Baseline LTP at 30 minutes in the Apoer2*[Δ16+19]* slices was significantly increased over LTP induced in Reelin treated Apoer2*[Δ16+19]* slices and untreated baseline LTP in Apoer2*[Δ16Δ19]* slices. * $p < 0.01$

approximately a 40% increase over normal baseline LTP, which is a result normally expected of Reelin stimulated slices. When the Apoer2*[Δ16+19]* slices were stimulated with Reelin the LTP induction came back down to WT baseline levels. This is the complete opposite result that is achieve with the Apoer2*[+19]* mice. In these mice, untreated slices show normal baseline LTP and only after Reelin treatment is there an increase in LTP induction (Beffert et al., 2005).

The LTP induction of untreated and Reelin treated slices was significantly different at 30 minutes for the Apoer2*[Δ16+19]* animals (Figure 3.17C). There was no difference between Reelin treated and untreated LTP induction in the Apoer2*[Δ16Δ19]* mice. These data suggests that, in the absence of exon 19, the alternatively spliced O-linked sugar domain has no affect on synaptic function and does not compound the phenotypes already seen from loss of exon 19. Loss of exon 19 seems to be the dominant mutation. On the other hand, if exon 19 is expressed, the loss of exon 16 complicates the regulation and function of Apoer2 through a mechanism that is yet to be explained.

In order to get a better idea of how exon 16 is affecting exon 19 mediated LTP modulation, input/output (I/O) curves were plotted for both of the Δ16 knockin mutant mouse lines (Figure 3.18A). Comparing I/O between the two lines shows that baseline synaptic transmission measured from the hippocampal CA1 stratum radiatum region seems to be significantly different between the two mouse lines. The Apoer2*[Δ16+19]* slices have an increased input/output ratio over the Apoer2*[Δ16Δ19]* slices (Figure 3.18A).

Paired pulse facilitation (PPF) was measured in the Δ16 animals to see if exon 16 deletion may have an impact on short term synaptic plasticity in the presence or absence of exon 19. Preliminary data reveal statistical significance only at the 50 ms interval between WT and Apoer2*[Δ16+19]* animals (Figure 3.18B). There is no difference between WT and Apoer2*[Δ16Δ19]* animals. Although the difference in PPF between the Apoer2*[Δ16+19]* mutants and WT animals is small, a presynaptic effect cannot be

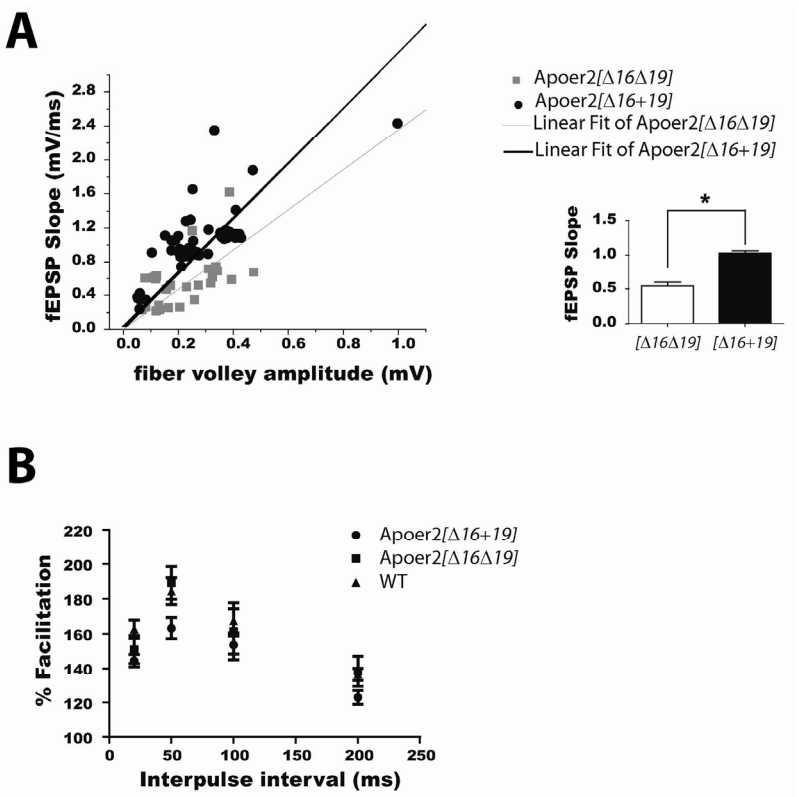

Figure 3.18: Synaptic transmission and PPF in Apoer2 Δ16 mice. (A) I/O plotted for Apoer2*[Δ16+19]* and Apoer2*[Δ16Δ19]* animals shows a significant difference in baseline synaptic transmission between the two mouse lines. Slope level I/O data fitted by linear regression model. * $p < 0.01$ (B) Preliminary paired pulse facilitation data reveals comparable short term synaptic plasticity between both Apoer2Δ16 mouse lines and WT mice. Inter pulse intervals of 20, 50, 100 and 200 ms were used. The 50 ms interpulse interval is the only interval at which there is a statistically significant difference between WT and Apoer2*[Δ16+19]* animals ($p < 0.05$).

entirely ruled out. Beffert et al., also saw a slight decrease in PPF, however, it was in the Apoer2*[Δ19]* animals. Even though Apoer2 is expressed in the postsynaptic density there is a possibility that through an unknown mechanism it may affect presynaptic function (Beffert et al., 2005).

Apoer2Δ16 animals show no significant deficiencies in the Morris Water Maze task

Apoer2*[Δ16+19]* animals show abnormal synaptic transmission and LTP induction in the hippocampus which is involved in learning and memory. It was important to test whether or not the Apoer2*[Δ16+19]* animals had altered, perhaps enhanced, abilities to learn. The first test that we subjected the animals to was the Morris Water Maze task which tests spatial learning. Animals were trained for 11 days straight, 4 trials per day, and the last day a probe test was performed during which the submerged platform was removed. WT and Apoer2Δ16 knockin mutants did not show any differences in latency or distance to the platform during the training portion of the experiment (Figure 3.19A, B).

During the probe test on day 12, the submerged platform was removed and the time spent searching and distance traveled in the goal quadrant where the submerged platform had been, was measured for each mouse. There were no significant differences between genotypes in either the time spent or distance traveled in the probe test (Figure 3.19C, D). However, there was an observed trend that the Apoer2*[Δ16Δ19]* animals spent less time and distance in the goal quadrant compared to WT animals. This decrease in the time spent in the goal quadrant was also observed in the Apoer2*[Δ19]* animals.

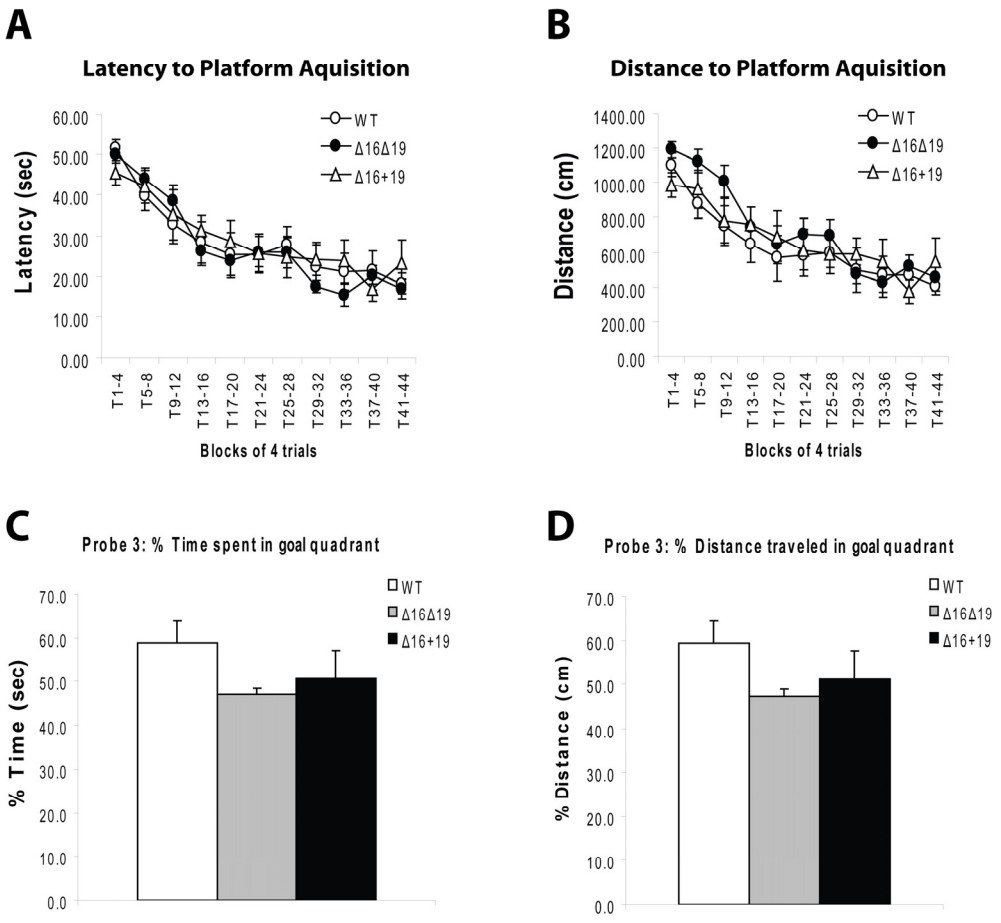

Figure 3.19: Apoer2Δ16 knockins have no significant deficiencies in the Morris Water Maze task. Ten mice were used for each genotype. (A) The amount of time it took mice from each genotype to find the platform was plotted in four block increments. Four trials were tested each day for eleven days. There was no difference in the learning curve between any of the genotypes (B) The distance the mice traveled before finding the submerged platform was plotted in the same four block increments as the latency. There was no difference between genotypes. (C) The percent time spent in the goal quadrant on day 12 of testing was not significantly different between genotypes. (D) The distance traveled in the goal quadrant on day 12 was not significantly different between genotypes. Apoer2Δ16 mouse lines were statistically compared to WT using the Student's t-test.

Thus, it may be concluded that the phenotypes seen in the water maze task are due to the lack of exon 19 and not exon 16.

No significant differences in other behavioral tests

The Apoer2Δ16 knockin mouse lines were also subjected to open-field, auditory prepulse inhibition (PPI), and tactile PPI tests. There were no significant differences in any of the tests between the WT mice and either of the two Apoer2Δ16 knockin mouse lines (data not shown). From these tests we can conclude that exon 16 regulation of Apoer2 expression may not play a role in regulating mouse activity, anxiety and sensorimotor gating.

Discussion

It is estimated that at least half of all proteins are posttranslationally modified by the addition of N- and O-linked sugars (Apweiler et al., 1999). Due to the large gamut of proteins that are glycosylated and the incredible variety of possible sugar trees which may glycosylate them, it is difficult to attribute a given set of functions to these sugar residues. However, protein glycosylation generally plays a role in protein folding, stability, sorting, and secretion. More specifically, sugar side chains on certain proteins can also function in mediating cell adhesion, cell/cell interaction, and inflammatory responses (Hanisch, 2001). Such diversity lends itself to characterizing the function of glycosylation based specifically on each protein being examined and its glycosylation pattern.

Apoer2 is fairly unique in having the ability to regulate its glycosylation through alternative splicing of the O-linked sugar domain encoded by exon 16. In this study, creation of Apoer2 knockin animals expressing splice variants lacking exon 16 has opened up a window through which the functional significance of the glycosylation, splicing, and processing of this particular exon can be explored.

Using data collected from these mice as well as transfected cells, I can conclude that glycosylation does, indeed, protect Apoer2 from proteolytic cleavage. There is also strong evidence that the extracellular cleavage site is located within the glycosylated O-linked sugar domain itself. Disruption of normal glycosylation and proteolytic processing causes an increase in Apoer2 protein levels and receptor misregulation *in vivo* and *in vitro*. Finally, inhibition of normal proteolytic processing of Apoer2, in conjunction with constitutive exon 19 expression, results in defective synaptic function and plasticity.

Although we have determined that glycosylation of the O-linked sugar domain protects the receptor from proteolytic cleavage, we are far from understanding why Apoer2 is expressed in alternatively spliced forms that can and cannot be glycosylated, can and cannot be cleaved. Apoer2 expressed from both the Apoer2*[Δ16+19]* and Apoer2*[Δ16Δ19]* mice resemble naturally occurring splice variants in the human brain. Thus, these splice variants should have some functional significance. The first clue that the knockin animals bestow, is the increase in Apoer2 protein levels in the Δ16 mouse lines. Because Apoer2*[Δ16Δ19]* and Apoer2*[Δ19]* mouse lines both lack exon 19 and have identical Apoer2 protein and mRNA expression levels, it can be suggested that the upregulation of protein and mRNA is an attempt to compensate for the loss of the

functional exon 19 and is not a result of misregulation of proteolytic processing. The dominant phenotype resulting from the loss of exon 19 seems to overshadow any affects that the deletion of exon 16 may exert. The same is true for the lack of Reelin stimulated increase in LTP induction. The Apoer2*[Δ16Δ19]* baseline and Reelin stimulated LTP results are identical to those from the Apoer2*[Δ19]* mice. In summary, comparison of the Apoer2*[Δ16Δ19]* and Apoer2*[Δ19]* mice only, could have led to the false assumption that loss of exon 16 has no effect on synaptic function or plasticity.

To the contrary, Apoer2*[Δ16+19]* and Apoer2*[+19]* mice have similar mRNA levels but the protein levels in the Δ16 mice are twice as high as those in the mice with normal exon 16 expression. Thus, on a constitutively expressed exon 19 background, loss of exon 16 results not only in a stabilization of Apoer2 protein but also affects synaptic function. Baseline LTP is significantly higher in Apoer2*[Δ16+19]* slices over Apoer2*[Δ16Δ19]* animals which are comparable to WT mice. Reelin stimulation of Apoer2*[Δ16+19]* slices decreases LTP induction to WT untreated baseline levels, the complete opposite result from Apoer2*[+19]* mice (Beffert et al., 2005). Traces from the LTP data reveal that Apoer2*[Δ16+19]* animals have increased responses (fEPSPs) to normal (non TBS) stimuli, corroborated by I/O data. This increased synaptic response is diminished upon the addition of Reelin.

Qui et al. demonstrated that prolonged Reelin treatment of WT hippocampal neurons increased AMPA receptor membrane insertion (Qiu et al., 2006). They supported this with electrophysiological recordings demonstrating increased AMPA receptor dependent activity in whole cell recordings after Reelin stimulation. It was suggested that this increase in AMPA receptor trafficking to the surface was dependent

on Reelin induced PI3K activation, independent of Src activity. Neurons expressing more Apoer2, such as those in the Apoer2*[Δ16+19]* mice, may be more sensitive to endogenous Reelin signaling and perhaps exhibit an increase in baseline PI3K activation. This would result in increased AMPA receptor membrane insertion and may augment normal synaptic transmission as seen in the traces for Apoer2*[Δ16+19]* mice. This could be easily tested in the Apoer2*[Δ16+19]* mice by looking at both AMPA EPSCs in hippocampal slices as well as AMPA receptor cell surface accumulation in cultured neurons and compare the results to WT controls. There would also be an increase in PI3K phosphorylation which could be easily compared in WT and mutant hippocampal slices or cultured neurons by Western blotting. The receptor associated protein (RAP) competes with Reelin for binding to the extracellular domain of Apoer2 (Willnow, 1998). Incubation of slices with GST-RAP should decrease Reelin signaling through Apoer2 in the sensitized Apoer2*[Δ16+19]* animals and return synaptic transmission back to WT levels if my hypothesis is true.

Exogenous Reelin stimulation of Apoer2*[Δ16+19]* animals, however, causes a decrease in normal synaptic transmission as well as LTP induction. I propose that if the mice are already sensitized to endogenous Reelin due to increased Apoer2 protein levels, addition of exogenous Reelin may force the neurons to reach an activity/excitation threshold which automatically activates neuroprotective pathways in an attempt to prevent excitotoxicity. Because Reelin is added to hippocampal slices at least 30 minutes prior to TBS induction of LTP, the slices may have enough time to respond to increased Reelin levels in a protective manner. This may include the internalization of glutamate receptors or their selective exclusion from synapses in order to prevent overexcitation.

This hypothesis could be explored in Apoer2*[Δ16+19]* neurons by analysis of cell surface NMDA and AMPA receptor levels using biotinylation techniques before and after Reelin treatment.

Exon 19 must play a role in the modulation of these synaptic events as Apoer2*[Δ16Δ19]* mice do not show any increase in normal synaptic transmission or even Reelin induced LTP. The alternatively spliced cytoplasmic insert of Apoer2 specifically binds both PSD95 and JIPs. PSD95 is involved in regulating activation of NMDARs and the JIPs interact with JNK which has been implicated in affecting synaptic function (Bhattacharyya et al., 2009; Li et al., 2007; Wang et al., 2004). It may be through these adaptor/scaffolding proteins that exon 19 exerts its effect on synaptic transmission in the Apoer2*[Δ16+19]* mice. If this hypothesis is true, assessment of normal synaptic transmission and LTP induction in the presence of cell permeable peptides mimicking the exon 19 amino acid sequence (which would prevent adaptor protein binding to the receptor) should counteract the synaptic function misregulation in a dose dependent manner in the Apoer2*[Δ16+19]* animals.

Many questions still remain to be answered regarding the significance of splicing of the O-linked sugar domain of Apoer2. Is Apoer2 differentially glycosylated in various regions of the brain or even different cell types based on whether increased or decreased proteolytic processing is needed for normal brain function? Is there a change in glycosylation of the receptor in an activity dependent manner? Is there a change in glycosylation of the receptor temporally? During aging? We already know that Apoer2 levels may change in the shift from development to adulthood, it may very well be that glycosylation of the receptor is also changed during the life time of the organism.

In my analysis of the electrophysiological data, I have made the assumption that proteolytic processing is functionally significant only in the manner of enabling protein degradation/turnover. However, it is possible that proteolytic processing of the receptor and release of the ICD may regulate transcriptional activation/inhibition of various genes. As previously mentioned, Apoer2 processing is potentially an activity dependent phenomenon (Hoe and Rebeck, 2005). This would cause activity dependent transcriptional gene regulation that may mediate functions such as synaptic function and plasticity. ChIP assays may elucidate any potential gene targets of the cleaved Apoer2 ICD.

Although only a few behavioral tests were used to assess learning, memory, and normal brain function in the Apoer2 Δ16 mice, with no significant conclusions, it may be beneficial to subject these mice to other tests such as the fear conditioning paradigm or the T-maze test. Behavioral testing generally requires large animal pools. Minimal numbers of mice ($20 > n > 10$) were used in the behavioral tests in this study, increasing the n number may yield statistically significant results.

The generation of the Apoer2 Δ16 mice has been fruitful in creating a mouse model through which not only can the functional significance of Apoer2 proteolytic processing be addressed but also the importance of multiple splice forms of the receptor. These KI mouse lines will also aid in the further elucidation of how Apoer2 regulates synaptic function and plasticity.

CHAPTER FOUR

THE ROLE OF THE APOER2 CYTOPLASMIC TAIL FUNCTIONAL DOMAINS IN SELENIUM UPTAKE AND SPERM FUNCTION

(Adapted from: Masiulis, I., Quill, T.A., Burk, R.F., Herz, J. (2009). Differential functions of the Apoer2 intracellular domain in selenium uptake and cell signaling. Biol Chem 390, 67-73.)

Abstract

Apolipoprotein E Receptor 2 (Apoer2) is a multifunctional transport and signaling receptor that regulates the uptake of selenium into the mouse brain and testis through endocytosis of selenoprotein P (Sepp1). Mice deficient in Apoer2 or Sepp1 are infertile, with kinked and hypomotile spermatozoa. They also develop severe neurological defects on a low selenium diet, due to a profound impairment of selenium uptake. Little is known about the function of Apoer2 in the testis beyond its role as a Sepp1 receptor. By contrast, in the brain, Apoer2 is an essential component of the Reelin signaling pathway, which is required for proper neuronal organization and synapse function. Using knockin mice, we have functionally dissociated the signaling motifs in the Apoer2 cytoplasmic domain from Sepp1 uptake. Selenium concentration of brain and testis was normal in the knockin mutants, in contrast to Apoer2 knockouts. Thus, the neurological defects in the signaling impaired knockin mice are not caused by a selenium uptake defect, but instead are a direct consequence of a disruption of the Reelin signal. Reduced sperm motility was observed in some of the knockin mice, indicating a novel

signaling role for Apoer2 in sperm development and function that is independent of selenium uptake.

Introduction

Apolipoprotein E receptor 2 (Apoer2), a member of the low-density-lipoprotein (LDL) receptor family, undergoes complex splicing and proteolytic processing. Apoer2 is predominantly expressed in the brain where it regulates neuronal migration, cortical lamination, and synapse function. One of the major signaling cascades responsible for controlling these processes in the brain involves the large extracellular signaling protein Reelin, which is a ligand for Apoer2 (Herz and Chen, 2006). Reelin binding to Apoer2 and the very low-density-lipoprotein receptor (Vldlr), another member of the LDL receptor family, results in receptor clustering at the plasma membrane. This clustering initiates the transphosphorylation of the adaptor protein Disabled-1 (Dab1) by Src family kinases (SFKs). Dab1 interacts with an NPxY tetraamino acid motif in the cytoplasmic intracellular domains (ICDs) of both receptors. Phosphorylation leads to a further increase in SFK activity, thereby activating multiple cellular signaling branches that control neuronal migration and synapse function.

Apoer2 is not only involved in the transmission of the Reelin signal but has also been implicated in regulating selenium uptake in the brain and testis. Selenium is a micronutrient that is crucial for brain function and sperm development. It is transported to target tissues by incorporation into proteins such as Selenoprotein P (Sepp1), a high capacity carrier of selenium, followed by endocytosis through Apoer2 (Burk and Hill, 2005; Olson et al., 2007).

Burk and colleagues have recently reported a remarkable phenotypic similarity between Apoer2 and Sepp1 deficient animals (Burk et al., 2007; Olson et al., 2005; Trommsdorff et al., 1999; Valentine et al., 2008). Apoer2 and Sepp1 deficiency both greatly impair selenium uptake in the testis by as much as 81%, resulting in male hypofertility and structural sperm defects (Andersen et al., 2003; Hill et al., 2003; Olson et al., 2005). In addition to revealing a critical role for selenium in the testis, these findings have also shown that selenium delivery through Sepp1 and Apoer2 is the primary route of selenium supply to this tissue. In an analogous manner, selenium deficiency in the brain, caused by lack of Sepp1 or Apoer2 in combination with a low selenium diet, leads to irreversible neurological (Burk et al., 2007) and hippocampal dysfunction (Peters et al., 2006) with progressive neurodegeneration throughout the brain (Valentine et al., 2008).

We have previously shown that mutations or deletions of certain functional sequence motifs within the Apoer2 ICD, generated through a knockin approach, can also lead to hippocampal dysfunction, defects in synaptic plasticity, accelerated neurodegeneration, and reduced neuronal survival after injury (Beffert et al., 2006a; Beffert et al., 2006b; Beffert et al., 2005). These sequences include the NPxY motif and a 59 amino acid sequence encoded by an alternatively spliced exon, which provides binding sites for adaptor and scaffolding proteins that regulate the activation of JNK signaling and NMDA receptors.

The phenotypic similarity between Apoer2 and Sepp1 deficient mice raised the possibility that the neurological defects of the Apoer2 knockin mice might be caused in part by a Sepp1 uptake defect, resulting in neuronal selenium deficiency, rather than a

direct effect of Apoer2 on neuronal JNK or NMDA receptor signaling. Distinguishing between these possibilities is of the utmost importance for proper interpretation of the physiological functions that have been attributed to Apoer2, in particular its critical roles in regulating synaptic transmission and neuronal survival. The purpose of the current study was to disentangle these confounding possibilities. To achieve this, we made use of the series of Apoer2 knockin mice we had generated (Beffert et al., 2006a; Beffert et al., 2006b; Beffert et al., 2005). Here, we investigated the ability of these mutant animals to mediate selenium uptake into brain and testis. We also measured a series of sperm motility parameters to reveal potential roles of the cytoplasmic signaling and docking motifs in sperm maturation and function. Our results unequivocally show that selenium uptake into the brain is not impaired in the knockin mutants, thereby effectively ruling out a compounding effect of selenium deficiency on the profound synaptic signaling defects that occur in the Apoer2 ICD mutants. Intriguingly, our findings also show that the signaling competent functional motifs in the cytoplasmic domain of Apoer2 play a previously unknown role in sperm development which is independent of selenium uptake.

Materials and Methods

Animals – Generation of Apoer2 KO (Trommsdorff et al., 1999), Apoer2*[ex19]* (Beffert et al., 2005), Apoer2*[Δex19]* (Beffert et al., 2005), Apoer2*[Stop]* (Beffert et al., 2006), Apoer2*[Dab^{-}]* (Beffert et al., 2006), Apoer2*[Δ16±19]*(Chapter 3) mice has been previously described. All mice were housed under a 12 h: 12 h light dark cycle and fed a normal chow diet unless otherwise stated. All animals were euthanized via inhalation of

isoflurane according to the National Institutes of Health's Guide for the Care and Use of Laboratory Animals and the UT Southwestern Animal Care and Use Committee.

Membrane Fraction Preparation – Testis tissue was homogenized using a polytron tissue grinder in 1 ml of Buffer I (20 mM Tris-HCl, pH 8.0, 120 mM NaCl, 1 mM $CaCl_2$, EDTA-free protease inhibitor cocktail (Complete, mini, protease Inhibitor Cocktail Tablets, Roche)) per mg of tissue. Homogenate was spun down at 800 rpm (rotor JS-5.2, Beckman J-6B centrifuge) for 5 minutes at 4ºC. Supernatant was spun again for 10 minutes at 10,000 x g, 4ºC. The supernatant of the intermediate spin was spun in an ultracentrifuge (TLA110 rotor, Beckman Optima TLX ultracentrifuge) at 55,000 rpm for 30 minutes at 4ºC. The resulting pellet was resuspended in Buffer II (50 mM Tris-HCl, pH 8.0, 80 mM NaCl, 2 mM $CaCl_2$, 1% Triton X-100, 0.1% SDS, EDTA-free protease inhibitor cocktail) and homogenized by forcing the suspension 15-20 times through a 23 gauge needle. The homogenate was solubilized on ice for 10 minutes and spun again at 55,000 rpm for 30 minutes at 4ºC. The supernatant after the last high speed spin contained the membrane enriched fraction. Equal amounts of protein were loaded on an 8% SDS-PAGE gel from each Apoer2 Δ16 genotype (homozygote KI, Heterozygote and WT). Proteins were transferred to nitrocellulose membranes and probed with the 2561 affinity purified polyclonal Apoer2 C-terminal tail antibody.

Tissue selenium level analysis – Mice were weaned at three weeks of age and fed a *Torula* yeast diet containing 0.25 mg/kg selenium as sodium selenite (Burk et al., 2007). The diet was purchased from Harlan-Teklad (Madison, WI, USA). Mice consumed this

diet for 4 weeks, after which they were euthanized and exsanguinated. Tissues were collected and selenium levels were measured as previously described (Olson et al., 2007).

Immunocytochemistry – **Testis**: Testes were fixed in 4% paraformaldehyde in PBS for 1 h at 4°C and cryoprotected in 20% sucrose in PBS overnight. Frozen sections (5 μm) from these testes were washed with TBST (20 mM Tris-HCl, pH 8.0, 150 mM sodium chloride, 0.025% sodium azide, 0.05% Tween 20) and incubated in blocking buffer (1% BSA and 1% glycine in TBST) for 1 h. Sepp1 monoclonal rat antibody (Olson et al., 2007) diluted in blocking buffer was added to the slices for 1 h at room temperature. The slides were washed 3 x 5 min with TBST and incubated with Alexa Fluor 594 chicken anti-rat fluorescent secondary antibody (Invitrogen, Carlsbad, CA, USA, 1:200) diluted in blocking buffer for 1 h. Sections were washed in TBST and coverslips were mounted using ProLong Gold with DAPI mounting medium (Invitrogen). Pictures were taken with a Zeiss Axioplan 2 (Thornwood, NY, USA) fluorescence microscope using identical exposure settings. At least three animals were analyzed per genotype.

Sperm: Adult males were euthanized, and cauda and caput sections of the epididymis were dissected free of connective tissue and fat deposits. The tissue was minced in 0.1 M sodium phosphate buffer (pH 7.4) and the spermatozoa were allowed to swim up for 10 min. The suspension was spun at 1,000 x *g* to remove any remaining tissue. Spermatozoa were fixed in 4% paraformaldehyde overnight at 4°C. The fixed spermatozoa were resuspended and streaked onto slides, dried, and permeabilized with

ice cold methanol for 15 min. Slides were washed, blocked for 1 h at room temperature (blocking buffer: 0.1% BSA, 10% goat serum, 1xPBS), and incubated overnight at 4°C with the primary antibody (1:200 dilution of a crossreacting polyclonal antibody against an unidentified sperm antigen). Slides were washed in PBS followed by the addition of Alexa Fluor 488 goat anti-rabbit fluorescent secondary antibody (Invitrogen, 1:200) for 1 h at room temperature in blocking buffer. The slides were washed in PBS and incubated with MitoFluor^{TM} (Invitrogen, 1:200 in PBS) for 10 min at room temperature. Finally, the slides were washed in PBS and coverslips were mounted using ProLong Gold with DAPI mounting medium (Invitrogen). Pictures were taken with a Zeiss Axioplan 2 fluorescence microscope.

Scanning Electron Microscopy – Adult Apoer2 ICD mutant spermatozoa were collected as described for immunocytochemistry. After centrifugation at 800 x *g* for 5 min the spermatozoa were fixed with 4% glutaraldehyde in 0.1 M cacodylate buffer overnight at 4°C. Spermatozoa were pelleted and resuspended in 0.1 M cacodylate buffer for plating on Poly-L-Lysine coated coverslips. After incubation in osmium tetroxide, graded ethanol dehydration, and treatment with hexamethyldisilazane (HMDS), the coverslips were sputter coated in a Denton DV-502A evaporator (Moorestown, NJ, USA) with a gold/palladium target. Scanning electron images were taken with a FEI XL30 ESEM (Hillsboro, Oregon, USA), spot 4.0, 20.0kV.

Morphological analysis – Mice 3-6 months of age were euthanized and epididymides were dissected free of connective tissue and fat deposits. Using fine scissors, a few small

incisions were made in a small section of the cauda epididymis and the tissue was incubated in 1 ml of Biggers-Whitten-Whittingham (BWW) medium (osmolarity, 310 mosmol/L) supplemented with 12 mg/ml BSA (Andersen et al., 2003). Spermatozoa were allowed to swim up for 10 min at 37ºC. Tissue was removed from the medium and spermatozoa were fixed in 4% paraformaldehyde overnight at 4ºC. Spermatozoa were streaked onto slides, covered with coverslips, visualized using normal light microscopy, and categorized according to tail morphology. One hundred spermatozoa were analyzed for each of three mice from every genotype. Percentages were averaged and statistical analysis was performed using the Student's t-test.

Sperm motility analysis – Spermatozoa, from adult male mice 3-6 months of age, were collected in the same manner as for morphological analysis, tissue was removed from the medium, and the spermatozoa were immediately placed into an 80 μm slide well warmed to 37ºC. Sperm motility was analyzed according to the methods previously described (Quill et al., 2003). Briefly, the slide was placed in The IVOS Sperm Analyzer (Version 12, Hamilton Thorne Research, Beverly, MA, USA) for motility analysis. Images were collected for 0.5 s at 60Hz. For each sample (three mice per genotype, one sample per mouse), 100 spermatozoa tracks were selected for unobstructed motion during the entire recording time and the following parameters were analyzed: % motility, curvilinear velocity (μm/s), average path velocity (μm/s), straight line velocity (μm/s), amplitude of lateral head displacement (the largest distance the head reaches away from the averaged path, μm), beat cross frequency (Hz), linearity (%).

Results

We have previously generated and used a series of Apoer2 ICD mutant mouse lines to molecularly define intracellular components of the Reelin signaling pathway. In this study we utilize six of these mutant lines to investigate the involvement of the Apoer2 ICD in selenium uptake both in the brain and testis (Figure 4.1). The Apoer2*[ex19]* and Apoer2*[Δex19]* mice constitutively express a splice variant of Apoer2 that contains or lacks exon 19, respectively. Exon 19 encodes a proline rich 59 amino acid sequence within the intracellular domain of the receptor that contains binding sites for the adaptor proteins postsynaptic density protein of 95kDa (PSD95) and JNK interacting proteins (JIPs). This exon is essential in the regulation of synaptic plasticity by the neuronal signaling protein Reelin. Exon 19 functionally couples Apoer2 to *N*-methyl *D*-aspartate receptors (NMDAR) probably through the adaptor protein PSD95, resulting in the activation of the ionotropic receptors and regulation of NMDAR dependent synaptic plasticity (Beffert et al., 2005).

Another Apoer2 ICD mutant line, Apoer2*[Stop]*, contains the deletion of the entire ICD five amino acids carboxyterminal of the NPxY motif. This deletion includes part of exon 18 and all of exons 19 and 20. These mice, along with the Apoer2*[Δex19]* mice, show an age-dependent loss of corticospinal neurons signifying the importance of exon 19 as a regulator of neurodegeneration, likely through the interaction with JIPs, adaptor proteins involved in the regulation of the JNK signaling pathway (Beffert et al., 2006).

The fourth Apoer2 ICD mutant line, Apoer2*[Dab^{-}]*, has a three amino acid mutation in the cytoplasmic ICD just prior to the NPxY motif. Mutation of residues

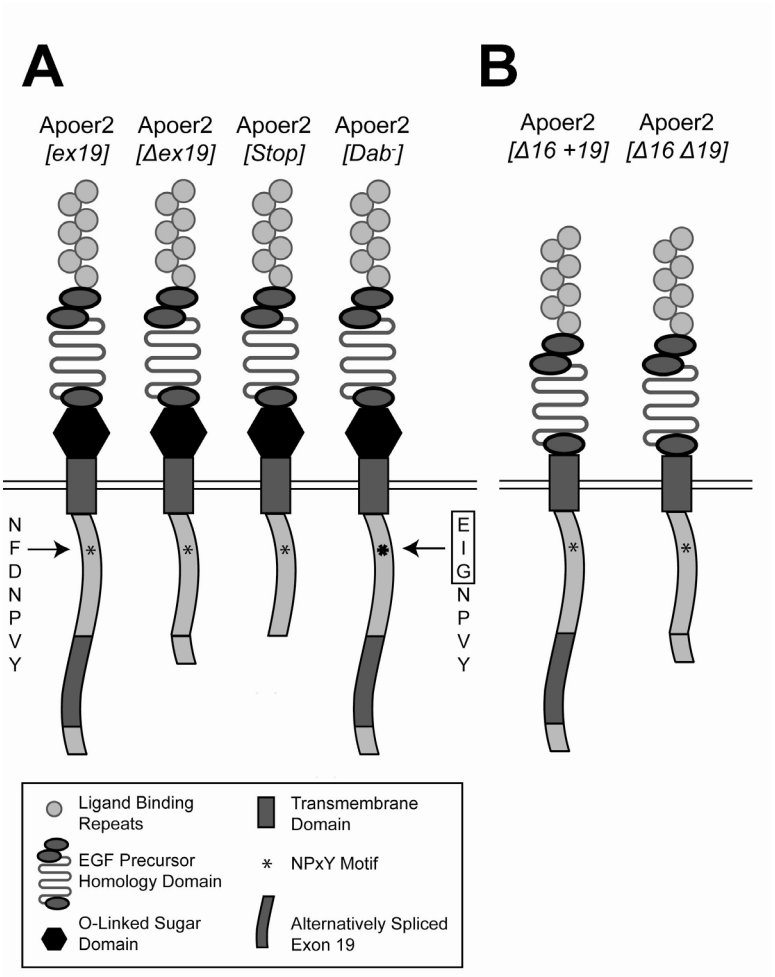

Figure 4.1: Apoer2 ICD mutant knockin mice. (A)Apoer2*[ex19]* mice constitutively express the full length receptor containing the alternatively spliced exon 19. Apoer2*[Δex19]* mice constitutively express the full length receptor without the alternatively spliced exon 19. Apoer2*[Stop]* mice express a truncated receptor lacking the C-terminal ICD after the NPXY domain. Apoer2*[Dab-]* Mice express the full length receptor with a mutation in the Dab-1 binding site. (B) Apoer2*[Δ16]* mice constitutively express a splice variant without exon 16. One mouse line constitutively expresses exon 19 (Apoer2*[Δ16+19]*) and the other lacks exon 19 (Apoer2*[Δ16Δ19]*).

N893E, F894I, and D895G in the cytoplasmic tail of the receptor abrogates binding of the adaptor protein Disabled-1 (Dab1), an obligatory component of the Reelin signaling

pathway. By preventing this interaction, the transmission of the Reelin signal through Apoer2 is disrupted. The NPxY motif is involved in the regulation of endocytosis of numerous proteins. Compared to other LDL receptor family members, the endocytosis coefficient of Apoer2 is very low. The three amino acid mutation so close to the NPxY motif affects, but does not completely abrogate, Apoer2 endocytosis (Beffert et al., 2006a). However, the mutation does severely impair synaptic plasticity further underscoring the importance of Apoer2 in the regulation of NMDA receptor function.

The last two Apoer2 knockin mutants mimic the Apoer2*[ex19]* and Apoer2*[Δex19]* animals however both lines also constitutively lack exon 16 (Figure 4.1B). This exon encodes the O-linked sugar domain and is involved in the proteolytic processing of the receptor (Chapter 3). These knockin mutants express 2-3 times more Apoer2 in the brain (Figure 3.11A, B). It was unknown if this increase in protein levels was a phenotype restricted to the brain or, if the testis also had increased Apoer2 levels. Membrane fractions from adult mouse testes from both Apoer2*[Δ16+19]* and Apoer2*[Δ16Δ19]* reveal that the testis also has increased Apoer2 protein levels (Figure 4.2).

Burk and colleagues have previously shown a profound effect of selenium deficiency on synaptic function and neuronal survival, which is strikingly similar to the defects we have observed in the Apoer2 ICD mutants (Beffert et al., 2006a; Beffert et al., 2006b; Beffert et al., 2005; Burk et al., 2007; Peters et al., 2006; Valentine et al., 2008). This raised the possibility that the phenotypes of our Apoer2 ICD mutant mice might be, at least in part, caused by selenium deficiency and not by the disruption of neuronal signaling pathways. To exclude this possibility, the Apoer2 ICD mutants, along with

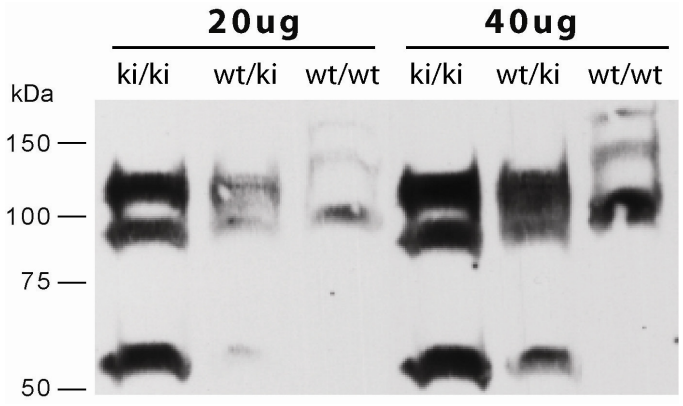

Figure 4.2: Testis Apoer2 protein levels are increased in Δ16 mice. Apoer2*[Δ16±19]* homozygous knockin animals (ki/ki) show consistently higher levels of Apoer2 protein in membrane fractions isolated from the testis than WT mice (wt/wt).

WT and Apoer2 KO controls, were fed a diet supplemented with a level of selenium that provides an adequate supply of this micronutrient to wild type mice. After four weeks the animals were euthanized and their brains, testes, and livers were collected for selenium level analysis. Consistent with previous reports, selenium levels were greatly reduced in both the brain (Figure 4.3A) and testis (Figure 4.3B) of Apoer2 KO mice (Hill et al., 2003; Olson et al., 2007). By contrast, none of the Apoer2 ICD mutants had significantly lower selenium levels in brain or testis, compared to wild type animals. Even the Apoer2 Δ16 mice which express more Apoer2 show no significant changes in selenium content in all three tissues. This confirms that selenium uptake into the brain and testis is highly regulated even with receptor misregulation. Because the Apoer2 Δ16 animals had normal selenium and fertility levels, they were excluded from further analyses. As a control, selenium levels in the liver, where Apoer2 is not expressed, were comparable across all genotypes (Figure 4.3C).

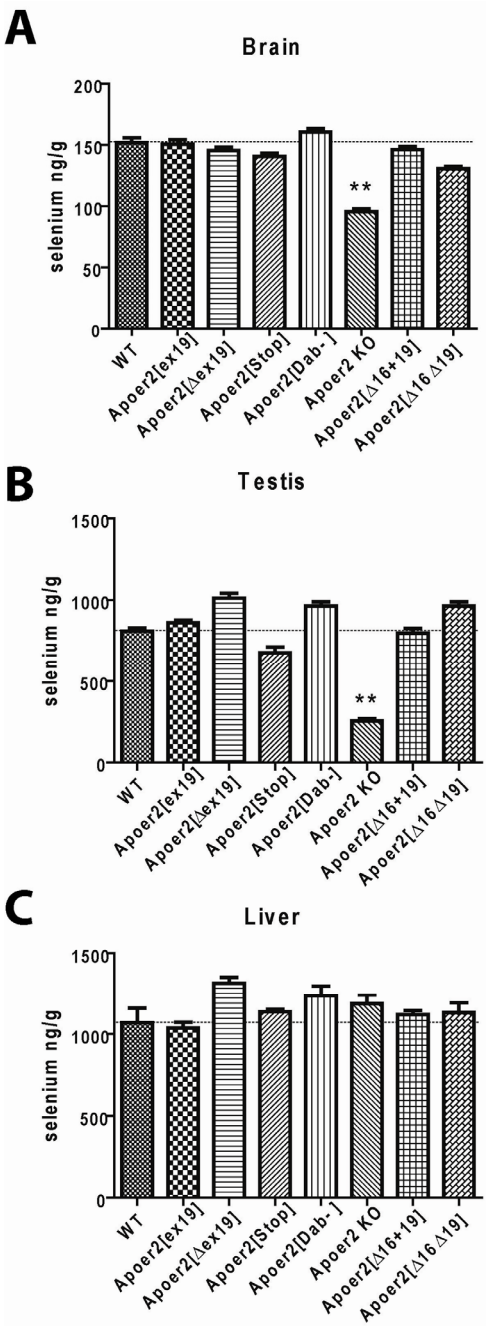

Figure 4.3: No significant difference in tissue selenium levels of Apoer2 ICD mutant mice from wild type. Tissue selenium values were measured from mice of all eight genotypes after four weeks on a 0.25 mg/kg selenium diet. Only Apoer2 KO mice presented with significantly lower selenium levels than wild type mice in the brain (A) and testes (B); $^{**}P<0.001$. Liver selenium levels were comparable among all genotypes (C).

Although endocytosis in the Apoer2*[Dab$^-$]* animals may be affected by the three amino acid mutation, it is not enough to decrease selenium levels in the brain or testis of these mice. We confirmed this conclusion by visualizing the localization of Sepp1 in the testis using immunohistochemistry. The WT animals and all of the Apoer2 ICD mutants showed vesicular Sepp1 staining at the basal lamina (Figure 4.4). As previously reported, there were no Sepp1 positive vesicles detected in the Apoer2 KO testes. These data indicate that the domains crucial for regulating synaptic function in the brain are not involved in the uptake of selenium in either of these tissues.

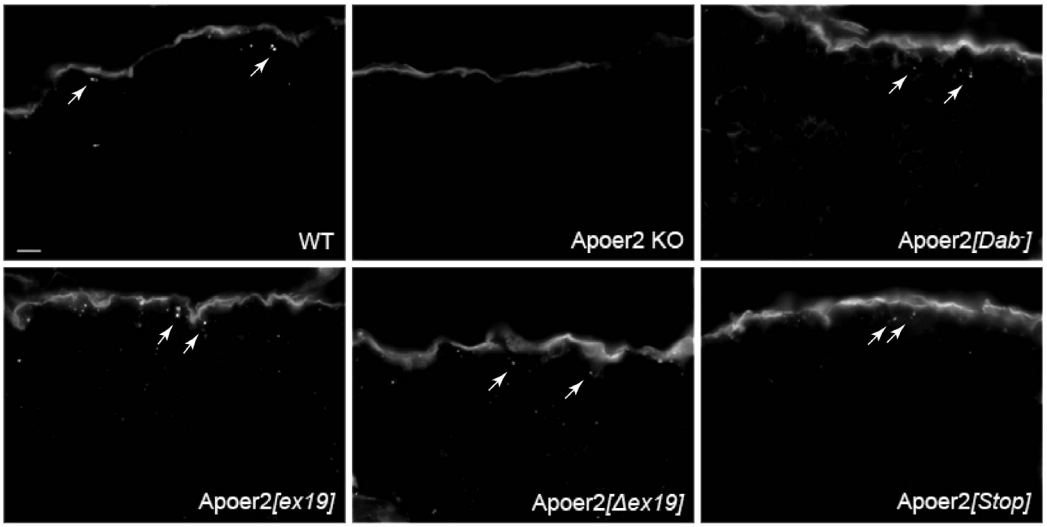

Figure 4.4: Vesicular Sepp1 staining observed in all Apoer2 ICD mutant mice. Fixed mouse testes were stained for Sepp1. Vesicular Sepp1 staining (arrows) is apparent in WT mice and all Apoer2 ICD mutants. As previously reported, there is no Sepp1 vesicular staining in Apoer2 KO testes. Scale bar = 10 μm.

Although none of the Apoer2 ICD mutant mice had significantly decreased selenium levels in the testis, we observed decreased pregnancy rates and small litter size in the Apoer2*[Dab^{-}]* ICD mutant animals. This impaired fertility in the Apoer2*[Dab^{-}]* mice indicated a role for Apoer2 in spermatogenesis that is independent of selenium uptake into the testis. Therefore, we investigated the morphology of spermatozoa from wild type and Apoer2 mutant lines by isolating, fixing, and staining spermatozoa with DAPI to label the nucleus, with MitoFluor^{TM} to stain the midpiece, and with a crossreacting polyclonal antibody against an unidentified sperm antigen that marks the acrosome and principal piece of the tail (Figure 4.5). The basic organization of the above mentioned sperm sections was identical between the spermatozoa collected from wild type mice and the Apoer2 mutants.

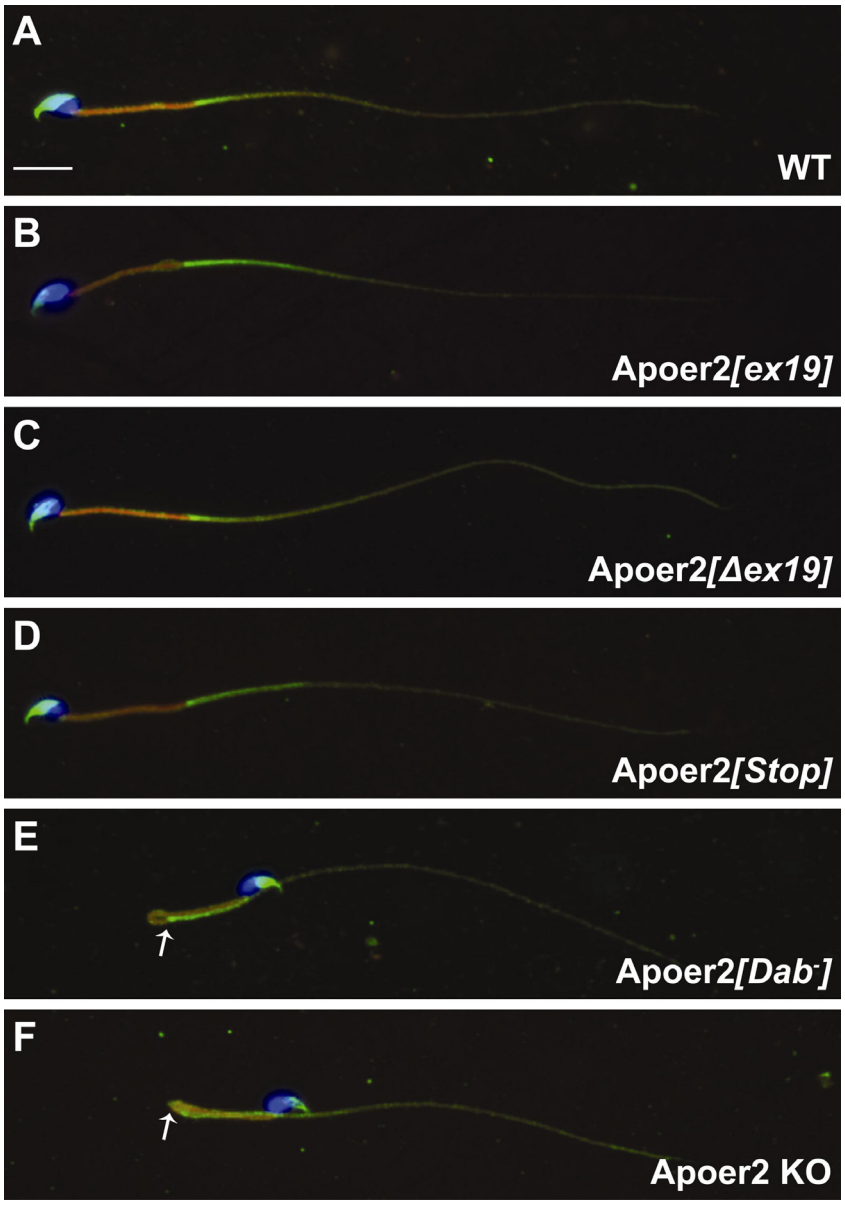

Figure 4.5: Sperm immunostaining reveals normal organization of spermatozoa. Fixed spermatozoa were immunostained with MitoFluor™ (midpiece; red), a crossreacting polyclonal antibody against an unidentified sperm antigen (acrosome and principal piece; green), and DAPI (nucleus; blue). (A) wild type (B) Apoer2*[ex19]* (C) Apoer2*[Δex19]* (D) Apoer2*[Stop]* (E) Apoer2*[Dab-]* (F) Apoer2 KO. Pictures are representative of the major morphological sperm population for each genotype. Arrows indicate location of annulus. Scale bar = 10 μm.

The Apoer2*[Dab$^-$]* mice, like the Apoer2 KOs, however, produced a larger fraction of spermatozoa with abnormal tail morphology than wild type mice. We morphologically analyzed spermatozoa from multiple mice ($n \geq 3$) from each genotype. Spermatozoa were classified by the shape of the tail as straight, hairpin, angled, or curled (Figure 4.6). Straight spermatozoa were defined as those with an absence of a bend in the tail between the neck and the distal tip of the tail. Hairpin spermatozoa were bent back on themselves 180 degrees at the annulus (arrowhead in Figures 4.6E, 4.6F and 4.6C). Angled spermatozoa were also bent at the annulus at an angle between 40-120 degrees with a cytoplasmic droplet often residing at the bend (Figure 4.6B). The midpieces of curled spermatozoa were looped adjacent to or around the head of the spermatozoon, frequently forming a complete circle. This particular conformation, confirmed by scanning electron microscopy (Figure 4.6D), appears to coincide with the cytoplasmic droplet failing to migrate down the midpiece and, instead, remaining at the neck. This can cause the head to curl around the droplet.

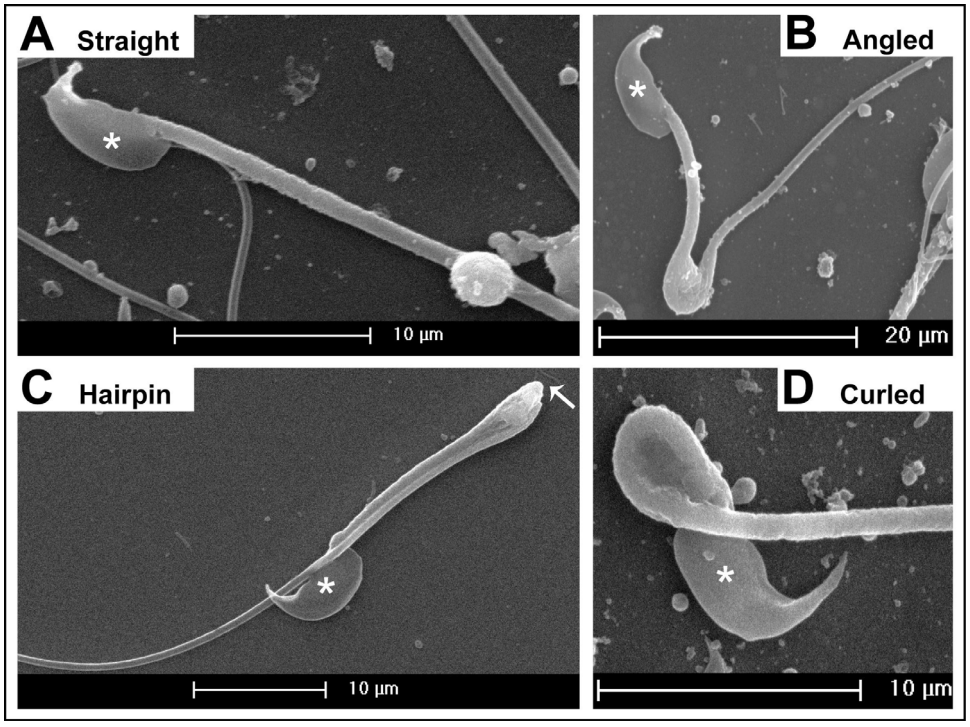

Figure 4.6: Sperm classification into four morphological categories. The majority of spermatozoa observed fell into one of four different morphological categories: straight, hairpin (sperm tail is bent back on itself at the annulus), angled (sperm tail is slightly bent at the annulus creating an angled tail), and curled (the tail is curled proximal to the head of the spermatozoon). Asterisks mark sperm head. Arrow marks annulus.

Table 4.1 summarizes the percent of the total population of spermatozoa in each of the four morphological conformations for all six mouse lines. As previously reported, we confirmed that the Apoer2 KO mice produce a considerably higher percentage of hairpin spermatozoa than wild type. The only Apoer2 ICD mutants that significantly differed from wild type with respect to tail morphology were the Apoer2*[Dab$^-$]* mice. Like the KOs, they had few straight spermatozoa, however, the majority of the Apoer2*[Dab$^-$]* spermatozoa were split between the hairpin (36.3%±4.1%) and the curled (35.0%±3.1%) conformations. By contrast, 66.3%±2.3% of Apoer2 KO spermatozoa

showed the hairpin conformation. This suggests that in the Apoer2*[Dab⁻]* mice, migration of the cytoplasmic droplet may be impaired as it remains arrested at the base of the neck in a significant proportion of the spermatozoa, a phenotype not seen in any other Apoer2 ICD mutant line.

	% Straight	% Hairpin	% Angled	% Curled
WT	64.7 ± 4.4	23.7 ± 5.0	6.3 ± 1.2	5.3 ± 1.2
Apoer2*[ex19]*	63.3 ± 4.4	23.3 ± 4.1	7.7 ± 1.2	5.7 ± 2.3
Apoer2*[Δex19]*	62.0 ± 4.2	18.7 ± 1.3	3.0 ± 1.7	16.3 ± 5.4
Apoer2*[Stop]*	57.7 ± 6.4	20.0 ± 7.1	10.3 ± 1.3	12.0 ± 0.6
Apoer2*[Dab⁻]*	17.7 ± 5.4 *	36.3 ± 4.1	11.0 ± 1.5	35.0 ± 3.1 *
Apoer2 KO	11.0 ± 1.7 *	66.3 ± 2.3 *	6.0 ± 0.0	16.7 ± 3.4

Table 4.1 Quantitative analysis of sperm morphology. One hundred spermatozoa from each of three animals per genotype were scored according to morphological category. (mean ± S.E.) *$P<0.005$

This abnormal morphology in the majority of the Apoer2*[Dab⁻]* spermatozoa could potentially affect sperm motility, and therefore cause impaired fertility in this mutant strain. To assess any defects in motility, spermatozoa were collected and various established parameters of sperm motility were measured (Table 4.2). Even though there was variability between animals, only the Apoer2 KO mice had a significantly lower percentage of motile spermatozoa compared to wild type. The motility of Apoer2*[ex19]* spermatozoa was essentially indistinguishable from wild type for all of the parameters tested. By contrast, spermatozoa from the Apoer2 *[Δex19]* and Apoer2*[Stop]* lines, both of which lack the alternatively spliced exon 19, had velocities that were considerably reduced compared to wild type but not as much as the KO spermatozoa. This suggests that exon 19, which is essential for synaptic plasticity and neuronal survival, may also

play a functional role in sperm motility. However, absence of exon 19 does not reduce motility enough to noticeably impair fertility. Although some of the velocity parameters of the Apoer2*[Dab$^-$]* spermatozoa were identical to those of the Apoer2 KOs, a larger percentage of the Apoer2*[Dab$^-$]* spermatozoa were motile compared to the KO mice. Even though fertility is impaired in the Apoer2*[Dab$^-$]* mice, this modest increase in percent motility may be the factor preventing this Apoer2 ICD mutant line from being infertile like the Apoer2 KOs.

	WT	Apoer2*[ex19]*	Apoer2*[Δex19]*	Apoer2*[Stop]*	Apoer2*[Dab⁻]*	Apoer2 KO
% Motile	69.0 ± 5.6	46.3 ± 10.3	30 ± 7.1	48.3 ± 7.5	32.7 ± 9.4	18.7 ± 7.3 *
Curvilinear velocity, μm/s	304.6 ± 4.0	283.1 ± 11.2	233.0 ± 2.7 *	242.6 ± 7.4 *	145.3 ± 7.1 *	160.4 ± 25.0 *
Average path velocity, μm/s	140.0 ± 0.4	142.1 ± 2.3	114.2 ± 3.6 *	116.4 ± 2.8 *	85.0 ± 6.2 *	80.1 ± 9.9 *
Straight line velocity, μm/s	103.2 ± 2.6	116.6 ± 1.6	87.1 ± 5.2	87.9 ± 5.0	66.9 ± 7.8	54.8 ± 7.5 *
Amplitude of lateral head displacement, μm	16.6 ± 0.2	14.0 ± 0.6	12.3 ± 0.2 *	12.8 ± 0.2 *	7.7 ± 0.4 *	9.2 ± 1.6
Beat cross frequency, Hz	24.7 ± 1.4	26.3 ± 1.1	28.2 ± 0.3	28.5 ± 0.7	30.2 ± 1.6	30.5 ± 1.3
Linearity, %	34.6 ± 0.6	42.6 ± 1.8	39.1 ± 1.8	37.1 ± 2.0	48.0 ± 4.9	37.5 ± 0.8

Table 4.2 Motility analysis of wild type and Apoer2 mutant sperm. Spermatozoa, 150 from each of three animals per genotype, were analyzed for percent motility and various motility parameters. (mean ± S.E.) *$P<0.01$

Discussion

The present study draws a clear distinction between two fundamentally different physiological functions of Apoer2: signal transduction and selenium transport. In the brain, Apoer2 relays the Reelin signal across the neuronal membrane and as a result controls neuronal migration, function, and survival. Here we have demonstrated that selenium uptake into the brains of mice expressing Apoer2 ICD mutations, which impair specific signaling functions in the brain, is not affected. Thus, the synaptic signaling role of Apoer2 is independent of its role in selenium uptake.

Using spermatogenesis as an independent model system, we further show that this separation between signaling and selenium uptake exists in the testis as well. None of the Apoer2 ICD mutants had lower testis selenium levels than wild type, yet we still observed significant defects in sperm morphology and motility in three of the Apoer2 ICD mutants. These data suggest that the intracellular domain regions that are crucial for normal brain function may also be relevant for determining sperm motility and maturation independent of selenium uptake.

The NPxY motif serves as a common endocytosis signal in numerous cell surface receptors. In the Apoer2 ICD it mediates the interaction with the PTB domain containing adaptor protein, Dab1. Mutation of the three amino acids prior to the NPxY motif marginally impairs endocytosis, however, it completely disrupts Dab1 binding to the ICD. This unique property of the Apoer2*[Dab$^-$]* mouse line has allowed us to differentiate between the function of Apoer2 in selenium uptake and signal transduction. Our data show that testis selenium levels in the Apoer2*[Dab$^-$]* mice are not lower than wild type. This indicates that selenium uptake remains unharmed by the mutation.

However, even under normal selenium levels, the Apoer2*[Dab$^-$]* line still produces spermatozoa with morphological and motility defects. These results suggest that Apoer2 may play a signaling role, through interaction with a PTB domain containing adaptor protein, which affects sperm maturation and function.

The significant number of spermatozoa with curled midpieces produced by the Apoer2*[Dab$^-$]* strain is not commonly observed. To our knowledge only one other mutant mouse line resembles this phenotype, the GOPC (Golgi-associated PDZ- and coiled-coil motif-containing protein) deficient mice (Suzuki-Toyota et al., 2004). The spermatozoa of these animals have rounded heads with the midpiece curled around the head. The proposed reason for this curl is the lack of a posterior ring that separates the cytoplasmic droplet from the rest of the perinuclear cytoplasm. Thus, as the cytoplasmic droplet migrates down the midpiece, the head of the spermatozoon is dragged along curling the tail around itself. The GOPC KO mice are more severely affected than the Apoer2*[Dab$^-$]* mouse line as the Apoer2 mutants do not have rounded heads. Furthermore, there is no evidence for the lack of a posterior ring as the cytoplasmic droplet seems to form normally and only a third of the spermatozoa display the curled phenotype.

This lack in the severity of phenotype does not rule out the possibility that the migration of the cytoplasmic droplet could play a role in the curled morphology of the Apoer2*[Dab–]* spermatozoa. To date, the cause and reason for the migration of the cytoplasmic droplet is unknown. However, it is accepted that in many species the droplet will migrate down the midpiece as the spermatozoon travels through the epididymis and matures (Cooper and Yeung, 2003). Because we find that a significant fraction of spermatozoa that have migrated to the cauda part of the epididymis retain their

cytoplasmic droplets proximal to the head, Apoer2*[Dab^{-}]* spermatozoa may fail to mature properly. Not only do we observe a proximal droplet, we also see the midpiece curled around it. When given an osmotic shock, immature sperm tails are more likely to curl than mature spermatozoa because they have not yet assembled the necessary molecular machinery for proper cell volume regulation (Yeung et al., 1999). These observations support a role for Apoer2 signaling through the intracellular domain of the receptor not only controls synaptic transmission in the brain, but similar pathways appear also to be important for sperm maturation in the epididymis. Further molecular definition of this novel signaling function may reveal new rational targets for male contraception and infertility therapies.

CHAPTER FIVE

DISCUSSION

The goal of this thesis was to uncover, explore, and explain novel functional roles of two receptors from the LDL receptor family, Vldlr and Apoer2, in the reproductive and central nervous systems. The process of elucidating novel functions of receptors as complex as Apoer2 and Vldlr requires exploration of protein function in a physiologically relevant, preferably endogenous, environment. The creation of transgenic animals was the powerful tool I employed which allows for such exploration.

Chapter 2 - The Interaction Between Vldlr and the Pafah1b Complex

My aim for Chapter 2 was to study the significance of the newly uncovered interaction between Vldlr and the Pafah1b complex (Zhang et al., 2007). The interaction is dependent upon a single amino acid which allows Vldlr, but not Apoer2, to bind to the alpha subunits of the Pafah1b complex. I successfully introduced this lysine to arginine mutation into the VLDL receptor, abrogating its binding to the alpha subunits and thereby mutating the first functional domain suggested to give Vldlr unique function independent from Apoer2. I believe that this interaction is an important link between Reelin signaling, the Pafah1b complex in the regulation of brain development and, as we postulate, synaptic function. The mutation was introduced into mice using two different techniques, BAC injection and ES cell homologous recombination. Employing two different techniques allowed for the exploration of advantages and disadvantages that pertain to each method of genetically altered mouse generation.

BAC transgenic vs. ES cell homologous recombination

The creation of mouse models in which genes are deleted, introduced, mutated, overexpressed, or modulated in any way that results in abnormal gene expression, has become an invaluable tool for exploring gene function and disease pathology. However, the creation of such mutant mouse lines is not trivial and, as explored in Chapter 2, presents an entirely unique set of challenges. BAC transgenic mouse generation does not require tedious cell culture work, but necessitates the analysis of multiple founder lines to confirm phenotypic consistency. ES cell techniques may be time consuming and technically more demanding, however the researcher modifies a gene in its natural environment using this technique. This allows for gene expression that may be more physiologically relevant than expression from a randomly integrated BAC locus. Random BAC genome integration sites can disrupt endogenous gene expression and create the potential for misleading conclusions regarding resultant phenotypes. Having created animals using both BAC transgenic and ES cell homologous recombination techniques, I strongly encourage scientists to carefully consider each method before embarking, and I promote using ES homologous recombination as a more powerful and reliable technique.

Pafah1b alpha subunits and Vldlr

Chapter 2 also discusses how the interaction between Pafah1b and Vldlr could be important for both neuronal migration and synaptic plasticity. These components of brain development and function are regulated by both Reelin signaling and functions of the Pafah1b complex and its subunits (Albrecht et al., 1996; Kato et al., 1994;

Trommsdorff et al., 1999; Weeber et al., 2002). The more we know about how Pafah1b regulates neuronal migration and synaptic plasticity, the closer the Pafah1b functional mechanisms encroach upon the Reelin signaling pathway. Interactions between Lis1 and phospho-Dab1, Pafah1b2 and Dab1, and now recently Lis1 and Pafah1b2/3, all indicate a convergence between the Reelin signaling pathway and the Pafah1b complex (Assadi et al., 2003; Zhang et al., 2007; Zhang et al., 2009). Compound mutant mouse lines removing Vldlr, Lis1, the alpha subunits, or Dab1 from synapses, reveal severe defects in neuronal migration, brain development, as well as synapse function (Assadi et al., 2003; Assadi et al., 2008). It has been postulated that binding of Vldlr to the alpha subunits of the Pafah1b complex may bring Lis1 in closer proximity to Disabled and promote downstream functions in neuronal migration. Thus, the significance of the interaction between Vldlr and Pafah1b2/3 could be no more than the need for protein scaffolding, thus highlighting Lis1 as the functional component in one of the mechanisms regulating neuronal migration which involves both Reelin signaling and the Pafah1b complex.

It is unfortunate that most studies exploring the relationship between Reelin signaling and components of Pafah1b ignore the catalytic activity of the Pafah1b complex. Pafah1b hydrolyzes PAF which has been shown to enhance memory in behavioral tasks as well as LTP induction in the hippocampus and rat medial vestibular nuclei (Clark et al., 1992; Grassi et al., 1998; Izquierdo et al., 1995; Kato, 1999). Kato et al. classified PAF as a potential retrograde messenger which is active subsequent to LTP induction, enhancing presynaptic neurotransmitter release (Kato et al., 1994). I propose the following model in which Reelin signaling may regulate presynaptic function through the catalytic activity of Pafah1b. The entire Pafah1b complex has the ability to interact

closely with the Reelin signaling machinery surrounding the NPxY motif of Vldlr. It may be that during Reelin signaling the interaction between Dab1 and Vldlr sequesters the three subunits of the Pafah1b complex (Vldlr binds the alpha subunits and pospho-Dab1 binds Lis1) within the Reelin signaling machinery. This prevents Pafah1b from hydrolyzing existing PAF in the synapse. This allows PAF to enter the synaptic cleft and acting as a retrograde messenger, enhance presynaptic neurotransmitter release upon Reelin stimulation and the induction of LTP. In the absence of Reelin, Pafah1b is free to move about the synapse and remove excess PAF, inhibiting any modulation of presynaptic function.

Measurement of Pafhah1b activity and PAF levels in synaptosomes from Reelin treated and untreated brain slices should reveal differences between WT, L838R Vldlr mutant, and Vldlr KO mice. If my hypothesis is correct, WT slices should exhibit decreased Pafah1b activity and increased PAF levels in the Reelin treated conditions. Both the L838R Vldlr mutant and Vldlr KO mice would show the opposite result, increased Pafah1b activity and decreased PAF levels. This is because the Vldlr receptor is mutated or absent from the synapse and cannot promote the sequestration of the enzyme and inhibition of its hydrolytic function.

Functionally, the frequency and amplitude of miniature EPSCs from slices or cultured neurons treated with and without Reelin would be different between WT mice and the L838R Vldlr mutants. If the L838R KI animals have decreased PAF levels due to increased Pafah1b activity, presynaptic neurotransmitter release should be dampened, resulting in less frequent or less intense mini-EPSCs both with and without Reelin

treatment. In the WT animals, Reelin treatment would increase mini-EPSC frequency or amplitude.

In the proposed mechanism, Vldlr and Reelin signaling do not directly stimulate LTP induction, however, they prepare the synaptic environment for LTP enhancement. Once LTP is induced in the Reelin stimulated synapses, PAF is available for release and can enhance LTP. This model supports previous studies showing no increase in LTP induction after Reelin treatment in Vldlr KO animals and suggests that whereas Apoer2 enhances Reelin induced LTP through a postsynaptic mechanism, Vldlr regulates presynaptic activity. This is model also introduces both pre- and postsynaptic mechanisms that need to be intact to promote increased induction of LTP upon Reelin stimulation. It also provides yet another way in which the functions of Apoer2 and Vldlr diverge, stressing the individual importance of each receptor.

Chapter 3 – The functional importance of the Apoer2 O-linked sugar domain

The O-linked sugar domain of Apoer2 is involved in the regulation of receptor stability and function through alternative splicing, glycosylation, and proteolytic processing (Chapter 3 and (Clatworthy et al., 1999; May et al., 2003)). The alternatively spliced cytoplasmic domain of Apoer2 functions through adaptor protein interactions, linking the receptor to the regulation of synaptic plasticity and neuronal survival (Beffert et al., 2006b; Beffert et al., 2005). Alternative splice variants expressing various permutations of these two domains are found in the human brain (Figure 3.4). However, reasons why Apoer2 processing is regulated by glycosylation and how cleavage of the receptor is important in synaptic function have not been determined.

In order to answer these questions, I created two knockin Apoer2 mouse lines constitutively expressing two of the O-linked sugar domain (exon16) and cytoplasmic tail insert (exon19) splice variants: Apoer2*[Δ16+19]* and Apoer2*[Δ16Δ19]*. Using these Apoer2 KI mouse lines along with cell culture data I was able to make four important conclusions regarding the function of the O-linked sugar domain in concert with the cytoplasmic tail insert. First, the O-linked sugar domain is necessary for specific proteolytic processing of Apoer2 in transfected cells and primary neuron cultures (Figures 3.10). I propose that there is a protease cleavage/recognition site within the O-linked sugar domain, however this hypothesis still needs to be confirmed by N-terminal sequencing of the cleaved Apoer2 tail. Second, glycosylation of Apoer2 within the O-linked sugar domain protects the receptor from proteolytic cleavage in transfected cells (Figure 3.12). Subsequently, disruption of Apoer2 proteolytic processing, resulting from the deletion of exon 16 *in vivo*, leads to protein stabilization and increased Apoer2 protein levels (Figure 3.9). Lastly, inhibition of proteolytic processing and an increase in Apoer2 brain membrane levels causes an increase in baseline synaptic transmission (Figure 3.16) and defects in Reelin stimulated LTP induction (Figure 3.15).

Although results from Chapter 3 suggest that the Apoer2 O-linked sugar domain and the functional cytoplasmic tail work together to regulate synaptic plasticity, it is still unclear why and how this is important *in vivo*. I believe that there are two mechanisms through which different Apoer2 splice variants regulate synaptic plasticity. First, during early LTP, the glycosylation state of Apoer2 in different regions of the brain or even different neurons/synapses controls the sensitivity of the neuron/synapse to LTP

induction in a Reelin dependent manner. Second, during late LTP, Apoer2 regulates synaptic strengthening by activating genes important for maintenance of LTP.

Prolonged Reelin incubation has been shown to increase AMPA receptor localization to synaptic membranes (Qiu et al., 2006). It is probable that increased baseline synaptic transmission seen in the Apoer2*[Δ16+19]* mice, which express twice as much Apoer2, is due to sensitization of the synapse to endogenous Reelin and increased AMPAR membrane insertion. However, cell surface biotinylation experiments from primary neuron cultures still need to be performed in the Apoer2*[Δ16]* animals to confirm this hypothesis. Because AMPA receptors mediate most of the fast, minute-by-minute synaptic activity they are also important for the induction of early LTP. Reelin stimulation may "prime" a synapse for LTP induction by increasing AMPAR localization to the membrane. If Apoer2 levels alter the sensitivity of a synapse to Reelin stimulation, and glycosylation regulates Apoer2 stability, then Apoer2 glycosylation should in turn modulate synapse "priming". Synapses in different regions of the hippocampus or cortex could express various glycosylated forms of Apoer2 depending on the sensitivity to Reelin that is needed for the function of the particular brain region. Hypoglycosylated Apoer2 will be removed from the membrane by increased proteolytic processing, causing desensitization of the synapse to Reelin and loss of "priming". Highly glycosylated Apoer2, or the Apoer2 splice variant lacking the O-linked sugar domain will increase Apoer2 protein levels and increase Reelin sensitivity as well as synapse "priming" for LTP induction.

Laser dissection of brain regions and subsequent protein and glycosylation analysis could uncover any regional Apoer2 glycosylation differences. Within a specific

brain region, excitatory and inhibitory neurons may also express differentially glycosylated Apoer2. Fluorescent activated cell sorting (FACS) could be used to separate excitatory or inhibitory neurons allowing for the measurement of Apoer2 protein levels and glycosylation states from both neuronal groups.

Switching to the function of Apoer2 in late LTP, gene expression and protein synthesis is required for the maintenance of late LTP. It is important to note that cleavage of hypoglycosylated Apoer2 leads to the release of the intracellular domain of the receptor, leaving it free to translocate to the nucleus and regulate gene transcription. Most protein nuclear localization signals (NLS) are short sequences of positively charged amino acids, typically lysines and arginines (Kalderon et al., 1984). The initial nine amino acids of the human Apoer2 cytoplasmic tail – R N W K R K N T K – include five lysines/arginines which suggests that the sequence could indeed function as a nuclear localization signal.

Although we have not yet tested Apoer2 effects on late-phase LTP, I propose that the Apoer2 ICD translocates to the nucleus and could be important for the regulation of genes involved in maintenance of synaptic plasticity. These genes may include Apoer2 itself, ionotropic glutamate receptors, or even the atypical PKC, Protein Kinase Mzeta (PKMζ). PKMζ, a constitutively active kinase, is upregulated after high frequency stimulation and is required for maintenance of late LTP (Sacktor, 2008; Yao et al., 2008). It is possible that the Apoer2 ICD could modulate the expression of the mRNA encoding a regulatory domain free PKCζ catalytic domain, from which the PKMζ is translated (Hernandez et al., 2003; Kelly et al., 2007).

The Apoer2 Δ16 knockin mice have not only allowed for the exploration of the significance of the O-linked sugar domain *in vivo* but have also provided new models which will be useful for further analysis of Apoer2 regulation of synaptic plasticity. These mice may help uncover the involvement of Apoer2 in the regulation of both early and late LTP as well as transcriptional regulation of genes involved in neuronal function, further augmenting the list of Apoer2 functions.

Chapter 4 – Roles of Apoer2 in selenium uptake and sperm function

The main focus of Chapter 4 was to emphasize the distinct roles of Apoer2 in signaling and endocytosis, both in the brain as well as the testis. Using a panel of Apoer2 mutant KI animals, I confirmed that none of the functional domains within the tail of the receptor, and including the O-linked sugar domain, participate in selenium uptake in the brain or in the testis. Although these domains, when mutated, affect normal Reelin signaling, they do not hamper the uptake of selenium via Sepp1.

The selenium study also uncovered a potential signaling role for the NFDNPVY motif within the cytoplasmic tail of Apoer2. Even though testis selenium levels from the Apoer2*[Dab^{-}]* mice (expressing the NFD → EIG mutation) were comparable to WT, these mice suffered from hypofertility, likely caused by impaired sperm morphology and motility. In the brain, the PTB domain containing protein Disabled binds to the NFDNPVY motif of Apoer2 and Vldlr. In the sperm, however, no proteins have yet been shown to bind to this particular sequence in the tail of Apoer2. It is likely that a PTB containing protein found in the sperm or testis is necessary for binding to Apoer2 and initiating signaling pathways that may regulate sperm maturation and function. This

signaling pathway may involve the regulation of osmotic pressure within the sperm tail or be involved in signaling for hyperactivation prior to egg fertilization.

It will be important to identify any adaptor/signaling proteins that bind to the Apoer2 tail in order to elucidate the signaling mechanism involving Apoer2 in sperm function. Apoer2 immunoprecipitated from sperm and testicular proteins from WT mice should pulldown any interacting proteins that can be further separated by electrophoresis. Silver stained bands that differ between WT and Apoer2*[Dab^{-}]* pulldowns may be candidate adaptor proteins which could be identified using mass spectrometry.

Previously unpublished data from our laboratory suggests that Apoer2 may be expressed in the acrosome of the mouse sperm. This could indicate that not only is Apoer2 important for sperm morphology and motility it may also be involved in the ability of the sperm to fertilize an egg. The acrosome is important in the capacitation, or "preparation", of the sperm for fusion with the egg (Visconti et al., 1995). To date nobody has looked at the capacitation efficacy of Apoer2 mutant spermatozoa. These experiments could further expand Apoer2 signaling function in the spermatozoon and again add to the growing list of Apoer2 functions in mammals.

Conclusion

In science, one answered question always brings up two more unanswered questions. As such, there are many more rocks waiting to be unturned which will further enlighten our knowledge of the independent and novel functions of both Vldlr and Apoer2. Existing and future mutant mouse lines will be crucial for further exploration of the functional divergence between Apoer2 and Vldlr and the potential involvement of

these LDL receptor family members in neurological diseases such as AD as well as potential treatments for infertility.

References

Albrecht, U., Abu-Issa, R., Ratz, B., Hattori, M., Aoki, J., Arai, H., Inoue, K., and Eichele, G. (1996). Platelet-activating factor acetylhydrolase expression and activity suggest a link between neuronal migration and platelet-activating factor. Dev Biol *180*, 579-593.

Alonso, A., Zaidi, T., Novak, M., Grundke-Iqbal, I., and Iqbal, K. (2001). Hyperphosphorylation induces self-assembly of tau into tangles of paired helical filaments/straight filaments. Proc Natl Acad Sci U S A *98*, 6923-6928.

Andersen, O.M., Yeung, C.H., Vorum, H., Wellner, M., Andreassen, T.K., Erdmann, B., Mueller, E.C., Herz, J., Otto, A., Cooper, T.G.*, et al.* (2003). Essential role of the apolipoprotein E receptor-2 in sperm development. J Biol Chem *278*, 23989-23995.

Angevine, J.B., Jr., and Sidman, R.L. (1961). Autoradiographic study of cell migration during histogenesis of cerebral cortex in the mouse. Nature *192*, 766-768.

Apweiler, R., Hermjakob, H., and Sharon, N. (1999). On the frequency of protein glycosylation, as deduced from analysis of the SWISS-PROT database. Biochim Biophys Acta *1473*, 4-8.

Arai, H. (2002). Platelet-activating factor acetylhydrolase. Prostaglandins Other Lipid Mediat *68-69*, 83-94.

Arnaud, L., Ballif, B.A., Forster, E., and Cooper, J.A. (2003). Fyn tyrosine kinase is a critical regulator of disabled-1 during brain development. Curr Biol *13*, 9-17.

Assadi, A.H., Zhang, G., Beffert, U., McNeil, R.S., Renfro, A.L., Niu, S., Quattrocchi, C.C., Antalffy, B.A., Sheldon, M., Armstrong, D.D.*, et al.* (2003). Interaction of reelin signaling and Lis1 in brain development. Nat Genet *35*, 270-276.

Assadi, A.H., Zhang, G., McNeil, R., Clark, G.D., and D'Arcangelo, G. (2008). Pafah1b2 mutations suppress the development of hydrocephalus in compound Pafah1b1; Reln and Pafah1b1; Dab1 mutant mice. Neurosci Lett *439*, 100-105.

Ballif, B.A., Arnaud, L., Arthur, W.T., Guris, D., Imamoto, A., and Cooper, J.A. (2004). Activation of a Dab1/CrkL/C3G/Rap1 pathway in Reelin-stimulated neurons. Curr Biol *14*, 606-610.

Ballif, B.A., Arnaud, L., and Cooper, J.A. (2003). Tyrosine phosphorylation of Disabled-1 is essential for Reelin-stimulated activation of Akt and Src family kinases. Brain Res Mol Brain Res *117*, 152-159.

Barmina, O.Y., Walling, H.W., Fiacco, G.J., Freije, J.M., Lopez-Otin, C., Jeffrey, J.J., and Partridge, N.C. (1999). Collagenase-3 binds to a specific receptor and requires the low density lipoprotein receptor-related protein for internalization. J Biol Chem *274*, 30087-30093.

Barr, A.M., Fish, K.N., and Markou, A. (2007). The reelin receptors VLDLR and ApoER2 regulate sensorimotor gating in mice. Neuropharmacology *52*, 1114-1123.

Beckett, D., Kovaleva, E., and Schatz, P.J. (1999). A minimal peptide substrate in biotin holoenzyme synthetase-catalyzed biotinylation. Protein Sci *8*, 921-929.

Beffert, U., Durudas, A., Weeber, E.J., Stolt, P.C., Giehl, K.M., Sweatt, J.D., Hammer, R.E., and Herz, J. (2006a). Functional dissection of Reelin signaling by site-directed disruption of Disabled-1 adaptor binding to apolipoprotein E receptor 2: distinct roles in development and synaptic plasticity. J Neurosci *26*, 2041-2052.

Beffert, U., Morfini, G., Bock, H.H., Reyna, H., Brady, S.T., and Herz, J. (2002). Reelin-mediated signaling locally regulates protein kinase B/Akt and glycogen synthase kinase 3beta. J Biol Chem *277*, 49958-49964.

Beffert, U., Nematollah Farsian, F., Masiulis, I., Hammer, R.E., Yoon, S.O., Giehl, K.M., and Herz, J. (2006b). ApoE receptor 2 controls neuronal survival in the adult brain. Curr Biol *16*, 2446-2452.

Beffert, U., Stolt, P.C., and Herz, J. (2004). Functions of lipoprotein receptors in neurons. J Lipid Res *45*, 403-409.

Beffert, U., Weeber, E.J., Durudas, A., Qiu, S., Masiulis, I., Sweatt, J.D., Li, W.P., Adelmann, G., Frotscher, M., Hammer, R.E.*, et al.* (2005). Modulation of synaptic plasticity and memory by Reelin involves differential splicing of the lipoprotein receptor Apoer2. Neuron *47*, 567-579.

Beisiegel, U., Weber, W., and Bengtsson-Olivecrona, G. (1991). Lipoprotein lipase enhances the binding of chylomicrons to low density lipoprotein receptor-related protein. Proc Natl Acad Sci U S A *88*, 8342-8346.

Bhattacharyya, S., Biou, V., Xu, W., Schluter, O., and Malenka, R.C. (2009). A critical role for PSD-95/AKAP interactions in endocytosis of synaptic AMPA receptors. Nat Neurosci *12*, 172-181.

Bielas, S., Higginbotham, H., Koizumi, H., Tanaka, T., and Gleeson, J.G. (2004). Cortical neuronal migration mutants suggest separate but intersecting pathways. Annu Rev Cell Dev Biol *20*, 593-618.

Bix, G.J., and Clark, G.D. (1998). Platelet-activating factor receptor stimulation disrupts neuronal migration In vitro. J Neurosci *18*, 307-318.

Bock, H.H., and Herz, J. (2003). Reelin activates SRC family tyrosine kinases in neurons. Curr Biol *13*, 18-26.

Bock, H.H., Jossin, Y., Liu, P., Forster, E., May, P., Goffinet, A.M., and Herz, J. (2003). Phosphatidylinositol 3-kinase interacts with the adaptor protein Dab1 in response to Reelin signaling and is required for normal cortical lamination. J Biol Chem *278*, 38772-38779.

Bos, J.L., de Rooij, J., and Reedquist, K.A. (2001). Rap1 signalling: adhering to new models. Nat Rev Mol Cell Biol *2*, 369-377.

Brion, J.P., Couck, A.M., Robertson, J., Loviny, T.L., and Anderton, B.H. (1993). Neurofilament monoclonal antibodies RT97 and 8D8 recognize different modified epitopes in paired helical filament-tau in Alzheimer's disease. J Neurochem *60*, 1372-1382.

Brown, M.S., and Goldstein, J.L. (1979). Receptor-mediated endocytosis: insights from the lipoprotein receptor system. Proc Natl Acad Sci U S A *76*, 3330-3337.

Brown, M.S., and Goldstein, J.L. (1986). A receptor-mediated pathway for cholesterol homeostasis. Science *232*, 34-47.

Burk, R.F., and Hill, K.E. (2005). Selenoprotein P: an extracellular protein with unique physical characteristics and a role in selenium homeostasis. Annu Rev Nutr *25*, 215-235.

Burk, R.F., Hill, K.E., Olson, G.E., Weeber, E.J., Motley, A.K., Winfrey, V.P., and Austin, L.M. (2007). Deletion of apolipoprotein E receptor-2 in mice lowers brain selenium and causes severe neurological dysfunction and death when a low-selenium diet is fed. J Neurosci *27*, 6207-6211.

Cam, J.A., Zerbinatti, C.V., Knisely, J.M., Hecimovic, S., Li, Y., and Bu, G. (2004). The low density lipoprotein receptor-related protein 1B retains beta-amyloid precursor protein at the cell surface and reduces amyloid-beta peptide production. J Biol Chem *279*, 29639-29646.

Caviness, V.S., Jr., and Sidman, R.L. (1973). Time of origin or corresponding cell classes in the cerebral cortex of normal and reeler mutant mice: an autoradiographic analysis. J Comp Neurol *148*, 141-151.

Chen, W.J., Goldstein, J.L., and Brown, M.S. (1990). NPXY, a sequence often found in cytoplasmic tails, is required for coated pit-mediated internalization of the low density lipoprotein receptor. J Biol Chem *265*, 3116-3123.

Chen, Y., Beffert, U., Ertunc, M., Tang, T.S., Kavalali, E.T., Bezprozvanny, I., and Herz, J. (2005). Reelin modulates NMDA receptor activity in cortical neurons. J Neurosci *25*, 8209-8216.

Clark, G.D., Happel, L.T., Zorumski, C.F., and Bazan, N.G. (1992). Enhancement of hippocampal excitatory synaptic transmission by platelet-activating factor. Neuron *9*, 1211-1216.

Clark, G.D., McNeil, R.S., Bix, G.J., and Swann, J.W. (1995). Platelet-activating factor produces neuronal growth cone collapse. Neuroreport *6*, 2569-2575.

Clatworthy, A.E., Stockinger, W., Christie, R.H., Schneider, W.J., Nimpf, J., Hyman, B.T., and Rebeck, G.W. (1999). Expression and alternate splicing of apolipoprotein E receptor 2 in brain. Neuroscience *90*, 903-911.

Collingridge, G.L., and Bliss, T.V. (1995). Memories of NMDA receptors and LTP. Trends Neurosci *18*, 54-56.

Cooper, J.A. (2008). A mechanism for inside-out lamination in the neocortex. Trends Neurosci *31*, 113-119.

Cooper, T.G., and Yeung, C.H. (2003). Acquisition of volume regulatory response of sperm upon maturation in the epididymis and the role of the cytoplasmic droplet. Microsc Res Tech *61*, 28-38.

Cordy, J.M., Hussain, I., Dingwall, C., Hooper, N.M., and Turner, A.J. (2003). Exclusively targeting beta-secretase to lipid rafts by GPI-anchor addition up-regulates beta-site processing of the amyloid precursor protein. Proc Natl Acad Sci U S A *100*, 11735-11740.

Costa, E., Grayson, D.R., and Guidotti, A. (2003a). Epigenetic downregulation of GABAergic function in schizophrenia: potential for pharmacological intervention? Mol Interv *3*, 220-229.

Costa, E., Grayson, D.R., Mitchell, C.P., Tremolizzo, L., Veldic, M., and Guidotti, A. (2003b). GABAergic cortical neuron chromatin as a putative target to treat schizophrenia vulnerability. Crit Rev Neurobiol *15*, 121-142.

Culi, J., Springer, T.A., and Mann, R.S. (2004). Boca-dependent maturation of beta-propeller/EGF modules in low-density lipoprotein receptor proteins. EMBO J *23*, 1372-1380.

D'Arcangelo, G., and Curran, T. (1998). Reeler: new tales on an old mutant mouse. Bioessays *20*, 235-244.

D'Arcangelo, G., Homayouni, R., Keshvara, L., Rice, D.S., Sheldon, M., and Curran, T. (1999). Reelin is a ligand for lipoprotein receptors. Neuron *24*, 471-479.

D'Arcangelo, G., Miao, G.G., Chen, S.C., Soares, H.D., Morgan, J.I., and Curran, T. (1995). A protein related to extracellular matrix proteins deleted in the mouse mutant reeler. Nature *374*, 719-723.

Delacour, D., and Jacob, R. (2006). Apical protein transport. Cell Mol Life Sci *63*, 2491-2505.

Derer, P. (1985). Comparative localization of Cajal-Retzius cells in the neocortex of normal and reeler mutant mice fetuses. Neurosci Lett *54*, 1-6.

Dobyns, W.B., Reiner, O., Carrozzo, R., and Ledbetter, D.H. (1993). Lissencephaly. A human brain malformation associated with deletion of the LIS1 gene located at chromosome 17p13. JAMA *270*, 2838-2842.

Falconer, D.S. (1951). Two new mutants "trembler" and "reeler" with neurological actions in the house mouse. J Genet *50*, 192-201.

Fass, D., Blacklow, S., Kim, P.S., and Berger, J.M. (1997). Molecular basis of familial hypercholesterolaemia from structure of LDL receptor module. Nature *388*, 691-693.

Fatemi, S.H. (2005). Reelin glycoprotein: structure, biology and roles in health and disease. Mol Psychiatry *10*, 251-257.

Fatemi, S.H., Snow, A.V., Stary, J.M., Araghi-Niknam, M., Reutiman, T.J., Lee, S., Brooks, A.I., and Pearce, D.A. (2005). Reelin signaling is impaired in autism. Biol Psychiatry *57*, 777-787.

Feng, Y., Olson, E.C., Stukenberg, P.T., Flanagan, L.A., Kirschner, M.W., and Walsh, C.A. (2000). LIS1 regulates CNS lamination by interacting with mNudE, a central component of the centrosome. Neuron *28*, 665-679.

Frykman, P.K., Brown, M.S., Yamamoto, T., Goldstein, J.L., and Herz, J. (1995). Normal plasma lipoproteins and fertility in gene-targeted mice homozygous for a disruption in the gene encoding very low density lipoprotein receptor. Proc Natl Acad Sci U S A *92*, 8453-8457.

Fuentealba, R.A., Barria, M.I., Lee, J., Cam, J., Araya, C., Escudero, C.A., Inestrosa, N.C., Bronfman, F.C., Bu, G., and Marzolo, M.P. (2007). ApoER2 expression increases Abeta production while decreasing Amyloid Precursor Protein (APP) endocytosis: Possible role in the partitioning of APP into lipid rafts and in the regulation of gamma-secretase activity. Mol Neurodegener *2*, 14.

Gerton, J.L., DeRisi, J., Shroff, R., Lichten, M., Brown, P.O., and Petes, T.D. (2000). Inaugural article: global mapping of meiotic recombination hotspots and coldspots in the yeast Saccharomyces cerevisiae. Proc Natl Acad Sci U S A *97*, 11383-11390.

Goffinet, A.M. (1992). The reeler gene: a clue to brain development and evolution. Int J Dev Biol *36*, 101-107.

Gotthardt, M., Hammer, R.E., Hubner, N., Monti, J., Witt, C.C., McNabb, M., Richardson, J.A., Granzier, H., Labeit, S., and Herz, J. (2003). Conditional expression of mutant M-line titins results in cardiomyopathy with altered sarcomere structure. J Biol Chem *278*, 6059-6065.

Grassi, S., Francescangeli, E., Goracci, G., and Pettorossi, V.E. (1998). Role of platelet-activating factor in long-term potentiation of the rat medial vestibular nuclei. J Neurophysiol *79*, 3266-3271.

Guidotti, A., Auta, J., Davis, J.M., Di-Giorgi-Gerevini, V., Dwivedi, Y., Grayson, D.R., Impagnatiello, F., Pandey, G., Pesold, C., Sharma, R.*, et al.* (2000). Decrease in reelin and glutamic acid decarboxylase67 (GAD67) expression in schizophrenia and bipolar disorder: a postmortem brain study. Arch Gen Psychiatry *57*, 1061-1069.

Gupta, A., Tsai, L.H., and Wynshaw-Boris, A. (2002). Life is a journey: a genetic look at neocortical development. Nat Rev Genet *3*, 342-355.

Hamosh, A., Scott, A.F., Amberger, J.S., Bocchini, C.A., and McKusick, V.A. (2005). Online Mendelian Inheritance in Man (OMIM), a knowledgebase of human genes and genetic disorders. Nucleic Acids Res *33*, D514-517.

Hanisch, F.G. (2001). O-glycosylation of the mucin type. Biol Chem *382*, 143-149.

Hattori, M., Adachi, H., Tsujimoto, M., Arai, H., and Inoue, K. (1994a). The catalytic subunit of bovine brain platelet-activating factor acetylhydrolase is a novel type of serine esterase. J Biol Chem *269*, 23150-23155.

Hattori, M., Adachi, H., Tsujimoto, M., Arai, H., and Inoue, K. (1994b). Miller-Dieker lissencephaly gene encodes a subunit of brain platelet-activating factor acetylhydrolase [corrected]. Nature *370*, 216-218.

Helenius, A., and Aebi, M. (2004). Roles of N-linked glycans in the endoplasmic reticulum. Annu Rev Biochem *73*, 1019-1049.

Hernandez, A.I., Blace, N., Crary, J.F., Serrano, P.A., Leitges, M., Libien, J.M., Weinstein, G., Tcherapanov, A., and Sacktor, T.C. (2003). Protein kinase M zeta synthesis from a brain mRNA encoding an independent protein kinase C zeta catalytic domain. Implications for the molecular mechanism of memory. J Biol Chem *278*, 40305-40316.

Herz, J. (2001). The LDL receptor gene family: (un)expected signal transducers in the brain. Neuron *29*, 571-581.

Herz, J., and Chen, Y. (2006). Reelin, lipoprotein receptors and synaptic plasticity. Nat Rev Neurosci *7*, 850-859.

Herz, J., Chen, Y., Masiulis, I., and Zhou, L. (2008). Expanding functions of lipoprotein receptors. J Lipid Res.

Herz, J., Clouthier, D.E., and Hammer, R.E. (1992). LDL receptor-related protein internalizes and degrades uPA-PAI-1 complexes and is essential for embryo implantation. Cell *71*, 411-421.

Herz, J., Hamann, U., Rogne, S., Myklebost, O., Gausepohl, H., and Stanley, K.K. (1988). Surface location and high affinity for calcium of a 500-kd liver membrane protein closely related to the LDL-receptor suggest a physiological role as lipoprotein receptor. EMBO J *7*, 4119-4127.

Herz, J., Kowal, R.C., Goldstein, J.L., and Brown, M.S. (1990). Proteolytic processing of the 600 kd low density lipoprotein receptor-related protein (LRP) occurs in a trans-Golgi compartment. EMBO J *9*, 1769-1776.

Herz, J., and Strickland, D.K. (2001). LRP: a multifunctional scavenger and signaling receptor. J Clin Invest *108*, 779-784.

Hiesberger, T., Trommsdorff, M., Howell, B.W., Goffinet, A., Mumby, M.C., Cooper, J.A., and Herz, J. (1999). Direct binding of Reelin to VLDL receptor and ApoE receptor 2 induces tyrosine phosphorylation of disabled-1 and modulates tau phosphorylation. Neuron *24*, 481-489.

Hill, K.E., Zhou, J., McMahan, W.J., Motley, A.K., Atkins, J.F., Gesteland, R.F., and Burk, R.F. (2003). Deletion of selenoprotein P alters distribution of selenium in the mouse. J Biol Chem *278*, 13640-13646.

Hirotsune, S., Fleck, M.W., Gambello, M.J., Bix, G.J., Chen, A., Clark, G.D., Ledbetter, D.H., McBain, C.J., and Wynshaw-Boris, A. (1998). Graded reduction of Pafah1b1 (Lis1) activity results in neuronal migration defects and early embryonic lethality. Nat Genet *19*, 333-339.

Hisatsune, C., Umemori, H., Mishina, M., and Yamamoto, T. (1999). Phosphorylation-dependent interaction of the N-methyl-D-aspartate receptor epsilon 2 subunit with phosphatidylinositol 3-kinase. Genes Cells *4*, 657-666.

Hobbs, H.H., Russell, D.W., Brown, M.S., and Goldstein, J.L. (1990). The LDL receptor locus in familial hypercholesterolemia: mutational analysis of a membrane protein. Annu Rev Genet *24*, 133-170.

Hoe, H.S., Cooper, M.J., Burns, M.P., Lewis, P.A., van der Brug, M., Chakraborty, G., Cartagena, C.M., Pak, D.T., Cookson, M.R., and Rebeck, G.W. (2007). The

metalloprotease inhibitor TIMP-3 regulates amyloid precursor protein and apolipoprotein E receptor proteolysis. J Neurosci *27*, 10895-10905.

Hoe, H.S., and Rebeck, G.W. (2005). Regulation of ApoE receptor proteolysis by ligand binding. Brain Res Mol Brain Res *137*, 31-39.

Hoffarth, R.M., Johnston, J.G., Krushel, L.A., and van der Kooy, D. (1995). The mouse mutation reeler causes increased adhesion within a subpopulation of early postmitotic cortical neurons. J Neurosci *15*, 4838-4850.

Hong, S.E., Shugart, Y.Y., Huang, D.T., Shahwan, S.A., Grant, P.E., Hourihane, J.O., Martin, N.D., and Walsh, C.A. (2000). Autosomal recessive lissencephaly with cerebellar hypoplasia is associated with human RELN mutations. Nat Genet *26*, 93-96.

Howell, B.W., Hawkes, R., Soriano, P., and Cooper, J.A. (1997). Neuronal position in the developing brain is regulated by mouse disabled-1. Nature *389*, 733-737.

Howell, B.W., Herrick, T.M., and Cooper, J.A. (1999a). Reelin-induced tyrosine [corrected] phosphorylation of disabled 1 during neuronal positioning. Genes Dev *13*, 643-648.

Howell, B.W., Lanier, L.M., Frank, R., Gertler, F.B., and Cooper, J.A. (1999b). The disabled 1 phosphotyrosine-binding domain binds to the internalization signals of transmembrane glycoproteins and to phospholipids. Mol Cell Biol *19*, 5179-5188.

Ignatova, N., Sindic, C.J., and Goffinet, A.M. (2004). Characterization of the various forms of the Reelin protein in the cerebrospinal fluid of normal subjects and in neurological diseases. Neurobiol Dis *15*, 326-330.

Impagnatiello, F., Guidotti, A.R., Pesold, C., Dwivedi, Y., Caruncho, H., Pisu, M.G., Uzunov, D.P., Smalheiser, N.R., Davis, J.M., Pandey, G.N.*, et al.* (1998). A decrease of reelin expression as a putative vulnerability factor in schizophrenia. Proc Natl Acad Sci U S A *95*, 15718-15723.

Izquierdo, I., Fin, C., Schmitz, P.K., Da Silva, R.C., Jerusalinsky, D., Quillfeldt, J.A., Ferreira, M.B., Medina, J.H., and Bazan, N.G. (1995). Memory enhancement by intrahippocampal, intraamygdala, or intraentorhinal infusion of platelet-activating factor measured in an inhibitory avoidance task. Proc Natl Acad Sci U S A *92*, 5047-5051.

Johnson, E.B., Hammer, R.E., and Herz, J. (2005). Abnormal development of the apical ectodermal ridge and polysyndactyly in Megf7-deficient mice. Hum Mol Genet *14*, 3523-3538.

Johnson, E.B., Steffen, D.J., Lynch, K.W., and Herz, J. (2006). Defective splicing of Megf7/Lrp4, a regulator of distal limb development, in autosomal recessive mulefoot disease. Genomics *88*, 600-609.

Jossin, Y., Ignatova, N., Hiesberger, T., Herz, J., Lambert de Rouvroit, C., and Goffinet, A.M. (2004). The central fragment of Reelin, generated by proteolytic processing in vivo, is critical to its function during cortical plate development. J Neurosci *24*, 514-521.

Kalderon, D., Roberts, B.L., Richardson, W.D., and Smith, A.E. (1984). A short amino acid sequence able to specify nuclear location. Cell *39*, 499-509.

Kato, K. (1999). Modulation of long-term potentiation in the CA1 area of rat hippocampus by platelet-activating factor. Adv Exp Med Biol *469*, 221-227.

Kato, K., Clark, G.D., Bazan, N.G., and Zorumski, C.F. (1994). Platelet-activating factor as a potential retrograde messenger in CA1 hippocampal long-term potentiation. Nature *367*, 175-179.

Kelly, M.T., Crary, J.F., and Sacktor, T.C. (2007). Regulation of protein kinase Mzeta synthesis by multiple kinases in long-term potentiation. J Neurosci *27*, 3439-3444.

Kim, D.H., Iijima, H., Goto, K., Sakai, J., Ishii, H., Kim, H.J., Suzuki, H., Kondo, H., Saeki, S., and Yamamoto, T. (1996). Human apolipoprotein E receptor 2. A novel lipoprotein receptor of the low density lipoprotein receptor family predominantly expressed in brain. J Biol Chem *271*, 8373-8380.

Kim, D.H., Magoori, K., Inoue, T.R., Mao, C.C., Kim, H.J., Suzuki, H., Fujita, T., Endo, Y., Saeki, S., and Yamamoto, T.T. (1997). Exon/intron organization, chromosome localization, alternative splicing, and transcription units of the human apolipoprotein E receptor 2 gene. J Biol Chem *272*, 8498-8504.

Kingsley, D.M., Kozarsky, K.F., Hobbie, L., and Krieger, M. (1986a). Reversible defects in O-linked glycosylation and LDL receptor expression in a UDP-Gal/UDP-GalNAc 4-epimerase deficient mutant. Cell *44*, 749-759.

Kingsley, D.M., Kozarsky, K.F., Segal, M., and Krieger, M. (1986b). Three types of low density lipoprotein receptor-deficient mutant have pleiotropic defects in the synthesis of N-linked, O-linked, and lipid-linked carbohydrate chains. J Cell Biol *102*, 1576-1585.

Knisely, J.M., Li, Y., Griffith, J.M., Geuze, H.J., Schwartz, A.L., and Bu, G. (2007). Slow endocytosis of the LDL receptor-related protein 1B: implications for a novel cytoplasmic tail conformation. Exp Cell Res *313*, 3298-3307.

Koren, A., Ben-Aroya, S., and Kupiec, M. (2002). Control of meiotic recombination initiation: a role for the environment? Curr Genet *42*, 129-139.

Kounnas, M.Z., Moir, R.D., Rebeck, G.W., Bush, A.I., Argraves, W.S., Tanzi, R.E., Hyman, B.T., and Strickland, D.K. (1995). LDL receptor-related protein, a multifunctional ApoE receptor, binds secreted beta-amyloid precursor protein and mediates its degradation. Cell *82*, 331-340.

Kubo, K., Mikoshiba, K., and Nakajima, K. (2002). Secreted Reelin molecules form homodimers. Neurosci Res *43*, 381-388.

Lambert de Rouvroit, C., de Bergeyck, V., Cortvrindt, C., Bar, I., Eeckhout, Y., and Goffinet, A.M. (1999). Reelin, the extracellular matrix protein deficient in reeler mutant mice, is processed by a metalloproteinase. Exp Neurol *156*, 214-217.

Langbein, S., Szakacs, O., Wilhelm, M., Sukosd, F., Weber, S., Jauch, A., Lopez Beltran, A., Alken, P., Kalble, T., and Kovacs, G. (2002). Alteration of the LRP1B gene region is associated with high grade of urothelial cancer. Lab Invest *82*, 639-643.

Li, X.M., Li, C.C., Yu, S.S., Chen, J.T., Sabapathy, K., and Ruan, D.Y. (2007). JNK1 contributes to metabotropic glutamate receptor-dependent long-term depression and short-term synaptic plasticity in the mice area hippocampal CA1. Eur J Neurosci *25*, 391-396.

Lichtenthaler, S.F., Dominguez, D.I., Westmeyer, G.G., Reiss, K., Haass, C., Saftig, P., De Strooper, B., and Seed, B. (2003). The cell adhesion protein P-selectin glycoprotein ligand-1 is a substrate for the aspartyl protease BACE1. J Biol Chem *278*, 48713-48719.

Liu, C.X., Musco, S., Lisitsina, N.M., Forgacs, E., Minna, J.D., and Lisitsyn, N.A. (2000a). LRP-DIT, a putative endocytic receptor gene, is frequently inactivated in non-small cell lung cancer cell lines. Cancer Res *60*, 1961-1967.

Liu, C.X., Musco, S., Lisitsina, N.M., Yaklichkin, S.Y., and Lisitsyn, N.A. (2000b). Genomic organization of a new candidate tumor suppressor gene, LRP1B. Genomics *69*, 271-274.

Logeat, F., Bessia, C., Brou, C., LeBail, O., Jarriault, S., Seidah, N.G., and Israel, A. (1998). The Notch1 receptor is cleaved constitutively by a furin-like convertase. Proc Natl Acad Sci U S A *95*, 8108-8112.

Magdaleno, S., Keshvara, L., and Curran, T. (2002). Rescue of ataxia and preplate splitting by ectopic expression of Reelin in reeler mice. Neuron *33*, 573-586.

Magrane, J., Casaroli-Marano, R.P., Reina, M., Gafvels, M., and Vilaro, S. (1999). The role of O-linked sugars in determining the very low density lipoprotein receptor stability or release from the cell. FEBS Lett *451*, 56-62.

Mariani, J., Crepel, F., Mikoshiba, K., Changeux, J.P., and Sotelo, C. (1977). Anatomical, physiological and biochemical studies of the cerebellum from Reeler mutant mouse. Philos Trans R Soc Lond B Biol Sci *281*, 1-28.

Marin-Padilla, M. (1998). Cajal-Retzius cells and the development of the neocortex. Trends Neurosci *21*, 64-71.

May, P., Bock, H.H., Nimpf, J., and Herz, J. (2003). Differential glycosylation regulates processing of lipoprotein receptors by gamma-secretase. J Biol Chem *278*, 37386-37392.

May, P., Herz, J., and Bock, H.H. (2005). Molecular mechanisms of lipoprotein receptor signalling. Cell Mol Life Sci *62*, 2325-2338.

May, P., Reddy, Y.K., and Herz, J. (2002). Proteolytic processing of low density lipoprotein receptor-related protein mediates regulated release of its intracellular domain. J Biol Chem *277*, 18736-18743.

Meyer, G., and Goffinet, A.M. (1998). Prenatal development of reelin-immunoreactive neurons in the human neocortex. J Comp Neurol *397*, 29-40.

Monyer, H., Burnashev, N., Laurie, D.J., Sakmann, B., and Seeburg, P.H. (1994). Developmental and regional expression in the rat brain and functional properties of four NMDA receptors. Neuron *12*, 529-540.

Myers, S., Bottolo, L., Freeman, C., McVean, G., and Donnelly, P. (2005). A fine-scale map of recombination rates and hotspots across the human genome. Science *310*, 321-324.

Nakazawa, T., Komai, S., Tezuka, T., Hisatsune, C., Umemori, H., Semba, K., Mishina, M., Manabe, T., and Yamamoto, T. (2001). Characterization of Fyn-mediated tyrosine phosphorylation sites on GluR epsilon 2 (NR2B) subunit of the N-methyl-D-aspartate receptor. J Biol Chem *276*, 693-699.

Nykjaer, A., Dragun, D., Walther, D., Vorum, H., Jacobsen, C., Herz, J., Melsen, F., Christensen, E.I., and Willnow, T.E. (1999). An endocytic pathway essential for renal uptake and activation of the steroid 25-(OH) vitamin D3. Cell *96*, 507-515.

Ogawa, M., Miyata, T., Nakajima, K., Yagyu, K., Seike, M., Ikenaka, K., Yamamoto, H., and Mikoshiba, K. (1995). The reeler gene-associated antigen on Cajal-Retzius neurons is a crucial molecule for laminar organization of cortical neurons. Neuron *14*, 899-912.

Ohazama, A., Johnson, E.B., Ota, M.S., Choi, H.J., Porntaveetus, T., Oommen, S., Itoh, N., Eto, K., Gritli-Linde, A., Herz, J.*, et al.* (2008). Lrp4 modulates extracellular integration of cell signaling pathways in development. PLoS ONE *3*, e4092.

Olson, G.E., Winfrey, V.P., Nagdas, S.K., Hill, K.E., and Burk, R.F. (2005). Selenoprotein P is required for mouse sperm development. Biol Reprod *73*, 201-211.

Olson, G.E., Winfrey, V.P., Nagdas, S.K., Hill, K.E., and Burk, R.F. (2007). Apolipoprotein E receptor-2 (ApoER2) mediates selenium uptake from selenoprotein P by the mouse testis. J Biol Chem *282*, 12290-12297.

Park, T.J., and Curran, T. (2008). Crk and Crk-like play essential overlapping roles downstream of disabled-1 in the Reelin pathway. J Neurosci *28*, 13551-13562.

Perez-Garcia, C.G., Gonzalez-Delgado, F.J., Suarez-Sola, M.L., Castro-Fuentes, R., Martin-Trujillo, J.M., Ferres-Torres, R., and Meyer, G. (2001). Reelin-immunoreactive neurons in the adult vertebrate pallium. J Chem Neuroanat *21*, 41-51.

Persico, A.M., D'Agruma, L., Maiorano, N., Totaro, A., Militerni, R., Bravaccio, C., Wassink, T.H., Schneider, C., Melmed, R., Trillo, S.*, et al.* (2001). Reelin gene alleles and haplotypes as a factor predisposing to autistic disorder. Mol Psychiatry *6*, 150-159.

Pesold, C., Impagnatiello, F., Pisu, M.G., Uzunov, D.P., Costa, E., Guidotti, A., and Caruncho, H.J. (1998). Reelin is preferentially expressed in neurons synthesizing gamma-aminobutyric acid in cortex and hippocampus of adult rats. Proc Natl Acad Sci U S A *95*, 3221-3226.

Peters, M.M., Hill, K.E., Burk, R.F., and Weeber, E.J. (2006). Altered hippocampus synaptic function in selenoprotein P deficient mice. Mol Neurodegener *1*, 12.

Petes, T.D. (2001). Meiotic recombination hot spots and cold spots. Nat Rev Genet *2*, 360-369.

Pinto-Lord, M.C., Evrard, P., and Caviness, V.S., Jr. (1982). Obstructed neuronal migration along radial glial fibers in the neocortex of the reeler mouse: a Golgi-EM analysis. Brain Res *256*, 379-393.

Prescott, S.M., Zimmerman, G.A., Stafforini, D.M., and McIntyre, T.M. (2000). Platelet-activating factor and related lipid mediators. Annu Rev Biochem *69*, 419-445.

Qiu, S., Zhao, L.F., Korwek, K.M., and Weeber, E.J. (2006). Differential reelin-induced enhancement of NMDA and AMPA receptor activity in the adult hippocampus. J Neurosci *26*, 12943-12955.

Quinn, K.A., Grimsley, P.G., Dai, Y.P., Tapner, M., Chesterman, C.N., and Owensby, D.A. (1997). Soluble low density lipoprotein receptor-related protein (LRP) circulates in human plasma. J Biol Chem *272*, 23946-23951.

Quinn, K.A., Pye, V.J., Dai, Y.P., Chesterman, C.N., and Owensby, D.A. (1999). Characterization of the soluble form of the low density lipoprotein receptor-related protein (LRP). Exp Cell Res *251*, 433-441.

Rademacher, T.W., Parekh, R.B., and Dwek, R.A. (1988). Glycobiology. Annu Rev Biochem *57*, 785-838.

Reiner, O., Carrozzo, R., Shen, Y., Wehnert, M., Faustinella, F., Dobyns, W.B., Caskey, C.T., and Ledbetter, D.H. (1993). Isolation of a Miller-Dieker lissencephaly gene containing G protein beta-subunit-like repeats. Nature *364*, 717-721.

Rice, D.S., and Curran, T. (2001). Role of the reelin signaling pathway in central nervous system development. Annu Rev Neurosci *24*, 1005-1039.

Roses, A.D., Saunders, A.M., Corder, E.H., Pericak-Vance, M.A., Han, S.H., Einstein, G., Hulette, C., Schmechel, D.E., Holsti, M., Huang, D.*, et al.* (1995). Influence of the susceptibility genes apolipoprotein E-epsilon 4 and apolipoprotein E-epsilon 2 on the rate of disease expressivity of late-onset Alzheimer's disease. Arzneimittelforschung *45*, 413-417.

Rudenko, G., Henry, L., Henderson, K., Ichtchenko, K., Brown, M.S., Goldstein, J.L., and Deisenhofer, J. (2002). Structure of the LDL receptor extracellular domain at endosomal pH. Science *298*, 2353-2358.

Sacktor, T.C. (2008). PKMzeta, LTP maintenance, and the dynamic molecular biology of memory storage. Prog Brain Res *169*, 27-40.

Saez-Valero, J., Costell, M., Sjogren, M., Andreasen, N., Blennow, K., and Luque, J.M. (2003). Altered levels of cerebrospinal fluid reelin in frontotemporal dementia and Alzheimer's disease. J Neurosci Res *72*, 132-136.

Sasaki, S., Shionoya, A., Ishida, M., Gambello, M.J., Yingling, J., Wynshaw-Boris, A., and Hirotsune, S. (2000). A LIS1/NUDEL/cytoplasmic dynein heavy chain complex in the developing and adult nervous system. Neuron *28*, 681-696.

Schiffmann, S.N., Bernier, B., and Goffinet, A.M. (1997). Reelin mRNA expression during mouse brain development. Eur J Neurosci *9*, 1055-1071.

Shah, S., Lee, S.F., Tabuchi, K., Hao, Y.H., Yu, C., LaPlant, Q., Ball, H., Dann, C.E., 3rd, Sudhof, T., and Yu, G. (2005). Nicastrin functions as a gamma-secretase-substrate receptor. Cell *122*, 435-447.

Shankar, G.M., Li, S., Mehta, T.H., Garcia-Munoz, A., Shepardson, N.E., Smith, I., Brett, F.M., Farrell, M.A., Rowan, M.J., Lemere, C.A.*, et al.* (2008). Amyloid-beta protein dimers isolated directly from Alzheimer's brains impair synaptic plasticity and memory. Nat Med *14*, 837-842.

Sheldon, M., Rice, D.S., D'Arcangelo, G., Yoneshima, H., Nakajima, K., Mikoshiba, K., Howell, B.W., Cooper, J.A., Goldowitz, D., and Curran, T. (1997). Scrambler and yotari disrupt the disabled gene and produce a reeler-like phenotype in mice. Nature *389*, 730-733.

Sheppard, A.M., and Pearlman, A.L. (1997). Abnormal reorganization of preplate neurons and their associated extracellular matrix: an early manifestation of altered neocortical development in the reeler mutant mouse. J Comp Neurol *378*, 173-179.

Simon-Chazottes, D., Tutois, S., Kuehn, M., Evans, M., Bourgade, F., Cook, S., Davisson, M.T., and Guenet, J.L. (2006). Mutations in the gene encoding the low-density lipoprotein receptor LRP4 cause abnormal limb development in the mouse. Genomics *87*, 673-677.

Sinagra, M., Verrier, D., Frankova, D., Korwek, K.M., Blahos, J., Weeber, E.J., Manzoni, O.J., and Chavis, P. (2005). Reelin, very-low-density lipoprotein receptor, and apolipoprotein E receptor 2 control somatic NMDA receptor composition during hippocampal maturation in vitro. J Neurosci *25*, 6127-6136.

Singh, P.P., Singh, M., and Mastana, S.S. (2006). APOE distribution in world populations with new data from India and the UK. Ann Hum Biol *33*, 279-308.

Six, D.A., and Dennis, E.A. (2000). The expanding superfamily of phospholipase A(2) enzymes: classification and characterization. Biochim Biophys Acta *1488*, 1-19.

Sonoda, I., Imoto, I., Inoue, J., Shibata, T., Shimada, Y., Chin, K., Imamura, M., Amagasa, T., Gray, J.W., Hirohashi, S.*, et al.* (2004). Frequent silencing of low density lipoprotein receptor-related protein 1B (LRP1B) expression by genetic and epigenetic mechanisms in esophageal squamous cell carcinoma. Cancer Res *64*, 3741-3747.

Sornarajah, L., Vasuta, O.C., Zhang, L., Sutton, C., Li, B., El-Husseini, A., and Raymond, L.A. (2008). NMDA receptor desensitization regulated by direct binding to PDZ1-2 domains of PSD-95. J Neurophysiol *99*, 3052-3062.

Strasser, V., Fasching, D., Hauser, C., Mayer, H., Bock, H.H., Hiesberger, T., Herz, J., Weeber, E.J., Sweatt, J.D., Pramatarova, A.*, et al.* (2004). Receptor clustering is involved in Reelin signaling. Mol Cell Biol *24*, 1378-1386.

Suzuki-Toyota, F., Ito, C., Toyama, Y., Maekawa, M., Yao, R., Noda, T., and Toshimori, K. (2004). The coiled tail of the round-headed spermatozoa appears during epididymal passage in GOPC-deficient mice. Archives of histology and cytology *67*, 361-371.

Sweeney, K.J., Clark, G.D., Prokscha, A., Dobyns, W.B., and Eichele, G. (2000). Lissencephaly associated mutations suggest a requirement for the PAFAH1B heterotrimeric complex in brain development. Mech Dev *92*, 263-271.

Trommsdorff, M., Borg, J.P., Margolis, B., and Herz, J. (1998). Interaction of cytosolic adaptor proteins with neuronal apolipoprotein E receptors and the amyloid precursor protein. J Biol Chem *273*, 33556-33560.

Trommsdorff, M., Gotthardt, M., Hiesberger, T., Shelton, J., Stockinger, W., Nimpf, J., Hammer, R.E., Richardson, J.A., and Herz, J. (1999). Reeler/Disabled-like disruption of neuronal migration in knockout mice lacking the VLDL receptor and ApoE receptor 2. Cell *97*, 689-701.

Tsao, K.L., DeBarbieri, B., Michel, H., and Waugh, D.S. (1996). A versatile plasmid expression vector for the production of biotinylated proteins by site-specific, enzymatic modification in Escherichia coli. Gene *169*, 59-64.

Ulery, P.G., Beers, J., Mikhailenko, I., Tanzi, R.E., Rebeck, G.W., Hyman, B.T., and Strickland, D.K. (2000). Modulation of beta-amyloid precursor protein processing by the low density lipoprotein receptor-related protein (LRP). Evidence that LRP contributes to the pathogenesis of Alzheimer's disease. J Biol Chem *275*, 7410-7415.

Utton, M.A., Vandecandelaere, A., Wagner, U., Reynolds, C.H., Gibb, G.M., Miller, C.C., Bayley, P.M., and Anderton, B.H. (1997). Phosphorylation of tau by glycogen synthase kinase 3beta affects the ability of tau to promote microtubule self-assembly. Biochem J *323 (Pt 3)*, 741-747.

Valentine, W.M., Abel, T.W., Hill, K.E., Austin, L.M., and Burk, R.F. (2008). Neurodegeneration in mice resulting from loss of functional selenoprotein P or its receptor apolipoprotein E receptor 2. J Neuropathol Exp Neurol *67*, 68-77.

Visconti, P.E., Bailey, J.L., Moore, G.D., Pan, D., Olds-Clarke, P., and Kopf, G.S. (1995). Capacitation of mouse spermatozoa. I. Correlation between the capacitation state and protein tyrosine phosphorylation. Development *121*, 1129-1137.

Wang, Q., Walsh, D.M., Rowan, M.J., Selkoe, D.J., and Anwyl, R. (2004). Block of long-term potentiation by naturally secreted and synthetic amyloid beta-peptide in hippocampal slices is mediated via activation of the kinases c-Jun N-terminal kinase, cyclin-dependent kinase 5, and p38 mitogen-activated protein kinase as well as metabotropic glutamate receptor type 5. J Neurosci *24*, 3370-3378.

Wang, Y.T., and Salter, M.W. (1994). Regulation of NMDA receptors by tyrosine kinases and phosphatases. Nature *369*, 233-235.

Watanabe, I., Zhu, J., Recio-Pinto, E., and Thornhill, W.B. (2004). Glycosylation affects the protein stability and cell surface expression of Kv1.4 but Not Kv1.1 potassium channels. A pore region determinant dictates the effect of glycosylation on trafficking. J Biol Chem *279*, 8879-8885.

Weatherbee, S.D., Anderson, K.V., and Niswander, L.A. (2006). LDL-receptor-related protein 4 is crucial for formation of the neuromuscular junction. Development *133*, 4993-5000.

Weeber, E.J., Beffert, U., Jones, C., Christian, J.M., Forster, E., Sweatt, J.D., and Herz, J. (2002). Reelin and ApoE receptors cooperate to enhance hippocampal synaptic plasticity and learning. J Biol Chem *277*, 39944-39952.

Willnow, T.E. (1998). Receptor-associated protein (RAP): a specialized chaperone for endocytic receptors. Biol Chem *379*, 1025-1031.

Willnow, T.E., and Herz, J. (1994). Homologous recombination for gene replacement in mouse cell lines. Methods Cell Biol *43 Pt A*, 305-334.

Willnow, T.E., Hilpert, J., Armstrong, S.A., Rohlmann, A., Hammer, R.E., Burns, D.K., and Herz, J. (1996a). Defective forebrain development in mice lacking gp330/megalin. Proc Natl Acad Sci U S A *93*, 8460-8464.

Willnow, T.E., Moehring, J.M., Inocencio, N.M., Moehring, T.J., and Herz, J. (1996b). The low-density-lipoprotein receptor-related protein (LRP) is processed by furin in vivo and in vitro. Biochem J *313 (Pt 1)*, 71-76.

Willnow, T.E., Nykjaer, A., and Herz, J. (1999). Lipoprotein receptors: new roles for ancient proteins. Nat Cell Biol *1*, E157-162.

Wyne, K.L., Pathak, K., Seabra, M.C., and Hobbs, H.H. (1996). Expression of the VLDL receptor in endothelial cells. Arterioscler Thromb Vasc Biol *16*, 407-415.

Yang, X.W., and Gong, S. (2005). An overview on the generation of BAC transgenic mice for neuroscience research. Curr Protoc Neurosci *Chapter 5*, Unit 5 20.

Yao, Y., Kelly, M.T., Sajikumar, S., Serrano, P., Tian, D., Bergold, P.J., Frey, J.U., and Sacktor, T.C. (2008). PKM zeta maintains late long-term potentiation by N-ethylmaleimide-sensitive factor/GluR2-dependent trafficking of postsynaptic AMPA receptors. J Neurosci *28*, 7820-7827.

Yeung, C.H., Sonnenberg-Riethmacher, E., and Cooper, T.G. (1999). Infertile spermatozoa of c-ros tyrosine kinase receptor knockout mice show flagellar angulation and maturational defects in cell volume regulatory mechanisms. Biol Reprod *61*, 1062-1069.

Yochem, J., and Greenwald, I. (1993). A gene for a low density lipoprotein receptor-related protein in the nematode Caenorhabditis elegans. Proc Natl Acad Sci U S A *90*, 4572-4576.

Zhang, B., Luo, S., Wang, Q., Suzuki, T., Xiong, W.C., and Mei, L. (2008). LRP4 serves as a coreceptor of agrin. Neuron *60*, 285-297.

Zhang, G., Assadi, A.H., McNeil, R.S., Beffert, U., Wynshaw-Boris, A., Herz, J., Clark, G.D., and D'Arcangelo, G. (2007). The Pafah1b complex interacts with the Reelin receptor VLDLR. PLoS ONE *2*, e252.

Zhang, G., Assadi, A.H., Roceri, M., Clark, G.D., and D'Arcangelo, G. (2009). Differential Interaction of the Pafah1b Alpha Subunits with the Reelin Transducer Dab1. Brain Res.

Zhang, H., Liu, X., Zhang, C., Mundo, E., Macciardi, F., Grayson, D.R., Guidotti, A.R., and Holden, J.J. (2002). Reelin gene alleles and susceptibility to autism spectrum disorders. Mol Psychiatry *7*, 1012-1017.

Zhao, S., Hu, X., Park, J., Zhu, Y., Zhu, Q., Li, H., Luo, C., Han, R., Cooper, N., and Qiu, M. (2007). Selective expression of LDLR and VLDLR in myelinating oligodendrocytes. Dev Dyn *236*, 2708-2712.

Zheng, H., and Koo, E.H. (2006). The amyloid precursor protein: beyond amyloid. Mol Neurodegener *1*, 5.

Zurhove, K., Nakajima, C., Herz, J., Bock, H.H., and May, P. (2008). Gamma-secretase limits the inflammatory response through the processing of LRP1. Sci Signal *1*, ra15.